

UNCLASSIFIED

CENTRAL RESEARCH LIBRARY  
DOCUMENT COLLECTION

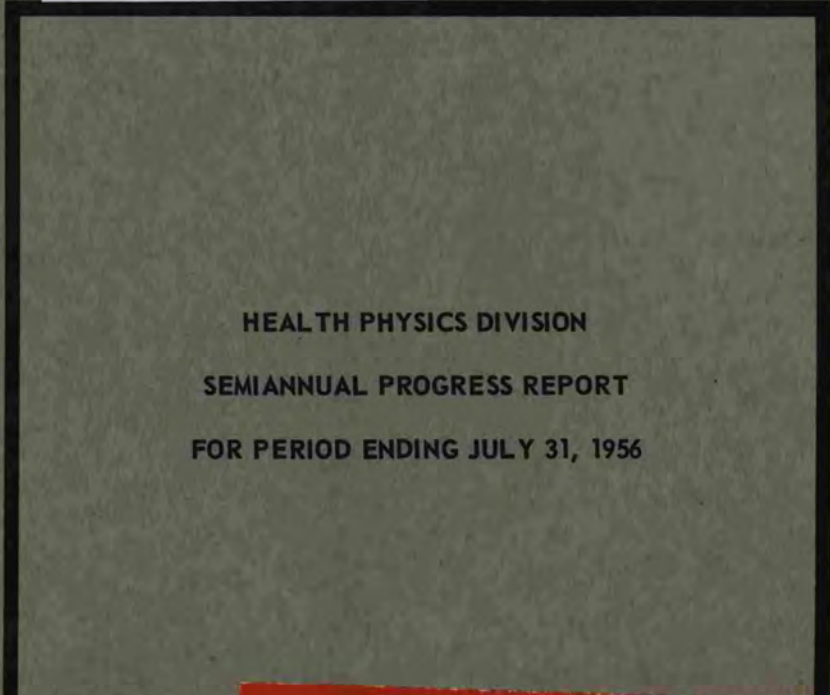
MARTIN MARIETTA ENERGY SYSTEMS LIBRARIES



3 4456 0060093 6

ORNL-2151  
Progress

*cg. 5*



HEALTH PHYSICS DIVISION  
SEMIANNUAL PROGRESS REPORT  
FOR PERIOD ENDING JULY 31, 1956



CENTRAL RESEARCH LIBRARY  
DOCUMENT COLLECTION

**LIBRARY LOAN COPY**

DO NOT TRANSFER TO ANOTHER PERSON

If you wish someone else to see this document,  
send in name with document and the library will  
arrange a loan.

OAK RIDGE NATIONAL LABORATORY

OPERATED BY

UNION CARBIDE NUCLEAR COMPANY

A Division of Union Carbide and Carbon Corporation



POST OFFICE BOX P • OAK RIDGE, TENNESSEE

UNCLASSIFIED

Printed in USA. Price 55 cents. Available from the

Office of Technical Services  
U. S. Department of Commerce  
Washington 25, D. C.

LEGAL NOTICE

This report was prepared as an account of Government sponsored work. Neither the United States, nor the Commission, nor any person acting on behalf of the Commission:

- A. Makes any warranty or representation, express or implied, with respect to the accuracy, completeness, or usefulness of the information contained in this report, or that the use of any information, apparatus, method, or process disclosed in this report may not infringe privately owned rights; or
- B. Assumes any liabilities with respect to the use of, or for damages resulting from the use of any information, apparatus, method, or process disclosed in this report.

As used in the above, "person acting on behalf of the Commission" includes any employee or contractor of the Commission to the extent that such employee or contractor prepares, handles or distributes, or provides access to, any information pursuant to his employment or contract with the Commission.

**UNCLASSIFIED**

ORNL-2151

Contract No. W-7405-eng-26

**HEALTH PHYSICS DIVISION SEMIANNUAL PROGRESS REPORT**

**For Period Ending July 31, 1956**

K. Z. Morgan, Director

DATE ISSUED

**OCT 18 1956**

---

OAK RIDGE NATIONAL LABORATORY  
Operated by  
UNION CARBIDE NUCLEAR COMPANY  
A Division of Union Carbide and Carbon Corporation  
Post Office Box P  
Oak Ridge, Tennessee



3 4456 0060093 6

**UNCLASSIFIED**

# UNCLASSIFIED

Semiannual reports previously issued by the Health Physics Division are as follows:

ORNL-1596	Period Ending July 31, 1953
ORNL-1684	Period Ending January 31, 1954
ORNL-1763	Period Ending July 31, 1954
ORNL-1860	Period Ending January 31, 1955
ORNL-1942	Period Ending July 31, 1955
ORNL-2049	Period Ending January 31, 1956

UNCLASSIFIED

ORNL-2151  
Progress

INTERNAL DISTRIBUTION

- 
1. C. E. Center
  2. Biology Library
  3. Health Physics Library
  - 4-6. Central Research Library
  7. Reactor Experimental Engineering Library
  - 8-24. Laboratory Records Department
  25. Laboratory Records, ORNL R.C.
  26. L. B. Emlet (K-25)
  27. J. P. Murray (Y-12)
  28. A. M. Weinberg
  29. J. A. Swartout
  30. E. D. Shipley
  31. E. J. Murphy
  32. M. L. Nelson
  33. K. Z. Morgan
  34. S. C. Lind
  35. A. S. Householder
  36. C. S. Harrill
  37. C. E. Winters
  38. A. H. Snell
  39. E. H. Taylor
  40. W. H. Jordan
  41. T. A. Lincoln
  42. A. Hollaender
  43. F. L. Culler
  44. D. W. Cardwell
  45. E. M. King
  46. M. T. Kelley
  47. E. E. Anderson
  48. R. S. Livingston
  49. C. P. Keim
  50. K. E. Cowser
  51. C. D. Susano
  52. L. B. Farabee
  53. F. J. Davis
  54. R. J. Morton
  55. C. E. Haynes
  56. Hugh F. Henry (K-25)
  57. E. G. Struxness
  58. W. E. Cohn
  59. H. H. Hubbell
  60. D. E. Arthur
  61. J. Neufeld
  62. D. D. Cowen
  63. P. M. Reyling
  64. G. C. Williams
  65. M. J. Skinner
  66. J. C. Hart
  67. T. H. J. Burnett
  68. W. J. Lacy
  69. B. G. Saunders
  70. G. S. Hurst
  71. T. E. Bortner
  72. J. A. Lane
  73. R. W. Johnson
  74. H. P. Yockey
  75. C. E. Clifford
  76. J. L. Gabbard
  77. R. A. Charpie
  78. G. E. Boyd
  79. S. J. Cromer
  80. L. C. Emerson (Y-12)
  81. D. M. Davis
  82. P. E. Brown
  83. E. D. Gupton
  84. J. C. Ledbetter
  85. R. L. Clark
  86. G. C. Cain
  87. L. C. Johnson
  88. W. Ogg
  89. O. D. Teague
  90. E. L. Sharp
  91. E. J. Kuna
  92. H. H. Abee
  93. C. R. Guinn
  94. A. D. Warden
  95. S. R. Bernard
  96. C. C. Sartain
  97. J. R. Muir
  98. J. A. Auxier
  99. M. F. Fair
  100. S. I. Auerbach
  101. G. W. Royster, Jr.
  102. R. R. Dickison
  103. ORNL - Y-12 Technical Library,  
Document Reference Section
  104. R. E. Yoder
  105. F. W. Sanders
  106. F. C. Maienschein
  107. W. J. Boegly, Jr.
  108. F. L. Parker

UNCLASSIFIED

# UNCLASSIFIED

109. W. E. Lotz  
110. B. Fish  
111. M. B. Edwards  
112. F. M. Empson  
113. G. G. Robeck  
114. R. D. Birkhoff

115. R. H. Ritchie  
116. J. A. Harter  
117. W. G. Stone  
118. J. S. Cheka  
119. P. N. Hensley  
120. R. W. Peelle

## EXTERNAL DISTRIBUTION

- 121. C. P. Straub, Public Health Service, Robert A. Taft Sanitary Engineering Center
- 122. R. M. Collier, University of Florida
- 123. Physics and Engineering Group, Balcones Research Center, RFD 4, Box 189, Austin, Texas
- 124. R. F. Bacher, California Institute of Technology
- 125. G. E. Thoma, USAF
- 126. H. J. McAlduff, AEC, Oak Ridge
- 127. Vanderbilt University (Physics Library)
- 128. Massachusetts Institute of Technology (Department of Electrical Engineering)
- 129. University of California (Gerhard Klein)
- 130. R. M. Richardson, U.S. Geological Survey, 2-C P. O. Building, Knoxville, Tennessee
- 131. C. V. Theis, U.S. Geological Survey, Box 433, Albuquerque, New Mexico
- 132. Lola Lyons, Librarian, Olin Industries, Inc., East Alton, Illinois
- 133. Jack Story, University of Chicago, Argonne Cancer Research Hospital, 950 East 59th Street, Chicago 37, Illinois
- 134. J. H. Ebersole, USSS Nautilus, c/o Fleet Post Office, New York, New York
- 135. David Smith, Electric Boat Division, Groton, Connecticut
- 136. Division of Research and Development, AEC, ORO
- 137. S. C. Sigoloff, USAF, The Radiobiological Laboratory, University of Texas and U.S. Air Force, Austin, Texas
- 138. Robert Wood, Department of Physics, Memorial Center, 444 E. 68th St., New York 21, New York
- 139-735. Given distribution as shown in TID 4500 (12th ed.) under Health and Biology category (200 copies - OTS)

DISTRIBUTION PAGE TO BE REMOVED IF REPORT IS GIVEN PUBLIC DISTRIBUTION

# UNCLASSIFIED

# UNCLASSIFIED

## CONTENTS

APPLIED RADIOBIOLOGY .....	1
Distribution and Excretion of Uranium in Man .....	1
Radiochemical Analysis .....	12
Distribution of Radioisotopes in Animal Tissue .....	12
Isotopic Distribution in Man .....	16
Ecology .....	16
SANITARY ENGINEERING RESEARCH .....	26
Field Investigations .....	26
Airborne-Radioactivity Studies .....	32
Chemistry and Soils Engineering .....	35
RADIATION DOSIMETRY .....	43
Experimental Physics of Dosimetry .....	43
Theoretical Physics of Dosimetry .....	57
Dosimetry Applications .....	64
EDUCATION, TRAINING, AND CONSULTATION .....	94
PUBLICATIONS .....	95
PAPERS .....	97
LECTURES .....	98

UNCLASSIFIED

# UNCLASSIFIED

## HEALTH PHYSICS DIVISION SEMIANNUAL PROGRESS REPORT

### APPLIED RADIOBIOLOGY

E. G. Struxness

#### DISTRIBUTION AND EXCRETION OF URANIUM IN MAN

S. R. Bernard	N. L. Gillum
G. J. Dodson	W. E. Lotz
M. B. Edwards	K. K. McDaniel
B. R. Fish	J. R. Muir
G. W. Royster, Jr.	

#### Application of Power Law to Excretion Data

The power law of excretion has been applied to the uranium excretion measurements made upon the brain tumor patients. The best fitting power function for the excretion was found by least squares to be  $\%/hr = 34.3 t^{-1.5}$ . A graph of this function plotted together with the excretion measurements appears in Fig. 1. The measurements made in the first 10 hr were omitted from the least-square calculation. Also omitted were the rate measurements on patients VII and VIII, since these patients were administered uranium compounds in the tetravalent state, while the others were injected with hexavalent compounds. Since tetravalent uranium, when injected into patients, shows a different excretion pattern, this omission is justified.

Some points of physiological interest can be noted in Fig. 1. Urinary excretion rates for patients IV, V, VI, VII, and VIII, measured immediately after injection of uranium, are noted to increase, rising to a maximum in about 3 to 5 hr and then decreasing. Patients I, II, and III do not increase; on the other hand, patients VII and VIII show a pronounced increase. This phenomenon correlates with the mass of uranium injected into the patients; patients I, II, and III received low doses, approximately 4 mg of uranium, while the others were administered larger doses.

For purposes of comparison, the urinary excretion data for six patients injected with  $UO_2(NO_3)_2 \cdot 6H_2O$  at the University of Rochester<sup>1</sup> have been plotted, and the best fitting power function for the ex-

cretion rate was found to be  $\%/hr = 57.2 t^{-1.8}$ , slightly different from that found for the Boston patients,  $\%/hr = 34.3 t^{-1.5}$ . Figure 2 shows the graph of the power function and excretion measurements for the Rochester patients. Rochester patient VI received a second injection, but the measurements of this excretion were not included in the computation. Also omitted from the calculations were those measurements in the first 10 hr.

These power function equations and the data have been submitted to the subcommittee<sup>2</sup> investigating the applicability of the power law to the calculation of maximum permissible concentrations.

#### Inhalation of Uranium Aerosols by Dogs

The past six months have been devoted to design of inhalation apparatus by which uranium aerosols could be generated and delivered quantitatively to experimental animals (dogs). This has involved the design and construction of (1) an aerosol generator, (2) a reservoir in which the dust is stored and from which the animal breathes, and (3) a suitable breathing apparatus (valve and mask). This equipment is shown in Figs. 3 and 4.

Uranium, being highly pyrophoric, lends itself readily to the production of aerosols through burning in the presence of oxygen. This being the case, a flask was designed which contained an electric furnace and an  $O_2$  inlet, permitting the flow of oxygen into a partial vacuum of 40–45 cm of mercury, Fig. 3.

From the generator the aerosol is transferred to a polyethylene bag which acts as reservoir from which the dog breathes a mixture of air and uranium dust. The reservoir consists essentially of two components: (1) a steel drum with 18-gage walls and  $\frac{1}{2}$ -in. Lucite ends, and (2) a collapsible polyethylene bag. The steel wall safely permits the production of a partial vacuum of approximately 50 cm of mercury, which is essential in the transfer process, while the Lucite ends permit visual observation of the filling and exhaustion of the

<sup>1</sup>S. H. Bassett et al., *The Excretion of Hexavalent Uranium Following Intravenous Administration. II. Studies on Human Subjects*, UR-37 (July 19, 1948).

<sup>2</sup>A special subcommittee, appointed by K. Z. Morgan and consisting of W. H. Langham, W. S. Snyder, A. M. Brues, and J. Healy.

# UNCLASSIFIED

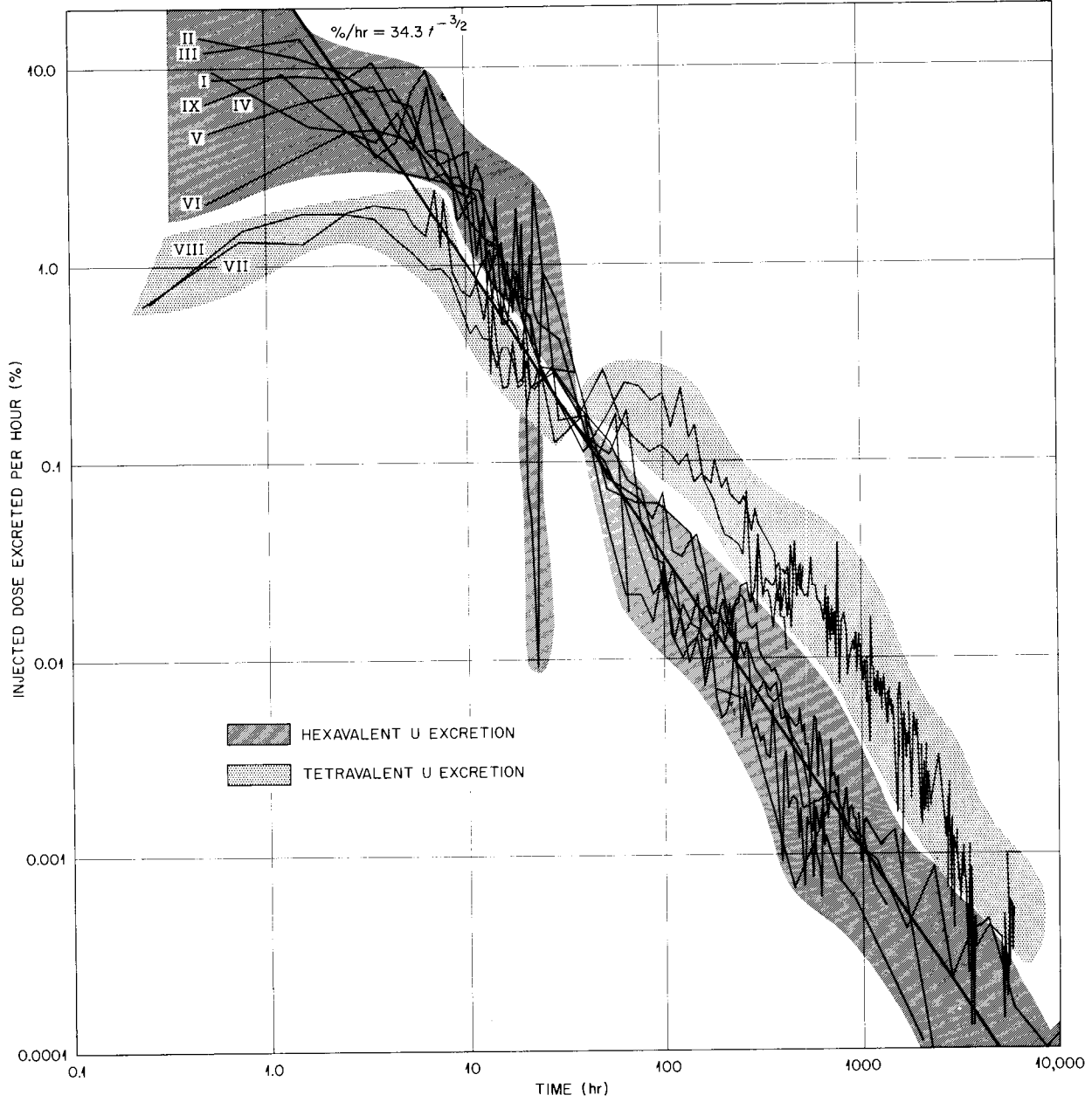


Fig. 1. Distribution and Excretion of Uranium in Man.

UNCLASSIFIED  
ORNL-LR-DWG 14395

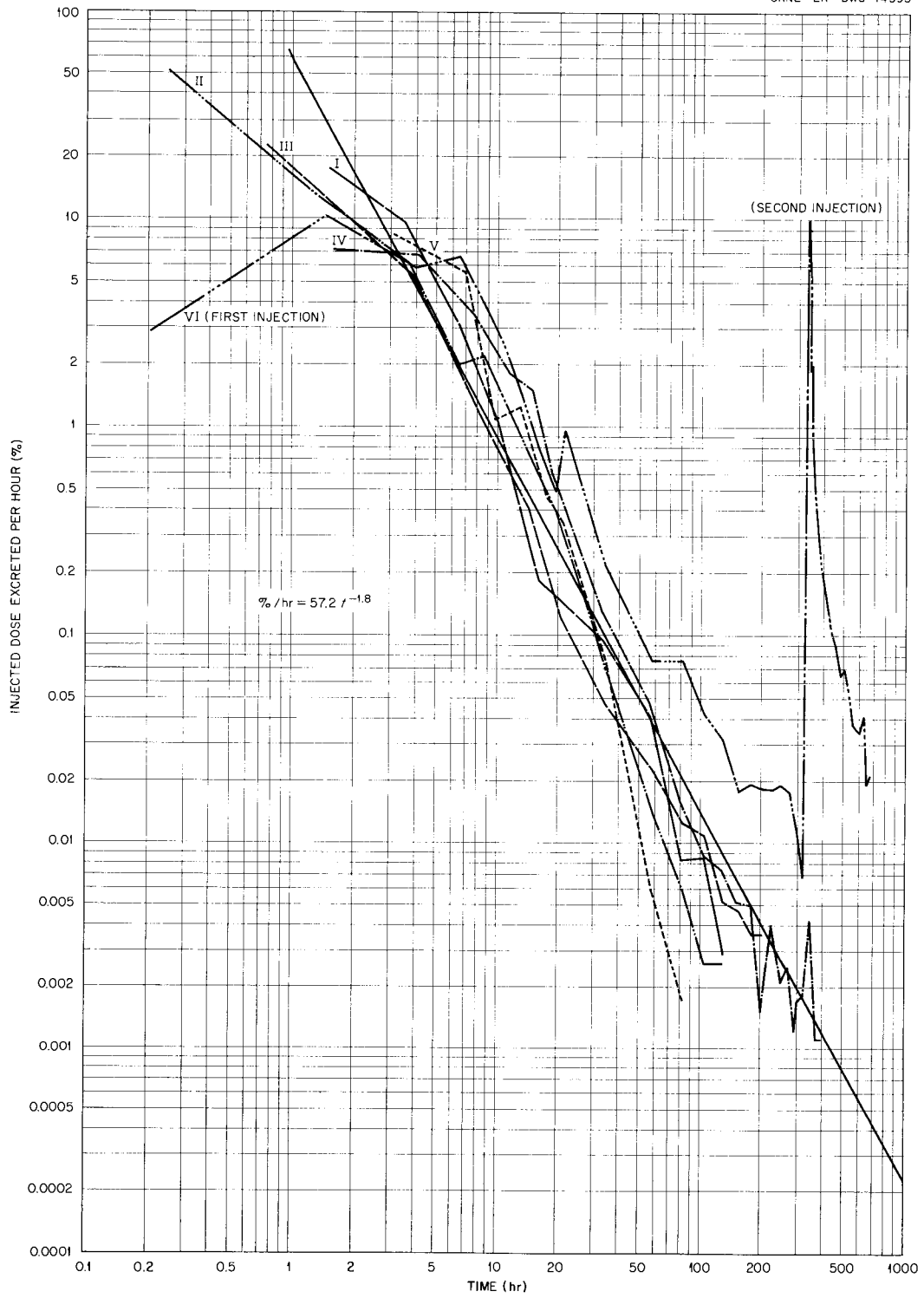


Fig. 2. Urinary Rate of Excretion for Six Patients at the University of Rochester After Intravenous Injection (from S. H. Basset et al.).

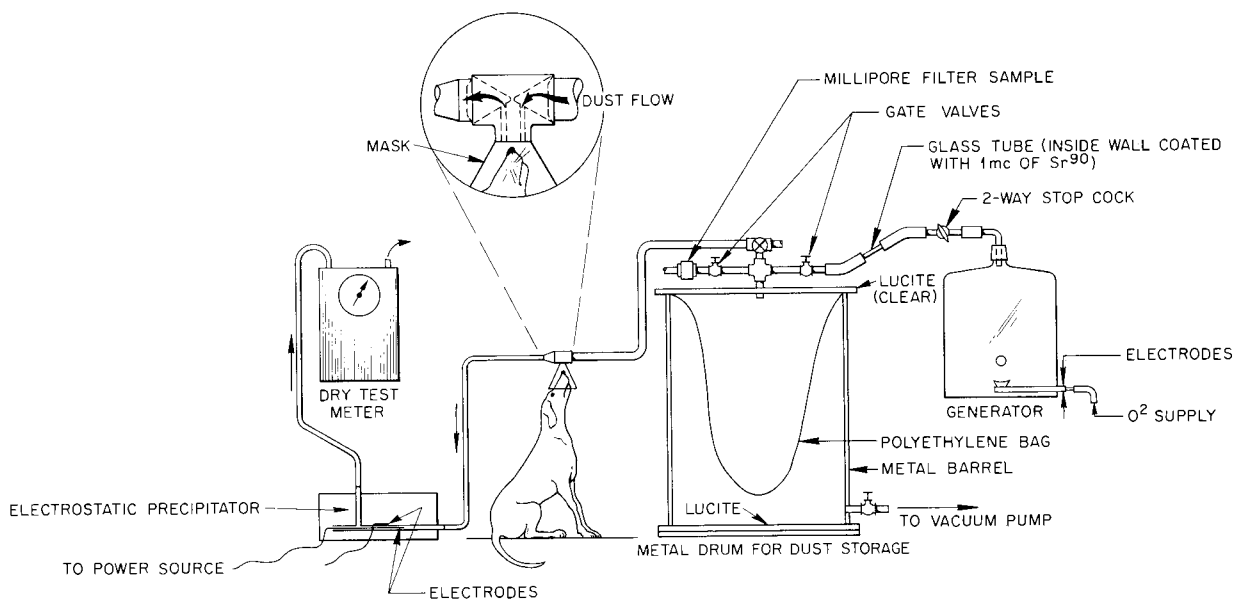


Fig. 3. Schematic Drawing of Inhalation Apparatus.

bag. The collapsible polyethylene bag permits a relatively constant concentration of dust and air, thus avoiding dilution and, therefore, facilitating the determination of the amount of inspired aerosol. The reservoir is pictured in Figs. 3 and 4.

The design of the valve and mask was obtained from the Chemical Warfare Laboratories of the Army Chemical Center. The valve housing was constructed of stainless steel to facilitate recovery, for quantitative purposes, of the residual uranium dust by washing with dilute nitric acid. The valve and mask are pictured also in Figs. 3 and 4.

Salvaged uranium chips at product levels of enrichment are burned in the furnace with an efficiency of 7–10% (ratio of total activity in the bag to total activity in the metal burned), producing an aerosol suitable for inhalation.

Electron photomicrographs of initial burnings show that the aerosol particles have a tendency to form chains of a mean size of  $2.22 \mu$ , Fig. 5. Very few particles of this mean size will enter the lungs of the dog, therefore it was necessary to prevent the formation of such chains. Investigation showed that the presence of a source of  $\beta$  radiation prevented the formation of such chains. A  $1\text{-}\mu\text{c}$  source of  $\text{Sr}^{90}$  was placed in the generator

and a  $1\text{-}\mu\text{c}$  source was placed also in the hose connecting the generator to the reservoir. This resulted in particles of uranium with a mean size of  $0.36 \mu$  (Fig. 6). These sources were plated as thin dry films and therefore do not contaminate the aerosol with  $\text{Sr}^{90}$ .

Electron diffraction studies of the aerosol deposits have shown the uranium to be in the form of the oxide,  $\text{U}_3\text{O}_8$ .

The following procedures are followed in the use of the equipment:

1. The polyethylene bag is completely deflated and closed to the outside atmosphere.
2. The steel drum is then partially exhausted to 40–45 cm of mercury.
3. A known weight of uranium metal is then introduced into the aerosol generator.
4. The generator is then exhausted by opening the gate valve (Fig. 3) between the generator and polyethylene bag. This results in the formation of a vacuum approximately equal to that within the drum.
5. The uranium chips are heated to glowing in the furnace, at which time  $\text{O}_2$  is allowed to flow over the chips. The combination of heat plus oxygen causes the uranium to ignite violently (analogous to the explosion of a photoflash bulb),

UNCLASSIFIED  
PHOTO 26626

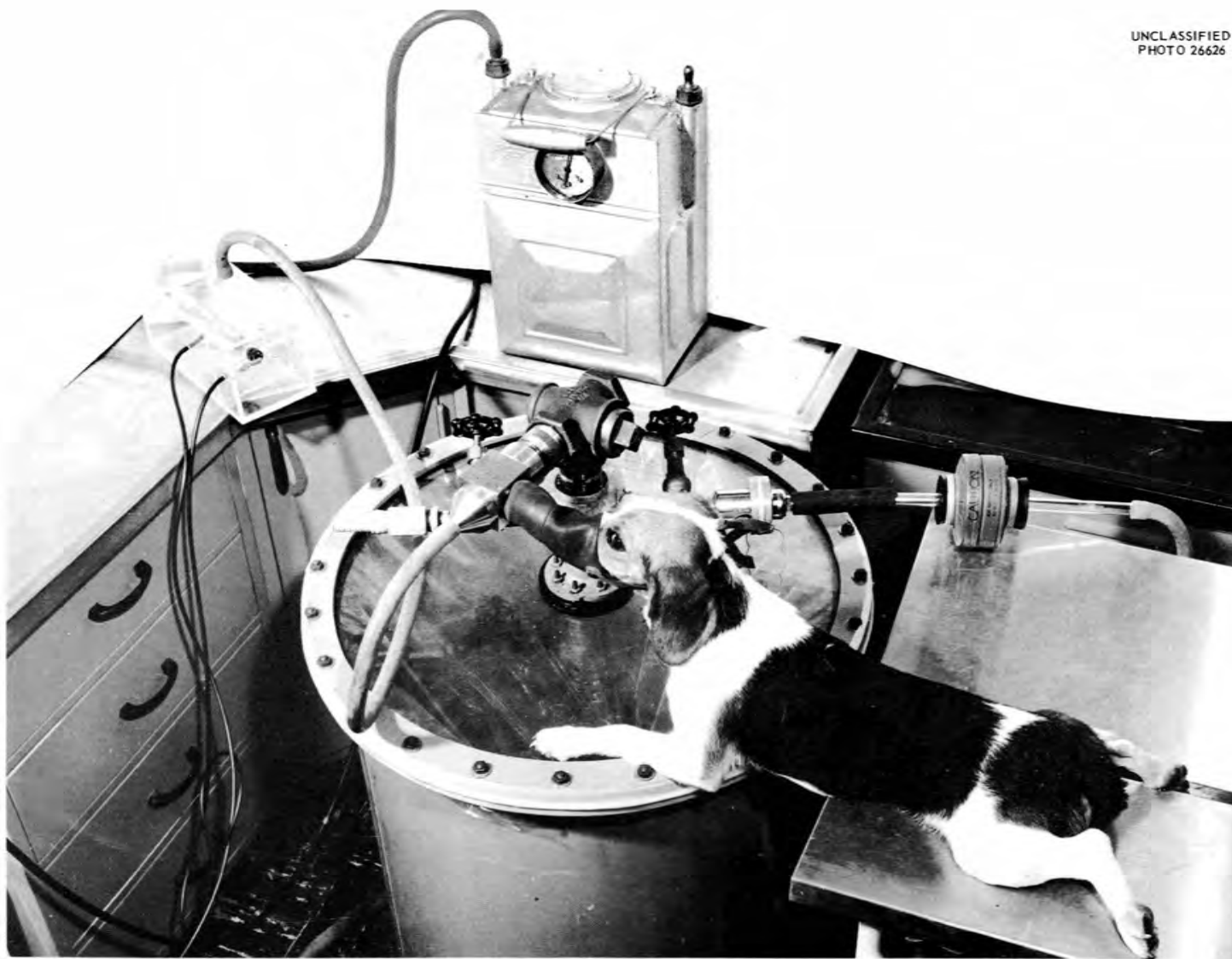


Fig. 4. Dog Breathing from the Aerosol Reservoir.

PERIOD ENDING JULY 31, 1956

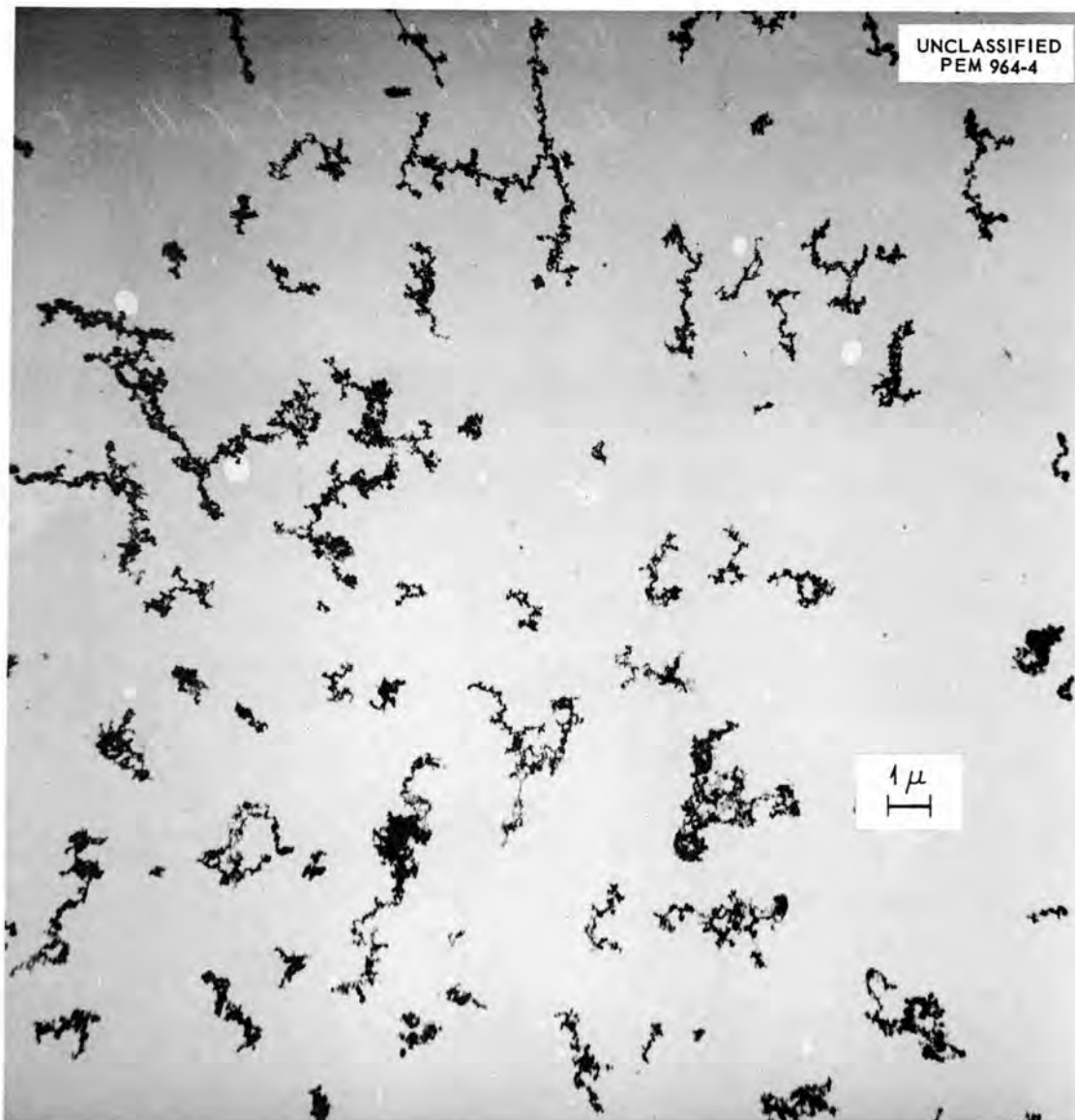


Fig. 5. Electron Photomicrograph of Aerosol Particles, Which Shows Chaining Effect. Mean chain size = 2.22  $\mu$ .

which results in the formation of the aerosol. In addition to supporting combustion, the flow of  $O_2$  tends to dilute rapidly the aerosol and to cause it to flow into the polyethylene bag.

6. The bulk of the aerosol transfer is effected by opening the aerosol generator to the outside atmosphere. This results in a rapid flow of air through the generator and into the bag, with resultant flushing of the generator and transfer of the aerosol.

7. The gate valve is again closed, isolating the contents of the polyethylene bag.

8. The dog is then attached to the bag assembly by means of a face mask and a three-way valve, Fig. 4. The valve arrangement permits the dog to breathe atmospheric air while periodic millipore samples are being taken for quantitative purposes. The capacity of the bag (150 liters) sustains the dog's normal breathing for 20-30 min. The state of the bag can be observed continuously, which

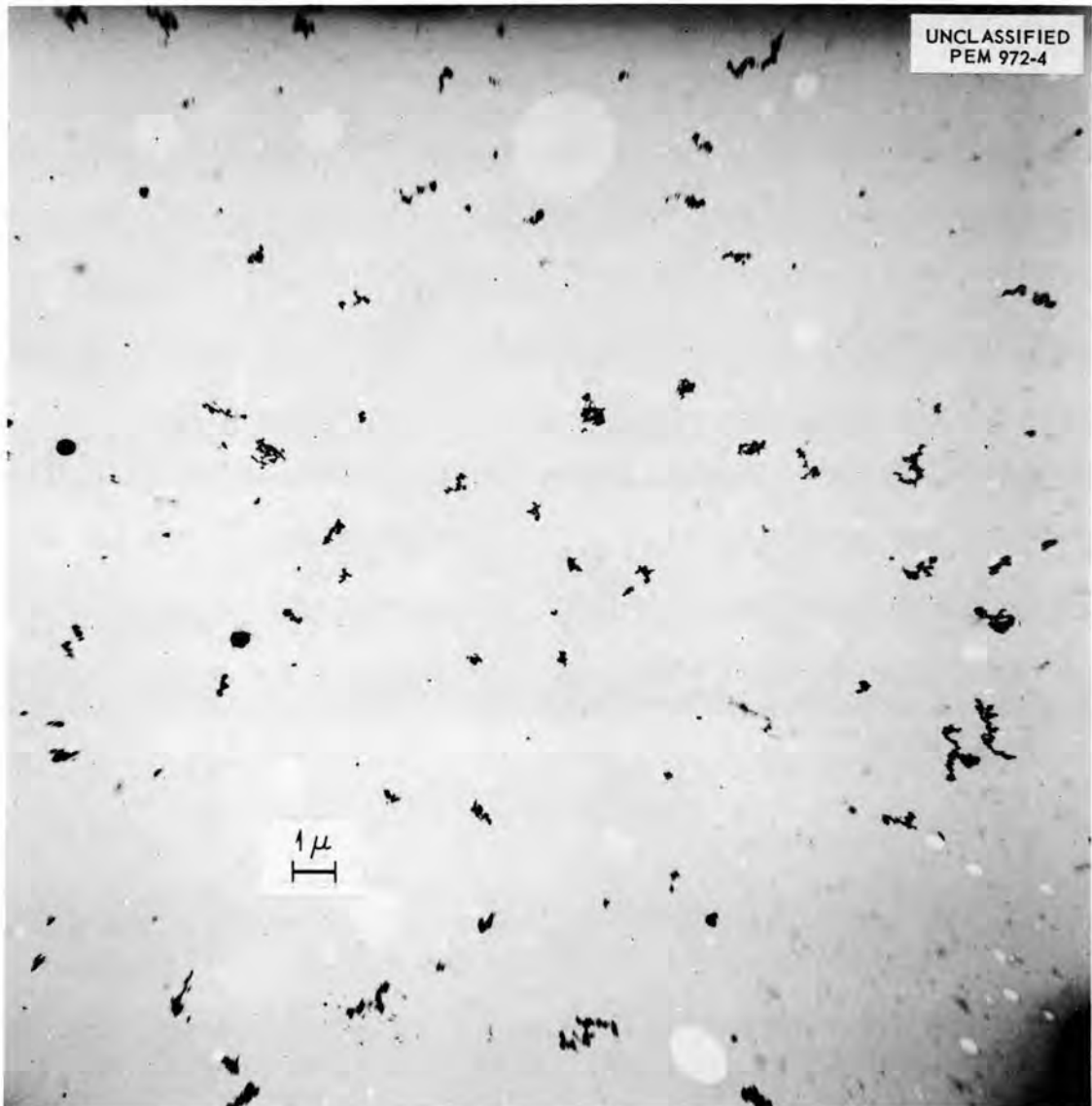


**Fig. 6. Electron Photomicrograph of Aerosol Particles, Which Demonstrates the Effect of a  $\beta$ -Emitting Source upon Chain Formation. Mean particle size =  $0.36 \mu$ .**

prevents asphyxiation of the animal resulting from abnormally heavy or rapid breathing.

The total amount of air breathed by the dog during the exposure is measured by passing the expired (effluent) air through a dry test meter, Figs. 3 and 4. Samples of dust from the reservoir are collected periodically on millipore filters, that is, immediately before permitting the dog to breathe from the bag, every 10 min thereafter, and at the termination of the exposure period. The sampling rate approximates the breathing rate of

the dog (3 liters per minute), thus the sample period of 1 min gives a total of three liters per sample.

The values of activity per liter (disintegrations per minute per liter) are plotted against the volume of air the dog breathes. The area beneath the curve gives the amount of activity which the dog inhaled. An electrostatic precipitator collects the aerosol in the effluent (expired air). This amount, plus the residual uranium recovered by washing all inlet and outlet hose and the mask and valve

assembly, when subtracted from the calculated amount of radioactive aerosol the dog was exposed to, gives the amount of uranium aerosol retained by the dog.

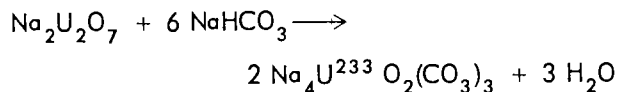
Quantitative tests are now being performed on the equipment by exposing mongrel dogs to uranium aerosols. The exposed dogs are sacrificed at designated intervals and analyses are made of the body organs in order to check between the calculated retained dose and that amount actually recovered from the dog's organs. Where the time interval between exposure and sacrifice is sufficiently long, urinary and fecal collections are made and analyses of the uranium content of the excreta are carried out.

### Blood-CSF Barrier Studies

It is known that some cations and some anions may penetrate the blood-cerebrospinal-fluid (CSF) barrier to a greater extent than others. With this in mind, an attempt has been made to find a uranium compound which might show a preferential disposition to penetrate the blood-CSF barrier.

The first chemical compound investigated<sup>3</sup> was sodium uranyl tricarbonate,  $\text{Na}_4\text{UO}_2(\text{CO}_3)_3$ .

The sodium uranyl tricarbonate compound was prepared with  $\text{U}^{233}$  according to the following stoichiometric equation:



Two dogs were used in a pilot experiment to test the differences, if any, between the anionic form, uranyl tricarbonate, and the cationic form, uranyl nitrate, with reference to the rates of removal from the blood and to the uptake and subsequent decline in the cerebral spinal fluid and in the urine. One dog was injected with uranyl tricarbonate,  $\text{Na}_4\text{UO}_2(\text{CO}_3)_3$ , and the other with uranyl nitrate,  $\text{UO}_2(\text{NO}_3)_2$ , care being taken to give an equal mass of uranium.

Blood, CSF, and urine samples were obtained at intervals, and analyses were made by standard radiochemical procedures. The blood was taken by vein puncture of the cephalic vein, the CSF was obtained by puncture of the cisterna magna, and the urine via catheterization.

<sup>3</sup>C. A. Blake et al., *Studies in the Carbonate-Uranium System; Part I. Investigation in the Four Component System  $\text{UO}_3 \cdot \text{Na}_2\text{O} \cdot \text{CO}_2 \cdot \text{H}_2\text{O}$* , AECD-3280 (Dec. 14, 1950).

Figures 7, 8, 9, and 10 give a comparison of the two compounds and show the disappearance in blood and CSF and the buildup and rate of excretion in the urine.

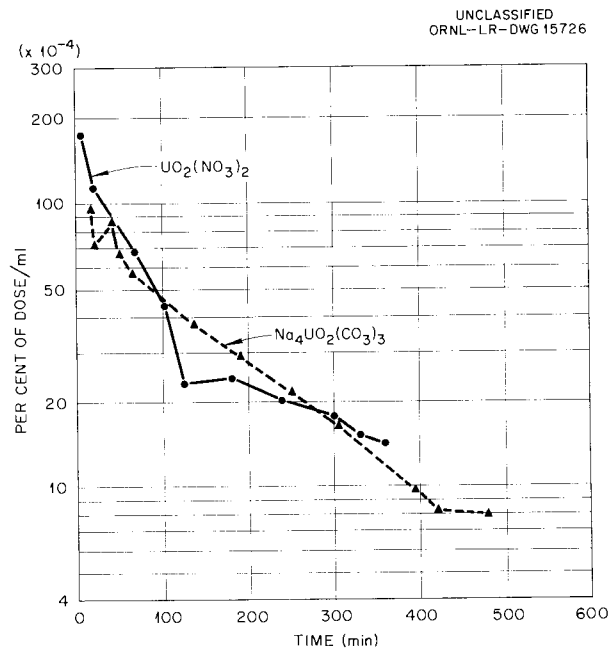


Fig. 7. Per Cent of Dose in Blood for Two Dogs After Intravenous Injection of Sodium Uranyl Tricarbonate in One and Uranyl Nitrate in the Other.

From Fig. 8 it may be noted that the disappearance from the CSF was more rapid for uranyl tricarbonate anion than for uranyl cation.

Further experiments must be carried out with additional dogs to substantiate (statistically) this difference. If this difference proves to be real, further work will be carried out in tumor-bearing rats to ascertain whether this disappearance from the CSF is reflected by a differential uptake between normal and tumorous brain tissue-implants.

### Application of the Analog Computer to Distribution and Excretion Models

Preliminary investigations in testing the application of analog computing equipment to direct simulation of various biological models for the distribution and excretion of U(VI) have been completed. With the help of E. R. Mann, F. P. Green, and R. S. Stone (ORNL Instrumentation and Controls Division) the Reactor Controls analog

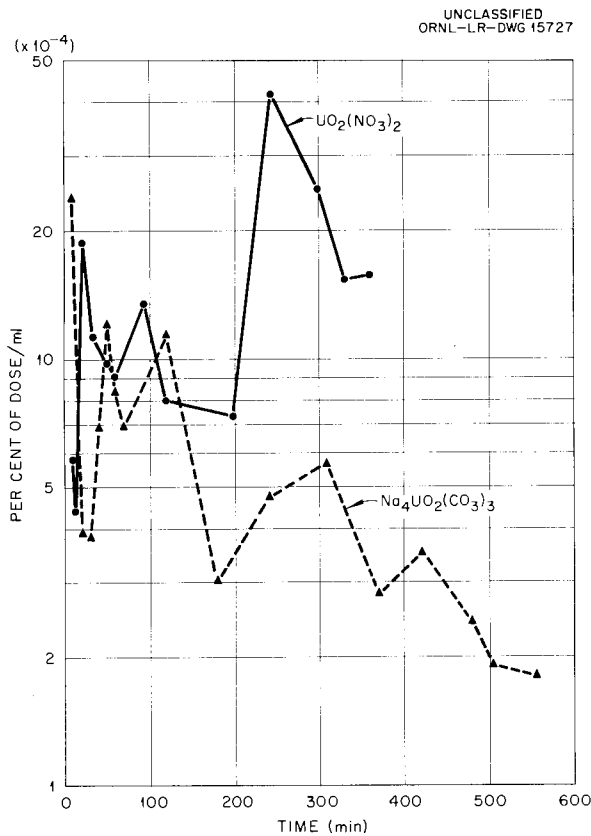


**Fig. 8. Per Cent of Dose in Cerebrospinal Fluid for Two Dogs After Intravenous Injection of Sodium Uranyl Tricarbonate in One and Uranyl Nitrate in the Other.**

facility was used in this study. The "four compartment model"<sup>4</sup> was simulated on the computer. The set of curves shown in Fig. 11 illustrates the simulator response to a single injection as compared to the male rat data reported by Newman.<sup>5</sup> The response to an arbitrary input function has been tested also and a method has been attempted whereby the input function might be derived from a set of output (urine excretion) data. The results showed considerable promise for a future study which is under consideration.

Although the simple model gives results in reasonable agreement with animal data, a somewhat more complex arrangement seems to be necessary

<sup>4</sup>S. R. Bernard *et al.*, *HP Semiann. Prog. Rep.* Jan. 31, 1955, ORNL-1860, p 1.

<sup>5</sup>C. Voegtlin and H. C. Hodge (eds.), *Pharmacology and Toxicology of Uranium Compounds*, Chapter 11, McGraw-Hill, New York, 1949.

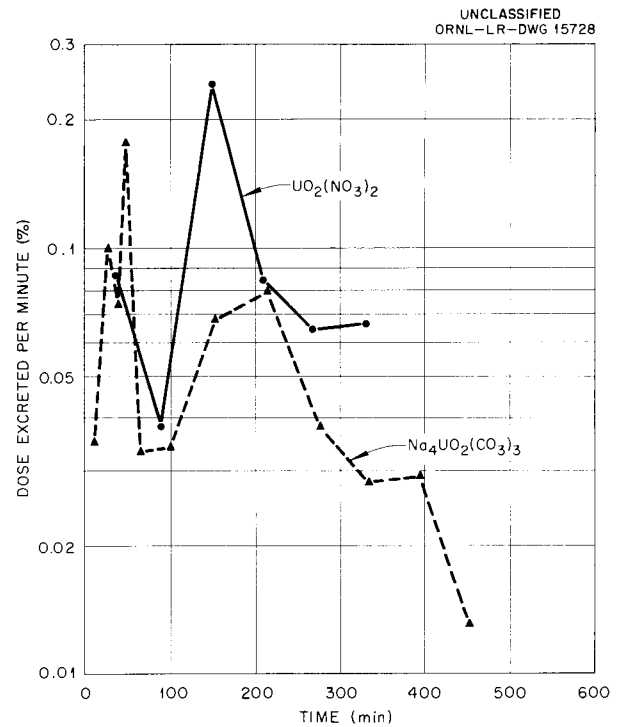
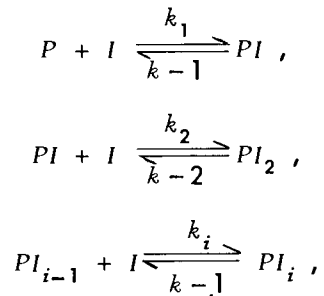


**Fig. 9. Urinary Rate of Excretion for Two Dogs After Intravenous Injection of Sodium Uranyl Tricarbonate in One and Uranyl Nitrate in the Other.**

to follow the response indicated by human data. An attempt has been made to incorporate the concept of the diffusible and nondiffusible complex of uranium in the blood stream. The paradigm of ion-protein interaction discussed by Klotz<sup>6</sup> appears to offer some promise for application to the model for distribution and excretion. Klotz writes a system of reversible second order reactions to describe how ions are bound to a protein molecule. The reactions are



where  $P$  is a molecule of protein and  $I$  is an ion.

<sup>6</sup>I. M. Klotz, "The Nature of Some Ion-Protein Complexes," *Cold Spring Harbor Symposia Quant. Biol.*, Vol. XIV, p 97-112 (1950).

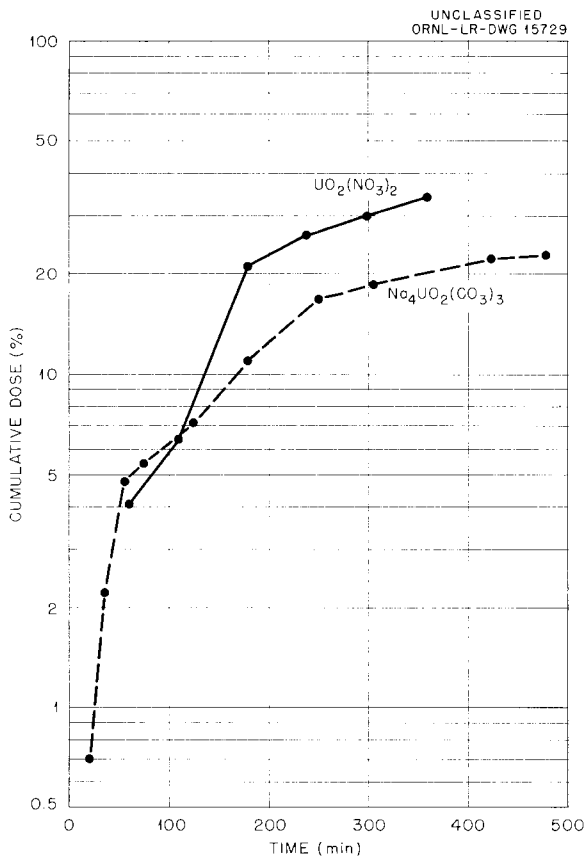


Fig. 10. Cumulative Per Cent of Dose in Urine for Two Dogs Following Intravenous Injection of Sodium Uranyl Tricarbonate in One and Uranyl Nitrate in the Other.

The  $k$ 's are velocity constants which are related to equilibrium constants  $K$  in the usual manner

$$K_1 = \frac{(PI)}{(P)(I)} = \frac{k_1}{k-1}$$

$$K_2 = \frac{(PI_2)}{(PI)(I)} = \frac{k_2}{k-2}, \text{ etc.}$$

In application to our model we consider a protein bound ion to be a nondiffusible type while ions not bound to protein are the diffusible type. To incorporate this scheme of chemical reactions in the model,  $S_1$  is denoted as the amount of diffusible complex present in site  $S_1$ , the blood stream. Let  $S_{1ni}$  be the amount of protein to which are

bound  $i$  ions, which species is also present in site  $S_1$ . Thus, the differential equations for site  $S_1$ , the blood stream, are

$$(1) \dot{S}_1 = \lambda_2 S_2 + \left( \sum_{i=1}^n k_{-i} S_{1ni} - S_1 \sum_{i=1}^n k_{i-1} S_{1ni} \right) - \lambda_1 S_1$$

$$(2) \dot{S}_{1nj} = S_1 \left[ k_j S_{1n(j-1)} - k_{(j+1)} S_{1n(j+1)} \right] + \left[ k_{-(j+1)} S_{1n(j+1)} - k_{-j} S_{1nj} \right]$$

$$j = 1, 2, 3, \dots, n.$$

When all  $\dot{S}_{1nj} = 0$  the summations appearing within parentheses in Eq. 1 cancel each other and the original differential equation for the blood stream is recovered.

The effect of the inclusion of these second order chemical reactions is examined by taking a special case  $n = 2$  and  $\dot{S}_{1n1} = 0$ . Thus, concern is with, at most, two uranyl ions bound to the protein  $P$ . By letting  $\dot{S}_{1n1}$  go to zero,  $S_{1n1}$ , the amount of complex of the type  $PI$ , is required to be zero. Furthermore, by the law of mass action, this dictates that  $k_1 S_1 S_{1no} = k_{-1} S_{1n1}$ . The system of equations then becomes:

$$(3) \dot{S}_1 = \lambda_2 S_2 + k_{-2} S_{1n2} - \left( \frac{k_1 k_2}{k-1} \right) S_{1no} S_1^2 - \lambda_1 S_1,$$

$$(4) \dot{S}_{1ni} = 0,$$

$$(5) \dot{S}_{1n2} = \left( \frac{k_1 k_2}{k-1} \right) S_{1no} S_1^2 - k_{-2} S_{1n2}.$$

Furthermore, it is required that  $S_{1no}$ , the amount of protein  $P$  in the system, be constant. Equations 3 and 5 can be handled as a simultaneous system.

UNCLASSIFIED  
ORNL-LR-DWG 45730

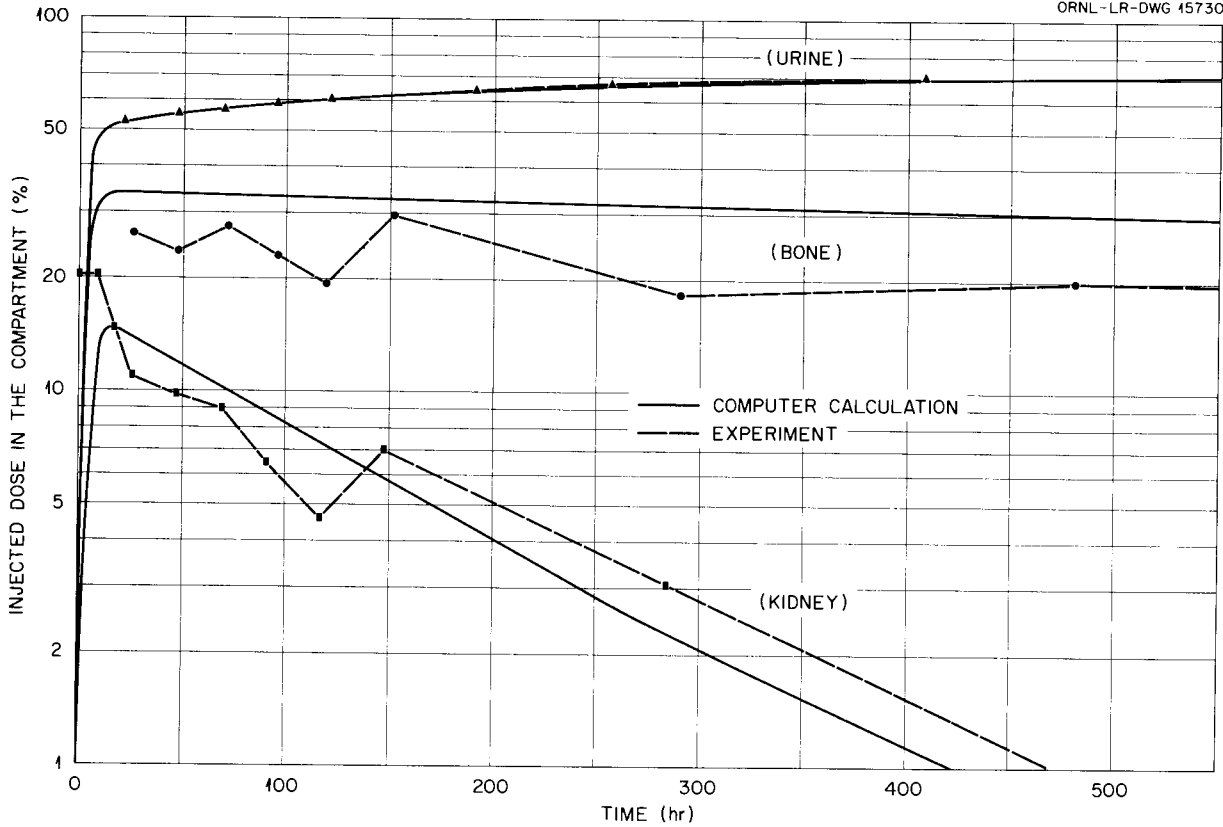


Fig. 11. A Comparison Between the Male Rat Data of Newman and Analog Computer Calculations.

After elimination of the  $S_2$  and  $S_{1n2}$  terms the following is obtained:

$$(6) \quad \overset{\dots}{S}_1 + (k_{-2} + \lambda_1 + \lambda_2) \overset{\dots}{S}_1 + [(1-f)\lambda_1\lambda_2 + k_{-2}(\lambda_1 + \lambda_2)] \overset{\cdot}{S}_1 + (1-f)\lambda_1\lambda_2 k_{-2} = -K'_2 [S_1 \overset{\dots}{S}_1 + (\lambda_2 S_1 + \overset{\cdot}{S}_1) \overset{\cdot}{S}_1] .$$

This is a third order, nonlinear differential equation that can be solved by perturbation methods, assuming

$$K'_2 = \left( \frac{k_1 k_2 S_{1no}}{k-2} \right)$$

to be small and the solution to be in the form

$$(7) \quad S_1 = f_1 + K'_2 f_2 + K'^2_2 f_3 + \dots$$

Since  $K'_2$  is small, the  $K'^2_2, K'^3_2$  terms are smaller still, and, hence, they are omitted. When this

method is used, the solution for  $S_1$  is

$$(8) \quad S_1 = \sum_{i=1}^3 C_i e^{-r_i t} + K'_2 \left( \sum_{i=1}^3 C'_i e^{-r_i t} \right)^2$$

where  $r_i$ 's are roots of the characteristic equation

$$(9) \quad r^3 + (\lambda_1 + \lambda_2 + k_{-2})r^2 + [(1-f)\lambda_1\lambda_2 + k_{-2}(\lambda_1 + \lambda_2)]r + (1-f)\lambda_1\lambda_2 k_{-2} = 0$$

and the  $C$ 's are arbitrary constants of integration.

After the solution for  $S_1$  is obtained,  $S_{1n2}$ ,  $S_2$ , etc. can be solved in turn. These solutions are not shown here. It should be pointed out that, by including one second order reaction describing the interaction of ionic uranium in blood with a molecule of protein and solving this system, the number of exponential terms describing the disappearance of uranium from the  $S_1$  compartment is increased. Obviously, this maneuver results in an equation which will yield a closer fit to the data, and, at the same time, it permits some possibilities for extrapolating to physiological mechanisms. In addition, the inclusion of this scheme of reactions permits some considerations of measurements of  $K$ 's, in vitro, which can be substituted into the kinetic equations for distribution and excretion of uranium. Further work is being done along this line.

#### Digital Computer

The initial work has begun in an attempt to adapt the Garwood method of curve-fitting to the analysis of distribution and excretion data. The program which has been written for the Oracle is presently being debugged and improved.

#### RADIOCHEMICAL ANALYSIS

L. B. Farabee

An analytical procedure has been developed for the determination of radioactive cesium in muscle tissue of fish. This procedure is simple in operation and the separation from other fission products and  $K^{40}$  is good. No radiochemical yield determination is necessary since the recovery is about 97%. Hazardous reagents such as perchloric acid are not required. As much as 10 g of fish muscle can be used in an analysis.

The analysis of radioactive cesium in solutions of long lived fission products by phosphotungstate precipitation has been studied by Mizzan.<sup>7</sup> The precipitation of cesium phosphotungstate is used as one step in this procedure. This precipitation is made from a 5N nitric acid solution and provides good decontamination from other fission products. Both cesium and potassium are precipitated quantitatively as the cobaltinitrite from a dilute acetic acid solution in the presence of an excess of reagent. This precipitation can be used as a means of concentrating these elements from the

<sup>7</sup>E. Mizzan, *Phosphotungstate Precipitation Method of Analysis of Radioactive Cesium in Solutions of Long Lived Fission Product Activities*, PDB-128 (July 1954).

large amount of inorganic residue in a 10 g muscle sample. Also it can be used as the final precipitation to facilitate the transfer of the cesium sample to a counting dish.

The essential steps in the procedure are: (1) oxidize the organic material by heating the sample in nitric acid and 30% hydrogen peroxide, (2) transfer the solution of the sample to a centrifuge tube and adjust the pH to 5, (3) add 10 mg of cesium carrier and precipitate the cesium and potassium as the cobaltinitrite by the addition of 10 ml of sodium cobaltinitrite reagent (57.2 g of cobaltous nitrate in 100 ml glacial acetic acid and water to make one liter; dissolve 360 g sodium nitrite in water and dilute to one liter; mix equal volumes and filter prior to use), let stand for 2 hr or longer and centrifuge, (4) add 1.5 ml of concentrated  $HNO_3$  and heat to dissolve the precipitate; add 12 ml of 5 N  $HNO_3$  and 2 ml of 0.05 M phosphotungstic acid; let stand for 10 min and centrifuge; wash the precipitate two times with 5 N  $HNO_3$ , (5) dissolve the cesium phosphotungstate in a minimum of 1 N NaOH; build the volume to 10 ml with water and adjust the pH to 5 (green color with bromcresol green); add 3 drops of glacial acetic acid and 5 ml of sodium nitrite; let stand for 1 hr and centrifuge; wash the precipitate one time with water, and (6) add 0.3 ml concentrated  $HNO_3$  and heat to dissolve the precipitate. Transfer the solution to a stainless steel dish and dry under a heat lamp.

By this procedure, the recovery of  $Cs^{137}$  tracer added to a 10-g fish muscle sample in 15 individual analyses was  $97.7 \pm 0.5\%$ . The separation from other beta-emitting fission products gave a decontamination factor of  $8 \times 10^3$ . The separation from  $K^{40}$  was good. This procedure can be applied to the analysis of cesium in soils, urine, and other forms of biological materials.

#### DISTRIBUTION OF RADIOISOTOPES IN ANIMAL TISSUE

M. J. Cook                      F. G. Karioris<sup>8</sup>  
K. Z. Morgan

The mathematical relations listed in publications by the National Committee on Radiation Protection<sup>9</sup>

<sup>8</sup>Summer research participant from Physics Department, Marquette University, Milwaukee, Wisconsin.

<sup>9</sup>United States National Bureau of Standards, *Maximum Permissible Amounts of Radioisotopes in the Human Body and Maximum Permissible Concentrations in Air and Water*, Handbook 53 (1953), Superintendent of Documents, Washington, D.C.

and the International Commission of Radiological Protection<sup>10</sup> and used to compute the maximum permissible concentration (MPC) of radionuclides in air and water for continuous exposure are based primarily on single exposure animal data. The biophysical factors  $f_w$  (fraction of the ingested amount that reaches the critical organ) and  $T_b$  (biological half life) are determined by extrapolation of the single exposure data, assuming exponential decay. Assuming continuous ingestion, a build-up curve can be derived of the form

$$(1) \quad qf_2 = \frac{CRTf_w}{0.693} (1 - e^{-0.693 t/T}) ,$$

where

$q$  =  $\mu\text{c}$  in total body,

$qf_2$  =  $\mu\text{c}$  in the organ studied,

$C$  = concentration of radioisotope in water ( $\mu\text{c}/\text{ml}$ ),

$R$  = rate of water intake ( $\text{ml}/\text{day}$ ),

$T$  = effective half life in days =  $\frac{T_b T_r}{T_b + T_r}$ ,

$T_b$  = biological half life,

$T_r$  = radioactive half life,

$f_w$  = fraction of the radioisotope that reaches the organ after ingestion.

A preliminary study with  $\text{Co}^{60}$  indicated that the mathematical relations used in the handbooks on internal dose are correct within a factor of 2 for this radionuclide.<sup>11</sup>

For the bone-seeker  $\text{Sr}^{90} + \text{Y}^{90}$ , a biological half life of greater than 200 days in the rat has been reported on the basis of single exposure data.<sup>12</sup> Chronic feeding of contaminated food to mice indicates that the bone burden is proportional to the concentration of  $\text{Sr}^{90} + \text{Y}^{90}$  in the food and that the bone burden accumulation curve reaches a plateau within 77 days.<sup>13</sup> Since, in general, a rapid equilibration is not consistent with a long biological half life, a study with mice was initiated to check the handbook relationships for  $\text{Sr}^{90} + \text{Y}^{90}$ .

<sup>10</sup>International Congress of Radiology, "Recommendations of International Commission of Radiological Protection," *Brit. J. Radiol. Supp.* 6: 23-59 (1955).

<sup>11</sup>M. J. Cook, K. Z. Morgan, and A. G. Barkow, *Am. J. Roentgenol., Radium Therapy Nuclear Med.* 75, 1177-1187 (1956).

<sup>12</sup>J. G. Hamilton, *Rev. Mod. Phys.* 20, 718-728 (1948).

<sup>13</sup>W. J. Gross, J. F. Taylor, and J. C. Watson. *Some Factors Influencing the Metabolism of Radio-Strontium by Animals*, UCL A-274 (Jan. 6, 1954).

A preliminary experiment to determine the nature of the build-up curves of  $\text{Sr}^{90} + \text{Y}^{90}$  in various tissues of the mouse is in progress. Ad lib. feeding of contaminated water was indicated since this method is less likely to disturb the metabolism of the animals than is the gavage method. The drinking apparatus previously described<sup>14</sup> makes it possible to determine within 1% the amount of water taken ad lib. by a cage of mice over a period of time. From the known concentration of  $\text{Sr}^{90} + \text{Y}^{90}$  in the drinking water, the average daily intake per mouse can be determined. Contaminated solutions are made up with tap water which the mice have drunk for two or more months preceding the experiment.

The preliminary study consists of two parts: (1) a short-term study with ad lib. feeding of 1.0  $\mu\text{c}/\text{ml}$  of  $\text{H}_2\text{O}$ , and (2) a longer-term study with 0.05  $\mu\text{c}/\text{ml}$  of  $\text{H}_2\text{O}$ . After various periods of feeding, the animals will be sacrificed and the following tissues taken: blood, liver, spleen, kidney and bladder, heart, lungs, reproductive organs, brain, stomach with contents, small intestine with contents, large intestine with contents, sigmoid colon with contents, pelt, femur, and carcass. These will be weighed, wet ashed, and assayed to determine the concentration and organ burden as a function of time and amount of  $\text{Sr}^{90} + \text{Y}^{90}$  ingested. Parts of the alimentary canal are assayed together with contents to check the possibility that, under conditions of continuous feeding, concentration in the canal may build up to critical levels.

The relatively high concentration (1  $\mu\text{c}/\text{ml}$ ) used in part 1 is required in order to study the beginning of the growth curves of the material in soft tissues as well as in bone. Sacrifices are scheduled at various times from 2 to 100 days. The results of the preliminary experiment will guide the selection of other concentrations and times of sacrifice. The possibility that the uptake may depend on the concentration will be checked by using several concentrations over a wide range.

Three groups of 10 mice have been sacrificed after 4, 8, and 14 days of feeding ad lib. on the 1.0  $\mu\text{c}/\text{ml}$  solution. Average intakes were 3.65, 3.45, and 3.70 ml/day/mouse for the three periods, respectively. Tissues have been assayed after

<sup>14</sup>M. J. Cook, F. G. Kariotis, and K. Z. Morgan, *HP Semiann. Prog. Rep. Jan. 31, 1956*, ORNL-2049, p 17.

allowing the  $Y^{90}$  to equilibrate with the  $Sr^{90}$  after the biochemical separation in the body.

The skeleton burden appears to increase linearly with time of feeding over the 14-day period (Fig. 12). Standard deviations are about 26% of the mean for these data. If Eq. 1 is written as

$$(2) \quad \frac{qf_2}{CR} = \frac{f_w T}{0.693} (1 - e^{-0.693 t/T}),$$

an approximation for  $t \ll T$  gives

$$(3) \quad \frac{qf_2}{CR} \sim f_w t.$$

On this basis, it appears that  $f_w \sim 0.04$  for  $Sr^{90} + Y^{90}$  in the mouse. In Handbook 52 (ref. 9) this factor is assumed to be 0.25 for man.

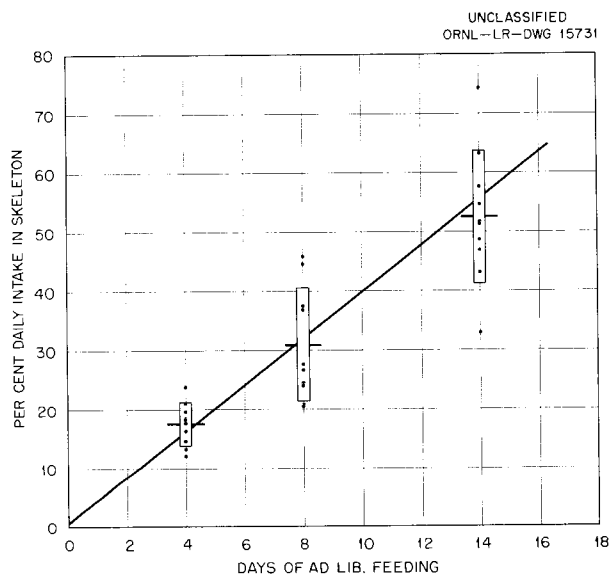


Fig. 12. Skeleton Burden of Mice as a Function of Time of ad lib. Feeding of Water Contaminated with  $1.0 \mu\text{c/ml}$ . Individual data, averages, and standard deviations shown.

The concentration in several tissues is shown in Fig. 13. Initially, the concentration in the lower alimentary canal is of the same order of magnitude as the concentration in bone. Concentration in the femur increases linearly with time over the period studied thus far. Many of the soft tissues appear to have reached an equilibrium concentration during this period.

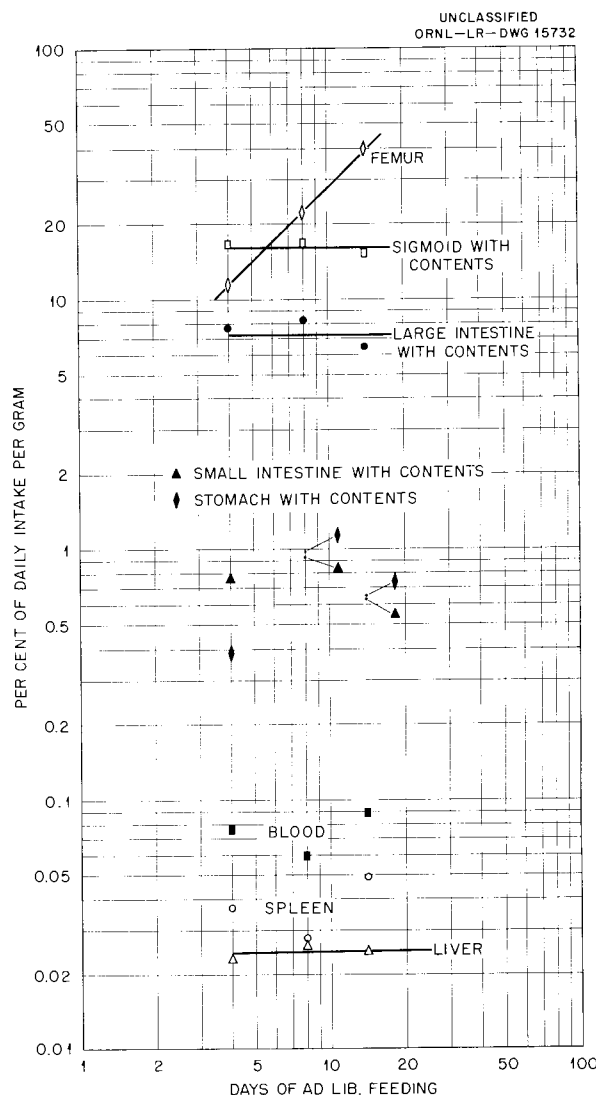


Fig. 13. Concentration of  $Sr^{90} + Y^{90}$  in Various Tissues of Mice After Periods of ad lib. Feeding of Water Contaminated with  $1.0 \mu\text{c/ml}$ . Tissues were pooled for assay.

In another phase of the experiment,<sup>14</sup> mice were given a single dose of  $10 \mu\text{c}$  of  $Sr^{90} + Y^{90}$  by stomach tube, and 16 tissues were analyzed after periods of time ranging from 1 to 275 days. Because of the large standard deviations (20-80%) it is difficult to deduce a mathematical relation of organ burden decay as a function of time. There are indications that the biological half life increases with time in the critical organ (bone) as

well as in noncritical soft tissues. The soft-tissue clearance is much more rapid than that of bone and most soft tissues seem to follow similar curves. (Figs. 14 and 15). The concentrations obtained in the various tissues of the mouse in this experiment are in good agreement with those obtained by other investigators for the rat.<sup>15</sup>

The factor  $f_2$  has been determined at 3, 5, 7, and 14 days following a single administration.

<sup>15</sup>J. G. Hamilton et al., *Metabolism of Fission Products Prog. Rep. Feb. 15, 1943, MDDC-1143.*

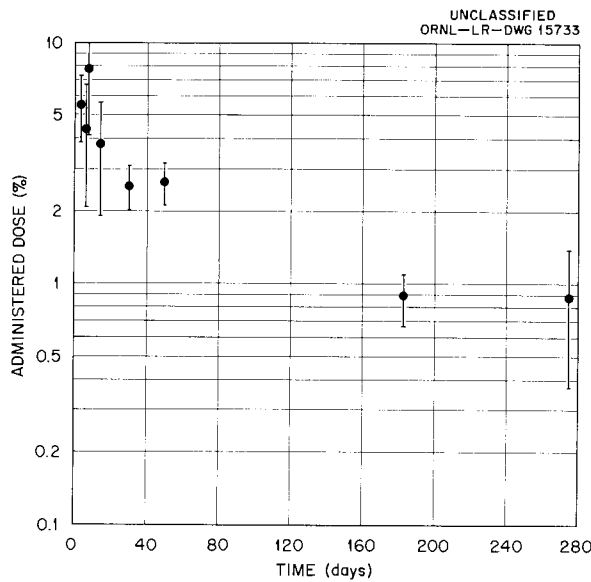


Fig. 14. Retention of Sr<sup>90</sup> + Y<sup>90</sup> in Skeleton of Mouse After Single Administration of 10 µc by Gavage.

Table 1 shows that  $f_2$  is about 0.96 for the skeleton of the mouse. In Handbook 52 (ref. 9) this factor is given as 0.7.

The effect of coprophagy and cross-contamination within a cage of mice following a single oral

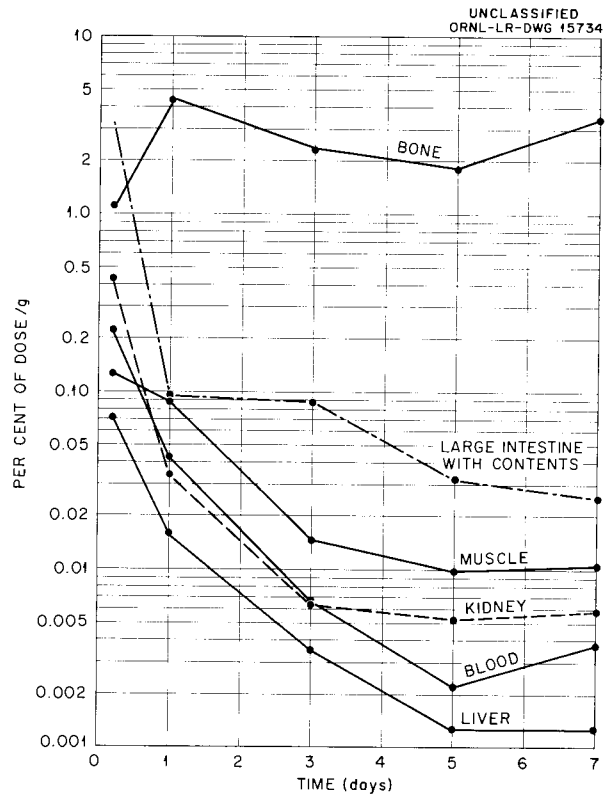


Fig. 15. Concentration of Sr<sup>90</sup> + Y<sup>90</sup> in Various Tissues of Mouse After Single Administration of 10 µc by Gavage.

TABLE 1. SOFT-TISSUE AND SKELETAL RETENTION OF Sr<sup>90</sup> + Y<sup>90</sup> IN MICE FOLLOWING A SINGLE ADMINISTRATION OF 10 µc

Time (days)	Number of Mice	Dose in Total Soft Tissue <sup>a</sup> (%)	Dose in Femur <sup>b</sup> (%)	Dose in Total Skeleton <sup>c</sup> (%)	Dose Body Burden (%)	$f_2$
3	10	0.31	0.128	5.50 ± 1.7	5.81	0.947
5	10	0.19	0.104	4.39 ± 2.3	4.58	0.959
7	8	0.25	0.215	7.79 ± 3.7	8.04	0.969
14	9	0.34	0.27	7.25 ± 6.0	7.59	0.955

<sup>a</sup>Soft tissues in mice amount to approximately 22 g.

<sup>b</sup>Femur weighs approximately 0.05 g.

<sup>c</sup>Skeletons analyzed individually, and standard deviation given. Other tissues grouped for analysis.

## HEALTH PHYSICS PROGRESS REPORT

administration of radioactive nuclide was investigated by placing untreated control animals in the cage. Analysis after 35 and 49 days shows that less than 0.01% of the administered dose is accumulated in the controls and that less than 0.3% of the total body burden of the experimental animals can be attributed to coprophagy and cross-contamination within the cage.

The influence of the strontium and the calcium in the diet is being considered. Spectroscopic analyses for these elements in food, water, and bone are in progress. Chemical analysis shows laboratory food to be 0.59% calcium and 130 ppm strontium.

### ISOTOPIC DISTRIBUTION IN MAN

#### Internal Dose

K. Z. Morgan                      M. J. Cook  
M. R. Ford

The National and International Handbooks<sup>9,10</sup> on internal dose are being revised. As the biological and physical data are completed, they are submitted to the members of both the National and International Committees on Internal Dose for review. For the majority of radioisotopes, biological data and maximum permissible concentration values in air and in water will be listed for the total body, first critical organ, second critical organ, and the gastrointestinal tract. Upon completion the number of nuclides listed in the Handbook by the National Committee will be increased by a factor of approximately 8.

#### Spectrographic Analysis of Tissues for Trace Elements

I. H. Tipton                      M. J. Cook  
K. K. McDaniel

During the past six months the collection of normal human tissue for spectrographic analysis of trace elements has been extended to include one more city in the United States, making a total of nine cities. Three cities have supplied tissues from the desired number of adult autopsies and all the tissues have been dry ashed and the ashes sent to the Physics Department, University of Tennessee, for spectrographic analysis. To date tissues have been obtained from a total of 175 autopsies.

The spectrographic laboratory has completed the analysis of tissue from two cities, and one-

third of the analysis of tissue from a third city has been done. A report<sup>16</sup> has been published that presents the results of the analysis of tissue from one city, and in November a detailed report will be issued to present like data for two additional cities.

Selections for "critical organ," values for concentration of the element in the critical organ, and values for the total body content have been determined and will be included in the revision of the Handbooks on internal dose by the National Committee on Radiation Protection<sup>9</sup> and by the International Commission on Radiological Protection.<sup>10</sup>

### ECOLOGY

S. I. Auerbach                      M. D. Engelmann<sup>17</sup>  
C. J. Rohde, Jr.                      R. J. Davis, Jr.<sup>17</sup>

#### Lethal Effects of Gamma Radiation upon Segments of a Natural Microbial Population

As part of an over-all ecological study of the effects of radiation upon components of the soil ecosystem, data on the gamma doses required to kill certain segments of a natural microbial population have been obtained.

The microflora used in this study were obtained from a mature beech tree cavity. Seven segments of this population were investigated, and these segments were discriminated physiologically through the use of the following media:

- I. basal medium - inorganic salts plus glucose, for enumerating bacteria without complex growth requirements;
- II. amino acid - basal medium plus amino acid mixture, for enumerating organisms requiring one or more amino acids;
- III. soil extract - basal medium plus soil extract, for enumerating organisms with nutritional requirements more complex than simple amino acids;
- IV. water insoluble cellulose-dextrin, for enumerating organisms able to utilize cellulose as the sole carbon source;
- V. Rose Bengal - peptone-dextrose medium containing Rose Bengal (1:30,000) and 30-gamma-per-ml streptomycin sulfate;

<sup>16</sup>I. H. Tipton *et al.*, *Progress Report, Spectrographic Analyses of Tissues for Tracer Elements, July 1, 1955-Dec. 31, 1955*, ORNL CF-56-3-60 (March 12, 1956).

<sup>17</sup>Temporary summer employee.

- VI. streptomycetes medium, for the enumeration of streptomycetes present;
- VII. sporulating organisms, medium II was repeated after the microbial suspensions had been held at 37°C for 20 min.

Material was transferred from the tree-hole into sterile polyethylene cylinders. These containers were stoppered, placed in thermos containers filled with crushed ice. To inhibit bacterial growth the material remained in the thermos from collection time until it was plated, except during irradiation and shaking. Ten grams of the material was weighed into a sterile 10-oz specimen jar and shaken with 100 ml of water in a wrist action shaker for 30 min. Controls were plated from dilutions made from this suspension. The remainder of the material was then placed in the radiation field, 10-g samples being removed after successive doses had been administered. The Co<sup>60</sup> source, located in the Biology Division, delivered an air dose at the rate of approximately

24 r/sec. Doses given in this experiment are listed in Table 2 and ranged from  $5 \times 10^3$  to  $4 \times 10^5$  r. In the experimental runs five plates were poured at three dilutions. Dilutions varied according to the media used, but the range was from 1:1000 to 1:500,000. All plates were incubated at a temperature of  $22 \pm 1^\circ\text{C}$  for seven days except the cellulose-dextrin plates. These were found to require ten days for all colonies to develop sufficiently to be counted.

The survival data are listed in Table 2 and shown in a semilogarithmic plot in Fig. 16. All the populations tended to drop off extremely rapidly at dosages up to  $10^4$  r, then level from 1 to  $2 \times 10^4$  r and continued to decrease at a fairly steady rate. At  $4 \times 10^5$  r there was but one type of colony on all of the bacterial plates. This organism produced rhizoid colonies and did not grow on the Rose-Bengal agar.

In general, the doses required for lethality reported here are in the range of those reported

TABLE 2. PER CENT SURVIVAL OF ORGANISMS GROWING ON VARIOUS MEDIA

Dose ( $r \times 10^3$ )	Medium						
	I	II	III	IV	V	VI	VII
5	$4.45 \times 10^{-1}$	$1.61 \times 10^{-1}$	$3.9 \times 10^{-1}$	$4.75 \times 10^{-1}$	$2.60 \times 10^{-1}$	$7.86 \times 10^{-1}$	$3.14 \times 10^{-1}$
10	$9.60 \times 10^{-2}$	$8.62 \times 10^{-2}$	$6.59 \times 10^{-2}$	$3.33 \times 10^{-1}$	$2.63 \times 10^{-1}$	$1.78 \times 10^{-1}$	$1.92 \times 10^{-1}$
20	$7.24 \times 10^{-2}$	$2.52 \times 10^{-2}$	$6.22 \times 10^{-2}$	$7.88 \times 10^{-2}$	$1.65 \times 10^{-2}$	$1.41 \times 10^{-1}$	$6.63 \times 10^{-2}$
25	$2.94 \times 10^{-2}$	$3.53 \times 10^{-2}$	$5.52 \times 10^{-2}$	$1.38 \times 10^{-1}$	$8.66 \times 10^{-2}$		$8.38 \times 10^{-2}$
30	$5.87 \times 10^{-2}$	$5.03 \times 10^{-2}$	$1.02 \times 10^{-1}$	$1.54 \times 10^{-1}$	$3.14 \times 10^{-1}$	$1.53 \times 10^{-1}$	$2.63 \times 10^{-1}$
40	$5.16 \times 10^{-2}$	$5.81 \times 10^{-2}$	$8.42 \times 10^{-2}$	$1.31 \times 10^{-1}$	$3.88 \times 10^{-2}$	$9.76 \times 10^{-2}$	$1.12 \times 10^{-1}$
50	$1.07 \times 10^{-2}$	$4.60 \times 10^{-3}$	$1.28 \times 10^{-2}$	$4.03 \times 10^{-2}$	$1.15 \times 10^{-2}$	$1.31 \times 10^{-1}$	$1.39 \times 10^{-2}$
75	$3.13 \times 10^{-3}$		$1.37 \times 10^{-2}$	$1.50 \times 10^{-2}$	$1.84 \times 10^{-3}$		$2.50 \times 10^{-3}$
100	$2.66 \times 10^{-3}$	$1.65 \times 10^{-3}$	$3.72 \times 10^{-3}$	$3.55 \times 10^{-2}$	$3.79 \times 10^{-3}$	$3.22 \times 10^{-3}$	$4.80 \times 10^{-3}$
125			$5.98 \times 10^{-3}$	$5.46 \times 10^{-3}$	$6.88 \times 10^{-4}$		$8.0 \times 10^{-4}$
150	$7.60 \times 10^{-4}$	$5.00 \times 10^{-4}$	$2.22 \times 10^{-3}$	$9.48 \times 10^{-4}$	$7.23 \times 10^{-4}$	$1.48 \times 10^{-3}$	$1.39 \times 10^{-3}$
200	$7.49 \times 10^{-5}$	$1.34 \times 10^{-4}$	$1.05 \times 10^{-3}$	$3.39 \times 10^{-4}$	$4.01 \times 10^{-4}$	$1.59 \times 10^{-5}$	$1.4 \times 10^{-3}$
250	$5.97 \times 10^{-5}$	$7.00 \times 10^{-5}$	$4.48 \times 10^{-4}$	$6.48 \times 10^{-5}$	$1.90 \times 10^{-4}$	$2.72 \times 10^{-6}$	$1.1 \times 10^{-3}$
400	$8.79 \times 10^{-7}$	$2.72 \times 10^{-6}$	$2.40 \times 10^{-6}$	$3.14 \times 10^{-6}$	$1.18 \times 10^{-5}$		$1.0 \times 10^{-7}$

UNCLASSIFIED  
ORNL-LR-DWG 13850A

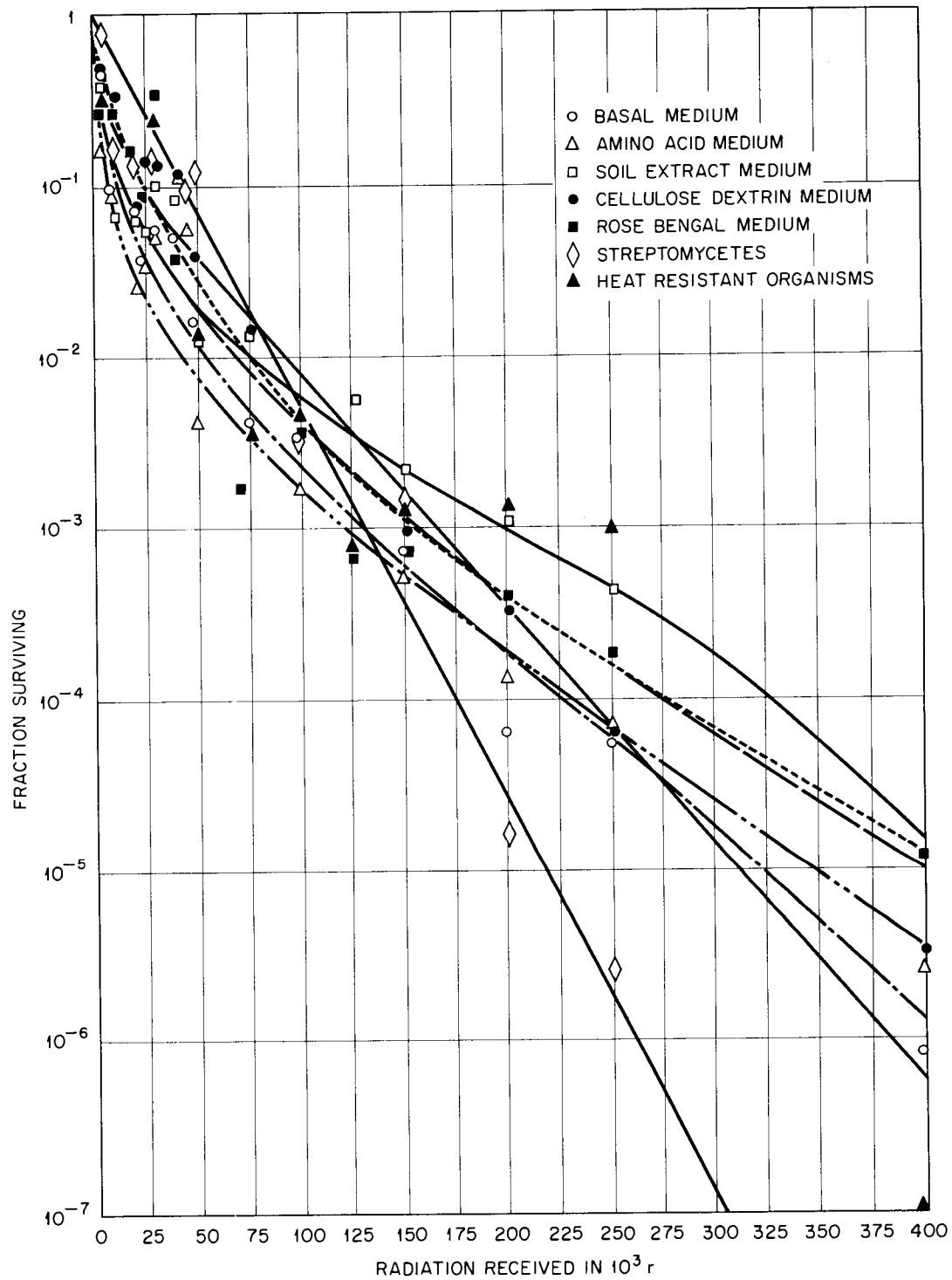


Fig. 16. Effects of Gamma Radiation on Seven Physiological Groups of a Microbial Population.

by workers studying pure cultures of various bacterial and fungal strains. Values for nine common bacterial species indicate that radiation of the order of  $10^4$ – $10^5$  r reduces most of these organisms to 1% (ref 18). Zelle and Hollaender<sup>19</sup> quote LD<sub>50</sub> for gamma radiation of  $5.2 \times 10^3$  r for *Escherichia coli* and  $1.3 \times 10^5$  r for *Bacillus mesentericus*. In only one case (the streptomycetes) in the present experiment did  $5 \times 10^3$  r, the lowest dose used, yield less than 50% mortality.

Reporting LD<sub>50</sub> values for mixed populations is hardly feasible. For the same reason regression lines were not calculated for the curves. The reason for deviation from an exponential function  $N = N_0 e^{-x}$  is in all probability due to the fact that in a natural population mixed species populations are dealt with, each species of which drops off at a rate peculiar to itself. The more exponential character of the streptomycetes curve is probably due to this group being composed of more closely related forms.

#### Delayed Effects of Gamma Radiation on Tree-Hole Arthropods

During the past six months, further analysis of the data on the study of delayed effects of gamma radiation on tree-hole arthropods has been completed. The experimental procedures and preliminary results of the study were reported previously.<sup>20</sup> It can be seen from Table 3, in which are summarized the relative radiosensitivities of the various soil arthropods, that the range of sensitivity to radiation for some of these common soil organisms is very broad. There appears to be no correlation with the degree of biological specialization; for example, within a single taxonomic group (Acarina) the approximate 50% mortality after 90 days varied from 5,000 r for one species to 75,000 r for another species.

Two other phenomena of ecological significance resulted from this study. The first is demonstrated by Fig. 17, in which the survival data for a single major arthropod group (the Collembola) are plotted. Shown here are curves for the total of all Collembola in each sample, a single species

TABLE 3. GAMMA DOSES WHICH PRODUCED APPROXIMATE 50% MORTALITY IN THE MORE ABUNDANT SOIL ORGANISMS USED IN THIS STUDY

Organism	Dose (r)		
	30-Day	60-Day	90-Day
Isopoda	2,000	2,000	
Chilopoda	15,000	12,000	
Protura	35,000	25,000	
Collembola			
Total	25,000	30,000	
<i>Folsomia elongata</i>	25,000	45,000	60,000
Poduridae sp	25,000	15,000	5,000
Acarina			
Belbidae-Eremaeidae sp	75,000	25,000	30,000
<i>Euphthiracarus</i> sp	125,000+	125,000	75,000
<i>Mesoplophora</i> sp	80,000	40,000	
Neoparasitidae sp	8,000	5,000	5,000
<i>Rhizoglyphus</i> sp	35,000	50,000	30,000

*Folsomia elongata* (Family Isotomidae), and members of the family Poduridae. Vertical lines through each point represent the standard error of that sample. At 30 days the species are closely grouped in a curve pattern which would be almost linear on a semilogarithmic plot. The 50% survival dose is about 25,000 r. Thirty days later (after 60 days) there is a marked change in the curves. All species have increased beyond the control population levels at doses up to 15,000 r except *F. elongata*. This species increased well above control levels at doses up to and including 25,000 r. The members of the family Poduridae do not manifest this pronounced increase over control numbers. After 90 days *F. elongata* numbers are still in excess of control numbers at dosages including 25,000 r. Meanwhile the curve of the Poduridae has shifted to the left giving an indication of being completely eliminated in an additional increment of time.

The problem that is posed by this particular piece of data is to account for this great increase in numbers of the species in irradiated substrate over the control levels in nonirradiated substrate. It is not believed that this represents any stimulatory effect of radiation, but, rather, that it represents an upset of the internal dynamics of the system in part due to radiation. The possible

<sup>18</sup>B. E. Proctor and S. A. Goldblith, *Progress Report*, Sept. 1, 1952–June 30, 1953, NYO-3340.

<sup>19</sup>M. R. Zelle and A. Hollaender, in *Radiation Biology*, vol. II, A. Hollaender (ed.), McGraw-Hill, New York (1955).

<sup>20</sup>S. I. Auerbach et al., *HP Semiann. Prog. Rep.* Jan. 31, 1956, ORNL-2049, p 5, esp 13.

HEALTH PHYSICS PROGRESS REPORT

UNCLASSIFIED  
ORNL-LR-DWG 43854A

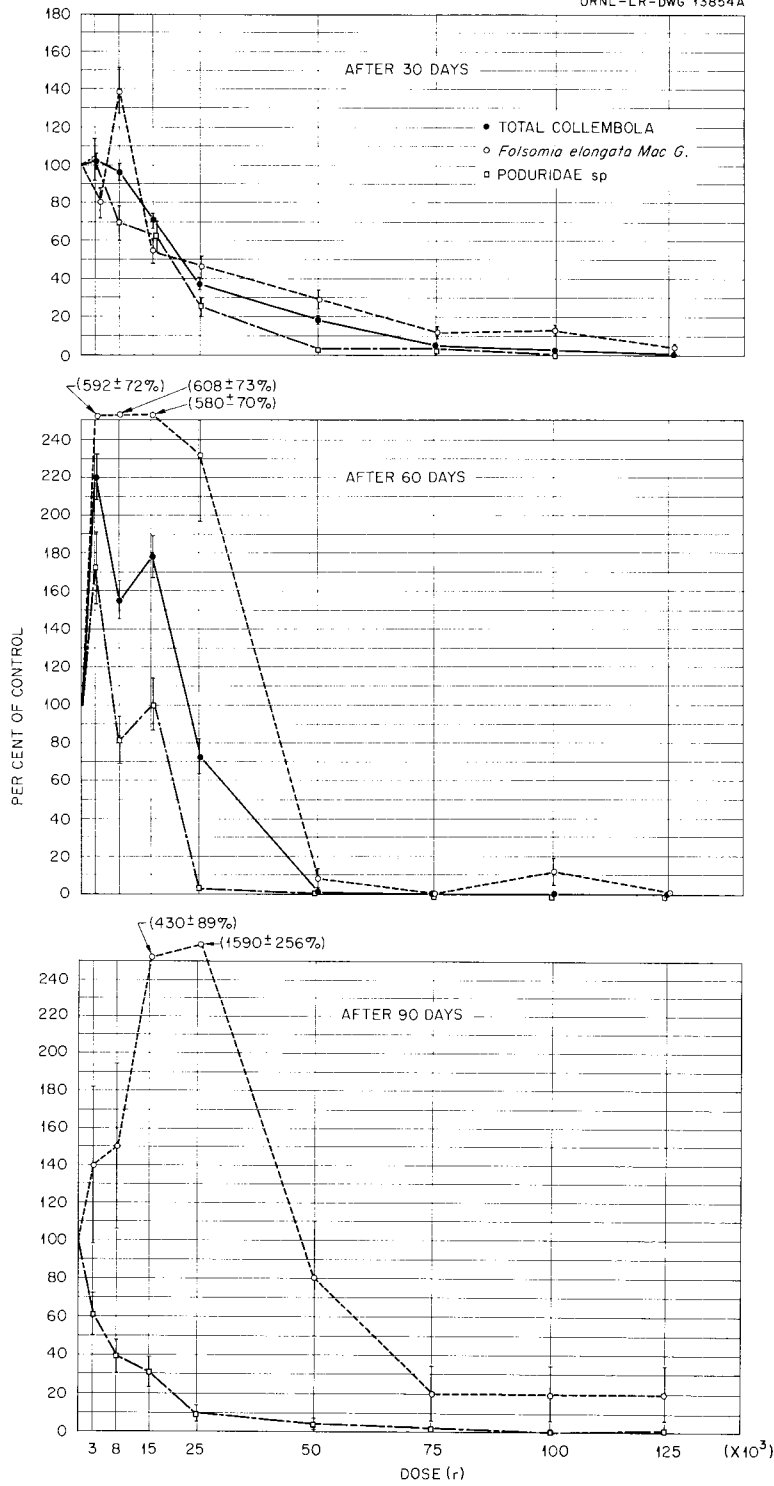


Fig. 17. Dose Survival Curves for Tree-Hole Collembola in Which Are Plotted Values for Total Collembola, Members of the Family Poduridae, and the Isotomid Species *Folsomia elongata*.

explanations include the destruction of more radiosensitive predators, parasites, and competitors for the same foods.

The second phenomenon of ecological significance is represented by the data shown in Fig. 18. These data are for two species of Acarina; one of which (*Rhizoglyphus* sp) is an herbivorous and saprophagous mite with a short life cycle and a high reproductive potential and the other species (*Neoparasitidae* sp) is a predator mite which, like most predator mites, is capable of exerting a high predator pressure on other mites. The latter species probably feeds on *Rhizoglyphus* sp, but not necessarily so. The curves for 30, 60, and 90 days suggest that through time the more radio-resistant prey species is increasing in numbers above control population levels while simultaneously the more radiosensitive predator species is decreasing in numbers. This suggests the hypothesis that biological balance can be upset by differences in radiosensitivity of predator-prey species. Further experimental work is currently under way to test this hypothesis.

#### Radiation Studies on a Single Species

The initial effort of the Ecology Group has been concerned with the effects of gamma radiation upon mixed-animal-species populations occurring naturally in the soil and its associated niches. The Acarina, or mites, being found in great abundance both in species and in individuals, are the largest single arthropod group present in these habitats.

The delayed effects of radiation on tree-hole arthropods are given elsewhere in this report. Presented here is a summary of the Acarina present in the beech tree-hole substrate. There are 27 families and 42 species of mites present. Of the latter, 31 are herbivores and 11 are predators. Apparently, five species are constant residents of the tree-hole habitat. Thirty-one species, or nearly 75% of the total, are also residents of the forest floor as determined qualitatively from soil samplings around ORNL environs and adjacent counties.

The correlation and interpretation of the data obtained on the effects of radiation on mixed species of a natural mite population have suggested the need for a detailed study of radiation effects at the single-species level. Little radiation data dealing with a mite is available from

the literature or from current investigations outside this Laboratory.

In order to utilize a mite as an experimental animal, it was necessary to develop rearing techniques and equipment as well as to select a species which would adapt itself to laboratory procedures. *Caloglyphus* sp (Acarina: Acaridae) is easily reared in the laboratory, produces a large number of eggs in its short life span and completes its cycle in a matter of seven to eight days. A single pair may produce as many as 106 eggs in a 24-hr period. Clone cultures were developed from the eggs of a single gravid female. These cultures are maintained in  $1\frac{3}{4} \times 1\frac{3}{4} \times \frac{3}{4}$  in. plastic boxes lined with a moisture-holding layer composed of one part activated charcoal to nine parts plaster of Paris.

For life history studies and for studies on the effects of radiation, other pieces of equipment utilizing the plaster-charcoal technique were designed. Several plastic cylinders of  $\frac{1}{2}$ -in. diameter with four holes at one end (Fig. 19) are inserted in a wet mass of charcoal and plaster in a  $4 \times 4\frac{1}{2} \times 1\frac{1}{4}$  in. plastic box with a snap cover. When the plaster sets, a series of rearing chambers, closed with cork stoppers, are contained in a box which can be handled with ease under the stereomicroscope (Fig. 20). A circular box of 1-in. height and  $1\frac{3}{4}$ -in. diameter and holding four cylinders imbedded in a plaster-charcoal mass has been developed for use in the  $\text{Co}^{60}$  source and allows for radiation of eggs, larvae, nymphs, and adults of *Caloglyphus*.

Life history investigations are essential to provide control data which can be correlated with observed effects of radiation on the mixed Acarine tree-hole population, where such comparisons can be made. These investigations include studies on (1) the food and feeding habits of the developmental stages as well as their morphological and ecological characteristics from egg to adult, (2) quantity of eggs laid and the periodicity of oviposition, and (3) longevity.

In most of the studies presented here pulverized lepidopterous larvae found in the same habitat niche with *Caloglyphus* were used as food. Later, freshly ground beef was used with equal success.

The high humidity of the rearing boxes was favorable to the production of mold. This growth was successfully eliminated by soaking the food in a 10,000 unit suspension of Mycostatin, a

HEALTH PHYSICS PROGRESS REPORT

UNCLASSIFIED  
ORNL-LR-DWG 13851A

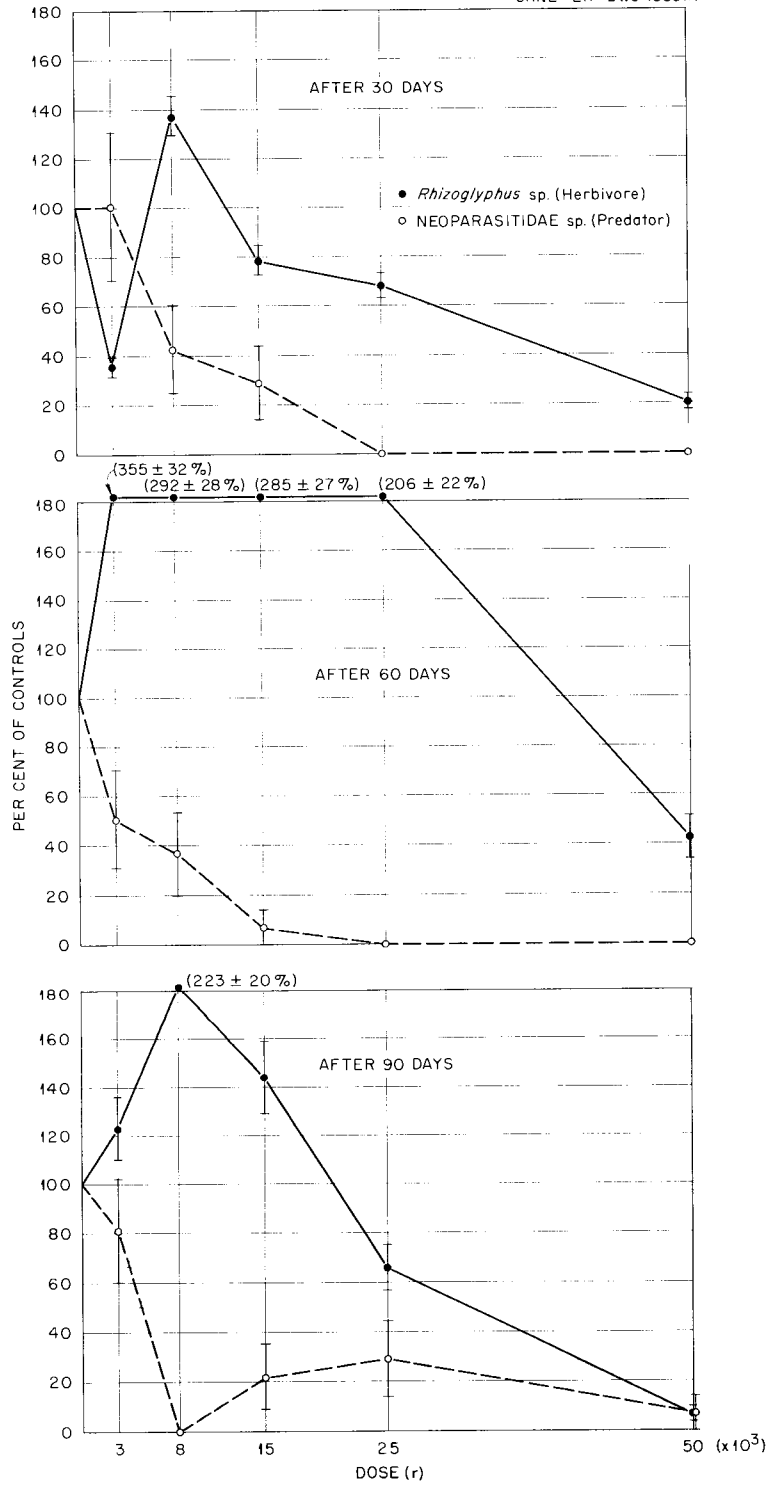


Fig. 18. Dose Survival Curve for Two Species of Tree-Hole Acarina.

UNCLASSIFIED  
ORNL-LR-DWG 13366A

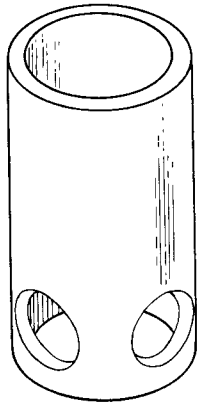


Fig. 19. Lucite Cylinder.

UNCLASSIFIED  
ORNL-LR-DWG 13365A

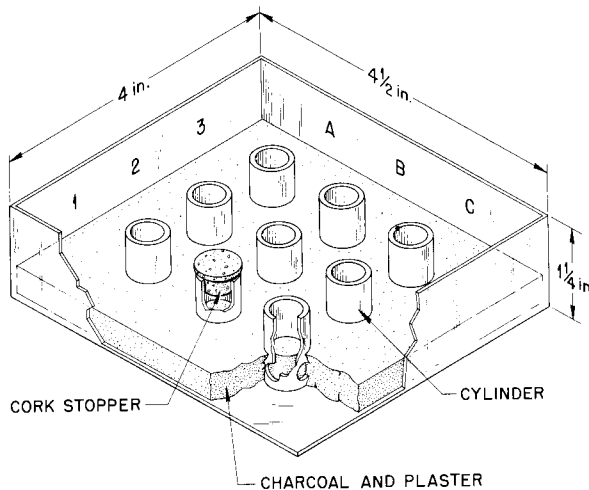


Fig. 20. Rearing Box.

fungistatic compound marketed by E. R. Squibb & Sons, New York.

Two hundred fifty eggs of known age were isolated in the chambers of ten rearing boxes and observations were made at 4-hr intervals until a sufficient number of adults were obtained. After hatching occurs, *Caloglyphus* passes through three stages (a fourth immature stage may be added under certain conditions) before it becomes an adult. From the egg emerges a hexapod larva which, after passing through an inert period

characterized by cessation of visible activity, molts to become the 8-legged protonymph. The protonymph also passes through an inert period and molts to give rise to the tritonymph. After a final inert period the tritonymph molts to the adult form. Thus this mite passes from the egg through three growth periods or stadia, three inert stadia, and three molts before the adult state is attained.

Under certain conditions a fourth stadium, inert period, and molt occurs between the protonymph and tritonymph stages. This is the deutonymph or hypopus, a stage unique in the Acaridae. Apparently adverse conditions predispose the transformation of protonymphs into hypopi or "wandernymphs." During this stadium no food is taken. With the aid of suckers on its underside, the hypopus is able to adhere to smooth surfaces. Collections of other mites, insects, birds, and small mammals frequently show the presence of clinging hypopi. This peculiar stage is a critical one in the development of *Caloglyphus* and enables the mite to remove itself from an unsatisfactory environment or situation by merely attaching to visitors entering its habitat niche.

Under the laboratory conditions employed in the life history study of *Caloglyphus*, no hypopus formation occurred. Table 4 summarizes the life history data obtained on this species at 25°C and under conditions of high humidity. Of the 247 mites (98.8% hatching) considered at the outset of this study, none passed through the incubation period in fewer than 9 hr and all but one completed this phase in fewer than 53 hr. One egg took as long as 79 to 83 hr to incubate. The distribution of hatchings in time is skewed to the left with 50% of the eggs completing incubation in less than 40.6 hr. All but one of the larvae completed this stadium in a period ranging from slightly less than one day to slightly less than four days. The distribution is skewed to the right with 50% of the observations at fewer than 43.5 hr. The three inert periods follow almost identical patterns. In somewhat less than a day all individuals completed these stadia. Over 85% of the total passed through each of the inert periods in fewer than 13 hr.

Distribution in the protonymph stadium is highly skewed to the right with 50% of the observations at fewer than 25.8 hr. One hundred and fifty-eight, or approximately two-thirds of the original number,

HEALTH PHYSICS PROGRESS REPORT

TABLE 4. FREQUENCIES OF IMMATURE STADIA IN CALOGLYPHUS

Time in Mid-point (hr)		Incubation	Larva	Inert	Protonymph	Inert	Tritonymph	Inert
Interval	Average							
4-8	6	0	0	99	0	97	0	16
9-13	11	4	0	117	10	101	0	122
14-18	16	8	0	21	40	4	1	20
19-23	21	15	1	1	32	0	13	0
24-28	26	19	29	0	55	0	56	0
29-33	31	35	33	0	13	0	25	0
34-38	36	15	32	0	8	0	17	0
39-43	41	85	31	0	4	0	10	0
44-48	46	60	44	0	10	0	14	0
49-53	51	5	10	0	5	0	7	0
54-58	56	0	16	0	9	0	4	0
59-63	61	0	12	0	4	0	2	0
64-68	66	0	14	0	3	0	5	0
69-73	71	0	10	0	3	0	1	0
74-78	76	0	4	0	0	0	2	0
79-83	81	1	2	0	1	0	0	0
84-88	86	0	3	0	3	0	0	0
89-93	91	0	1	0	0	0	1	0
94-98	96	0	0	0	1	0	0	0
99-103	101	0	0	0	0	0	0	0
104-108	106	0	0	0	0	0	0	0
109-113	111	0	0	0	0	0	0	0
114-118	116	0	1	0	1	0	0	0
Total		247	243	238	202	202	158	158
Range of observations, hr		9-83	19-118	4-23	9-118	4-18	14-93	4-18
Modal class		39-43	44-48	9-13	24-28	9-13	24-28	9-13
Median		40.6	43.5		25.8		30.8	
Mean		37.2	45.1		30.4		35.0	
Standard deviation		9.62	15.43		17.71		13.22	

remained at the tritonymph stadium. The distribution is skewed to the right with a median time of 30.8 hr and a modal class of 24 to 28 hr.

An approximate record, to within a 4-hr interval, was kept on the duration of time between egg and adult for 158 mites. The average duration of the life cycle, as computed from these observations, is 151.26 hr, or approximately  $6\frac{1}{3}$  days. The shortest observed cycle is between 88 and 92 hr, or just less than 4 days. The longest was between 220 and 224 hr, or slightly more than 9 days.

Two pilot experiments, in which were used virgin adults irradiated with a single 5000 r gamma dose, showed that at this dose no effect was observed in four females, neither in the hatching of their eggs nor upon the fertility of their offspring.

There is a temporary effect upon fertility in the male *Caloglyphus*, as observed in two irradiated individuals (Fig. 21). After the fifth day of continuous pairing, egg viability begins to approach that observed in the controls.

Experiments concerning the susceptibility of the egg to gamma radiation are completed. The manner of collecting eggs for irradiation purposes was to allow approximately two males and three females to reside for 24 hr in each chamber of the circular plastic box described. Each chamber contained a small amount of food. Prior to the end of the 24-hr oviposition period all adults were removed. Under these conditions, the maximum egg age is 24 hr at the time of irradiation.

Successive egg clutches were exposed to increasing instantaneous dosages at increments of 250 r up to 3750 r. At the expiration of a 5-day maximum waiting period hatched larvae were killed with a few drops of boiling water. Counts of larvae and eggs were made at this time. Any unhatched eggs were presumed inviable since previous studies indicated maximum hatching to be under two days and the maximum incubation observed (Table 4) also falls within the limit of the waiting period.

Susceptibility to gamma radiation begins at 1250 r when 90% hatching occurs (Fig. 22). Viability appears to decrease linearly as the dose increases. At 3750 r a 34.9% hatchability is noted.

As compared with such arthropods as *Habrobracon*,<sup>21</sup> *Melanoplus*,<sup>22</sup> and *Drosophila*,<sup>23</sup> the egg of *Caloglyphus* appears less susceptible to radiation. This same situation apparently exists with the adult *Caloglyphus* when compared with related studies on the adults of *Habrobracon*<sup>24</sup> and *Drosophila*.<sup>25</sup>

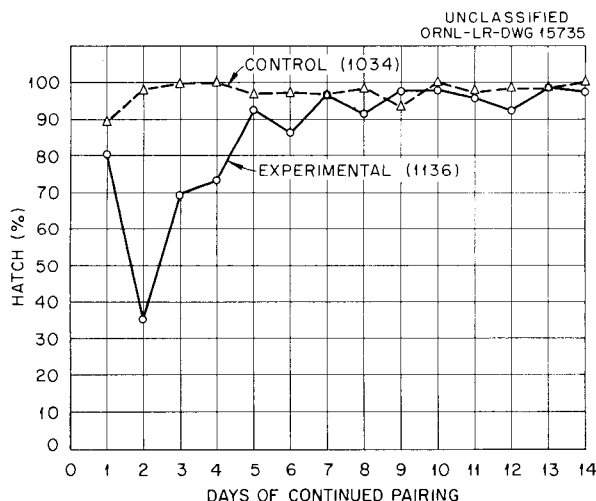


Fig. 21. Per Cent Hatchability of Eggs from Two Irradiated Male *Caloglyphus* Paired with Normal Virgin Females as Compared with Controls.

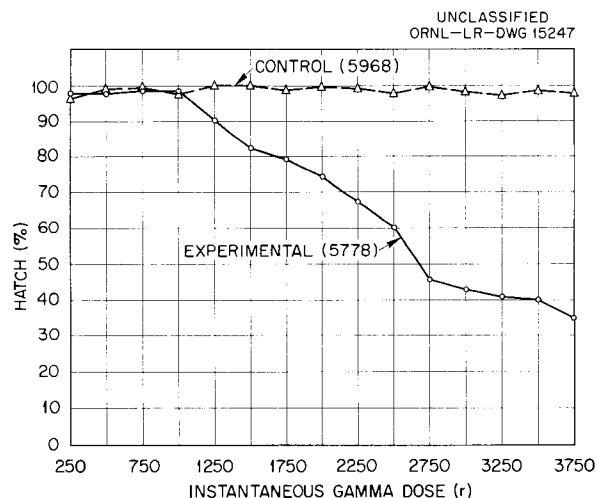


Fig. 22. Effect of Gamma Radiation on Eggs of the Mite, *Caloglyphus* sp (Maximum Egg Age, 24 hr).

## SANITARY ENGINEERING RESEARCH

E. G. Struxness

R. J. Morton

## FIELD INVESTIGATIONS

W. E. Boegly	L. Hemphill
K. E. Cowser	F. W. Sanders
F. M. Empson	R. E. Yoder
W. de Laguna	H. E. Wyrick
F. L. Parker	

## Aerosol Entrainment Well

The aerosol entrainment well<sup>1</sup> was designed to study the evolution and de-entrainment of radioactive aerosols produced by hot reactor wastes. The well is now being operated with two objectives, an investigation of the entrainment of radioactive aerosols from hot and boiling solutions and a study of the effectiveness of sand and other materials as filter media for wet aerosols. During the report period, data were secured for the first of these objectives and for the filtration effectiveness of two types of sand.

**Boiling Data.** — Initial tests with the well were carried out at a water level of 10 ft in the 20-ft-deep well, followed by a number of tests with 15 ft of water in the well. These data are shown in Table 5. The data are too erratic to permit the drawing of firm conclusions. In general, with a level in the well of 10 ft, the decontamination factor (DF) by boiling is approximately  $1 \times 10^5$ . The decontamination factor is defined as:

$$DF = \frac{\text{counts/min/ml in well liquid}}{\text{counts/min/ml in condensate}}$$

Reducing the temperature to 98, 95, and 93°C lowered the DF to  $2 \times 10^4$ . When the water level was raised to 15 ft, the DF increased to  $1 \times 10^6$  at boiling. At 98°C the DF was not significantly different.

**Sand Filter Data.** — Entrainment well tests have been made of the filtering properties of two types of sand: the Ottawa standard testing sand, ASTM designation C-190, and a local river sand, which is referred to as the Clinch sand. The data are shown in Table 6. The Ottawa standard testing sand gives DF's greater than the Clinch sand by a factor of 10.

By pressurizing the system, allowing the moisture to force itself through the sand filter, the DF's are

<sup>1</sup>K. E. Cowser *et al.*, *HP Semiann. Prog. Rep. Jan. 31, 1956*, ORNL 2049, p 27.

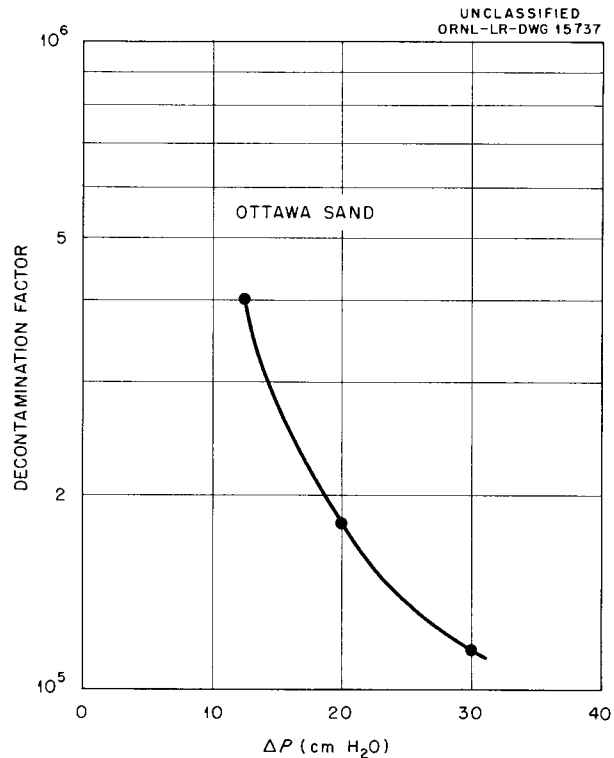


Fig. 23. Decontamination Factor Variation with Pressure.

found to increase as the internal pressure of the system decreases, Fig. 23.

## Pilot Pit Experiments

**Pilot Pit No. 1.** — Construction of pilot pit No. 1, described previously,<sup>1</sup> has been completed. A mixture of 720 gal of nonradioactive acid aluminum nitrate simulated waste solution, 720 lb of soda ash, 720 lb of limestone, and 2405 lb of Conasauga shale was added to the pit and heated. First water and then nitrogen oxides were evolved. After 28 days of heating, dryness was reached, at which time a 3-ft layer of insulation was placed over the mass. Heating was continued until, after 41 days of heating, an equilibrium temperature of 650°C was reached at the center of the cake, with a power input of 4.2 kw. This temperature was thought to be sufficiently above the minimum sintering temperature of 550°C indicated by the laboratory study. The cake was then cooled and

TABLE 5. DECONTAMINATION BY EVAPORATION

Test No.	Temperature (°C)	Air Flow (liters/min)	Radioactivity (counts/min/ml)		DF
			Well	Condensate	
Water level, 10 ft					
6	100	1	7,514	0.082	$0.92 \times 10^5$
7	100	1	7,514	0.082	$1.25 \times 10^5$
4	100	2	9,701	0.136	$0.713 \times 10^5$
5	100	2	9,701	0.082	$1.18 \times 10^5$
8	100	2	5,961	0.042	$1.42 \times 10^5$
9	100	2	5,961	0.085	$0.70 \times 10^5$
2	100	4	10,000	0.105	$0.95 \times 10^5$
3	100	4	10,000	0.096	$1.04 \times 10^5$
26	100	10	11,920	0.036	$3.31 \times 10^5$
30	100	10	9,448	0.049	$1.93 \times 10^5$
27	100	20	11,920	0.108	$1.1 \times 10^5$
29	100	20	9,448	0.066	$1.43 \times 10^5$
41	98	10	11,055	0.320	$3.45 \times 10^4$
42	98	20	10,755	1.64	$0.66 \times 10^4$
29	95	20	15,563	0.43	$3.6 \times 10^4$
31	95	20	15,563	0.46	$3.4 \times 10^4$
40	93	10	23,823	0.603	$3.95 \times 10^4$
38	93	20	23,823	0.90	$2.64 \times 10^4$
39	93	20	23,823	1.01	$2.38 \times 10^4$
Water level, 15 ft					
46	100	10	19,258	0.139	$1.38 \times 10^6$
47	100	10	19,258	0.146	$1.32 \times 10^6$
44	100	20	19,258	0.212	$0.91 \times 10^6$
48	98	10	19,258	0.218	$0.88 \times 10^6$
50	98	10	19,258	0.198	$0.97 \times 10^6$
54	98	10	7,914	0.074	$1.1 \times 10^5$
49	98	20	19,258	0.240	$0.80 \times 10^6$
51	98	20	19,258	0.185	$1.04 \times 10^6$
53	98	20	7,914	0.064	$1.2 \times 10^5$

TABLE 6. DECONTAMINATION BY SAND FILTRATION

Sand, 1 ft  
Water level, 10 ft  
Temperature, 100°C

Sand	Test No.	Air Flow (liters/min)	Radioactivity (counts/min/ml)		DF
			Well	Condensate	
Clinch	15	1	11,356	0.086	$1.32 \times 10^5$
	16	1	11,356	0.088	$1.21 \times 10^5$
	17	2	11,356	0.054	$2.10 \times 10^5$
	18	2	11,356	0.087	$1.30 \times 10^5$
	11	4	11,356	0.16	$0.71 \times 10^5$
	12	4	11,356	0.10	$1.14 \times 10^5$
Ottawa	31	1	9,448	0.003	$3.2 \times 10^6$
	32	1	9,448	0.031	$3.0 \times 10^5$
	33	1	9,448	0.020	$4.7 \times 10^5$
	34	1	9,448	0.031	$3.0 \times 10^5$
	28	1	11,920	0.007	$1.7 \times 10^6$
	21	2	10,878	0.060	$1.81 \times 10^5$
	24	2	14,930	0.003	$4.9 \times 10^6$
	25	2	14,930		
	19	4	11,356	0.113	$1 \times 10^5$
	20	4	11,054	0.052	$2.13 \times 10^5$
	22	4	20,245	0.012	$1.7 \times 10^6$
23	4	14,930	0.005	$3 \times 10^6$	

removed from the pit and liner. Gross physical examination of the sinter showed that the cake was not homogeneous. Chemical analyses of samples taken throughout the cake are in progress.

Figure 24 shows variations of temperature and input power with time. Input power was regulated by heater temperature.<sup>1</sup> Thermocouples 1, 2, and 4 were located on a level 1 ft above the bottom of the ceramic mixture in the pit - No. 1 at the center, No. 2 at the outer surface of the mixture, and No. 4 on the outer surface of the liner. Thermocouple No. 3 was 1 ft directly above No. 2. Thermocouple No. 13 was attached to one of the four heaters of the upper bank; thermocouple No. 14 was on a heater of the lower bank. The arrangement of thermocouples is shown in Fig. 25. The power

input of 4.2 kw required was about 12% higher than that predicted from scaling-up the laboratory experiments, which was within the expected accuracy of the prediction. The results of this experiment indicate the necessity for improvements in mixing technique and in heater design in future experiments.

**Pilot Pit No. 2.** - The design of pilot pit No. 2 was completed during the past six months. The pit will operate with tracer levels of mixed fission products in the waste-clay-flux slurry and will provide a radioactive cake for leaching analysis. Also to be studied in this pit is the nature and character of the off-gases. Pilot pit No. 2 differs from pilot pit No. 1 (described above) in that (1) the mixing operation will be performed in one batch of

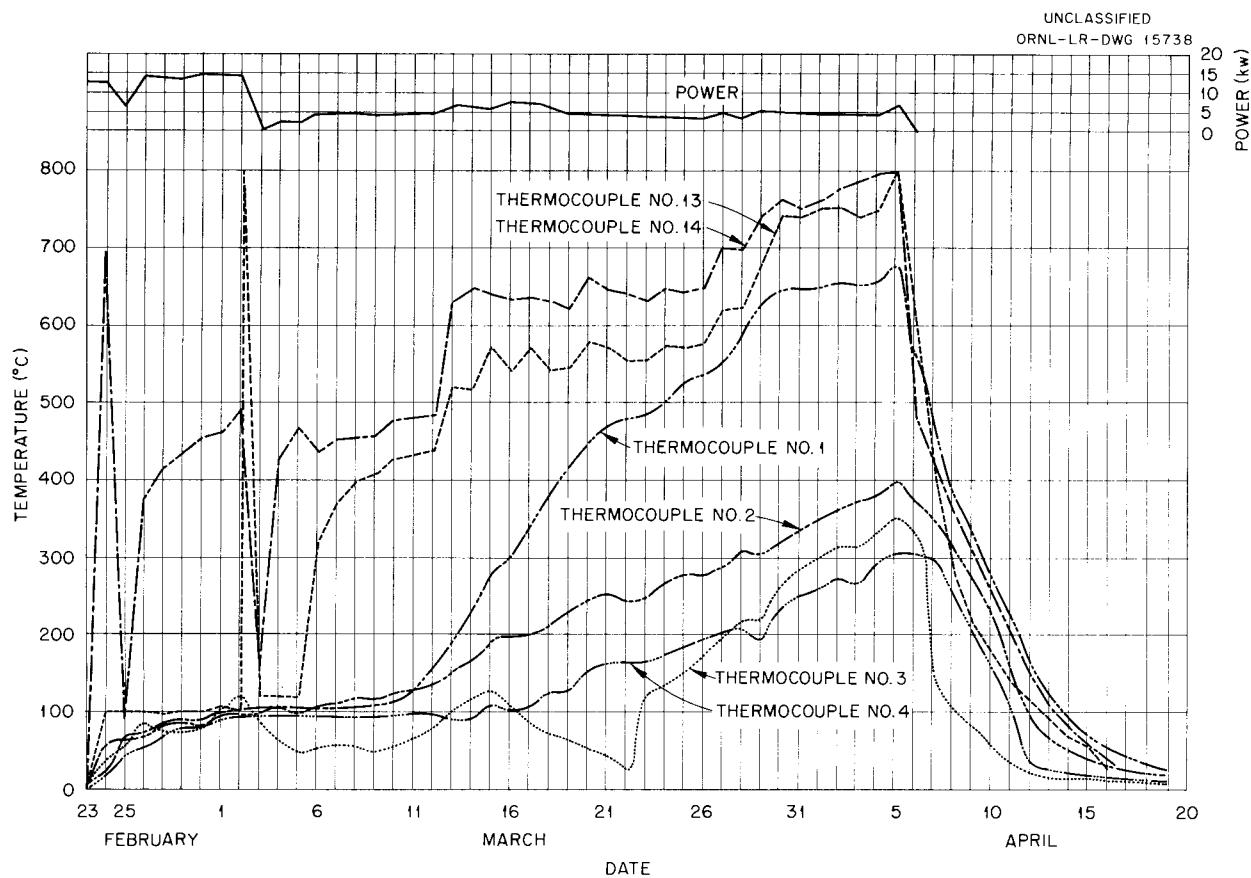


Fig. 24. Temperatures and Power Level vs Time for Pilot Pit No. 1.

720 gal, (2) a new and better heater layout has been designed, and (3) an air cleaning system will be provided for the off-gases.

A trial run of the facilities designed for pilot pit No. 2 will be made in order to test the performance of the heater and air cleaning systems. No radioactive material will be used in this test. It is proposed to run this test with the highest power during the initial stages and gradually decrease to a low power at the end, which is a power distribution similar to that in the actual hot waste solution. In an operation of this fashion a cake should be produced which will be more representative of the cake expected in the actual self-sintering pits than that produced in pilot pit No. 1.

#### Chemical Waste Seepage Pits

Waste pit No. 4 was placed in operation on April 4, 1956, when approximately 400,000 gal of waste containing 900 curies of beta activity was decanted

from pit No. 2. Copper tubing was installed in the pit for sampling at fixed points, while polyethylene tubing is used for sampling at any depth at selected points in the pit. Composite samples are taken as the waste is transferred from pit No. 2 to pit No. 4 and samples are also taken of the contents of pit No. 4 at various times. Stilling wells were installed to obtain a continuous recording of the liquid stage in the pit.

The lowering of the liquid levels in pits No. 2 and No. 3 exposed the radioactive nuclides adsorbed and precipitated on the side wall of these pits, thus increasing the external radiation fields in the immediate vicinity and thus reducing the permissible working time in the pit area. The results of a survey made on May 17, 1956, are shown in Fig. 26, where the radiation contour intervals (solid lines) are in units of milliroentgens per hour.

**Liquid Inventory.** - Equipment has been installed to obtain meteorological data for computing the loss

UNCLASSIFIED  
ORNL - LR - DWG 10960B

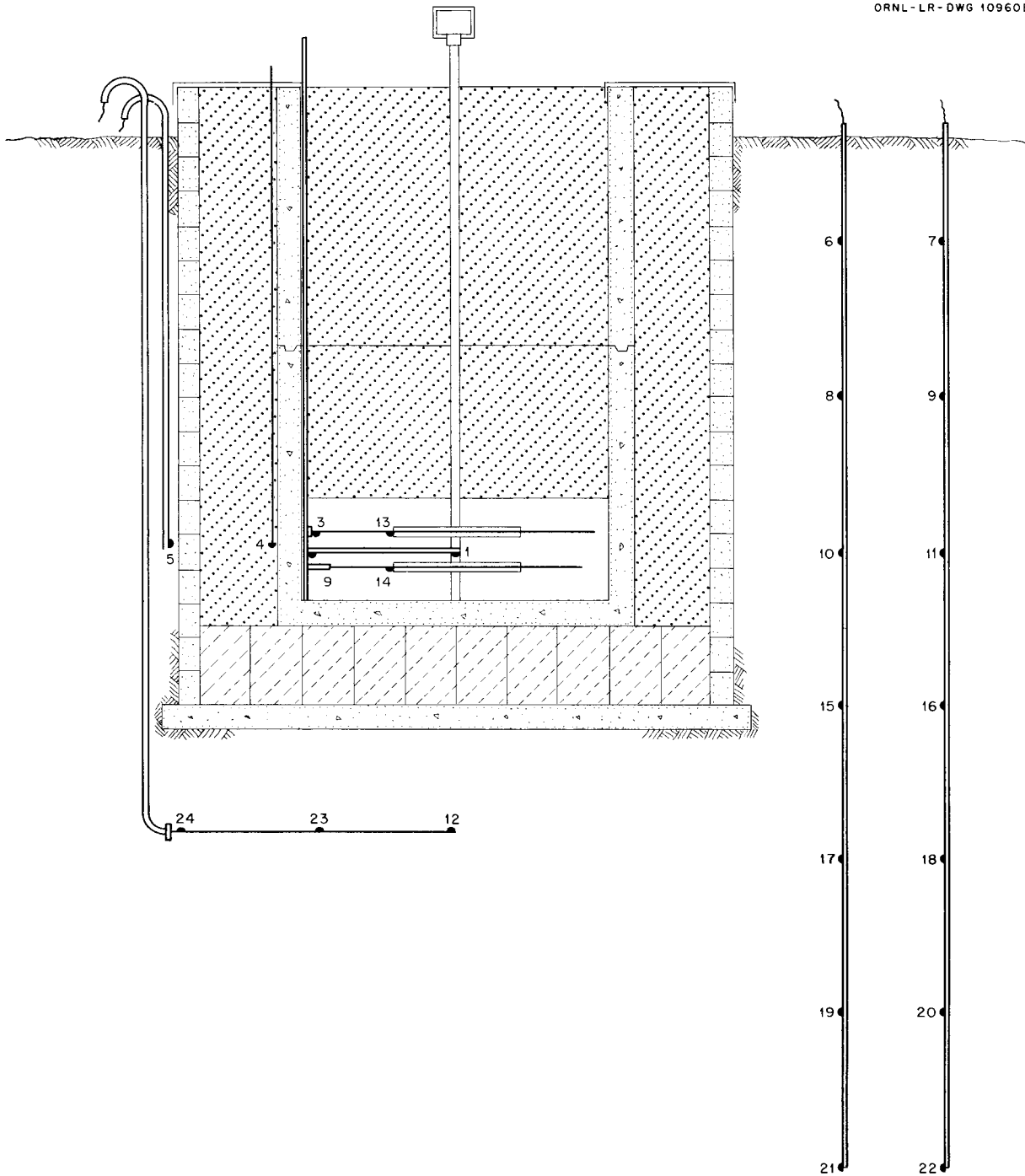


Fig. 25. Arrangement of Thermocouples in Pilot Pit No. 1.



of liquid due to evaporation. Wind movement and air temperatures are measured by means of anemometers and thermocouples supported at 2 and 8 meters above the ground surface. Humidity determinations are obtained at the 2-meter height by means of a Foxboro dew cell. Float-supported thermocouples and an anemometer measure the liquid temperature and surface wind speed in pit No. 4. Figure 27 is a photograph of the waste pit showing the installed floats and appurtenant sampling tubes and stilling well.

**Chemical and Radiochemical Inventory.** – Through May, 1956, a total of 4,050,000 gal of waste had been released to the seepage pits. The gross beta activity was measured at the time that each batch was transferred; the total of these measurements is 57,000 curies of  $\beta$  activity. Qualitatively, the predominant radionuclides in the waste are  $\text{Cs}^{137}$  and  $\text{Ru}^{106}$ , while Na and  $\text{NO}_3$  account for the largest part of the chemical constituents.

**Definition of Underground Contamination.** – The vertical movement of radioactive waste through the soil under pit No. 4 is followed by radiologging well No. 78, which is located in the center of the pit. The well casing was grouted in the boring and extends above the maximum liquid stage of the pit. The installation of the monitoring equipment is shown in Fig. 27; the probe is mounted in the well casing, and the recording equipment and cable reel are offset in the portable trailer. Radiologs show (see Fig. 28a) a continuous zone of activity which has penetrated to a depth of 6 ft below the bottom of the pit. Because of rapid seepage, the pit became dry in approximately 5 weeks and since that time only a small additional vertical movement of the activity zone has occurred. Several discrete zones of activity have developed below the continuous zone of activity and are associated with the influence of the geologic structure upon the waste movement. From the radiologs it is apparent that the bulk of the cation activity in the waste seeping from the bottom of the pit has been removed within the upper foot of the shale material. Available information suggests that the side walls of the pit which expose the strike of the formation exert the greatest influence on the volume of waste seeping from the pit.

Radiologs of well No. 82 (grout well) located adjacent to pit No. 4 have shown that the majority of activity intercepted by the well occurs in discrete zones and is limited to a depth of 40 ft (see

Fig. 28b). There are responses developing at greater depths, but their magnitude is substantially less than the responses above 40 ft. By probing well 74 (an open boring 20 ft from well 82) after flushing with tap water (see Fig. 28c and d), discrete peak responses typical of those detected in other open borings were observed. These responses occur to a depth of 100 ft, which was the limit of the flushing procedure.

The series of wells surrounding pit 4 have been analyzed to determine the dispersion of the radioactive wastes. Background measurements were made prior to the time that the pit went into operation and the increase of activity in the wells has been followed since that time. The initial measured increase in activity was found in the culvert near well 84, to the east of the waste pit. Gradual increases in activity have been found in the wells to the east and west of the waste pit. These results are in the process of being analyzed.

A simple slide mechanism was developed to permit rapid sampling of the wells with little likelihood of cross-contamination of the samples.

**The Use of Helium as a Tracer in Ground Water Studies.** – In order to test the feasibility of helium as a ground water tracer, a program of laboratory experimentation has been initiated to determine the increase in solubility of helium with the increase in amount of nitrogen in the water. The leak detector (a simplified mass spectrometer) is being calibrated to read directly the concentration of helium in water.

**Column Studies of Storage Pit Waste.** – A series of tests of the absorption of the wastes from the chemical storage pits on the waste storage pit soil has commenced. Preliminary work indicates that, with the present volume and composition of wastes, the cation exchange and absorption capacity of the soil is not being exceeded. It is surmised that the seeps of nitrates and ruthenium that have developed are from flow along fissures and cracks.

#### AIRBORNE-RADIOACTIVITY STUDIES

F. M. Empson                      F. W. Sanders  
R. E. Yoder

#### Sand Filters

The sand filter studies have been expanded to include three types of sand.<sup>2</sup> The last sand

<sup>2</sup>E. G. Struxness *et al.*, *HP Semiann. Prog. Rep.* Jan. 31, 1956, ORNL-2049, p 40.

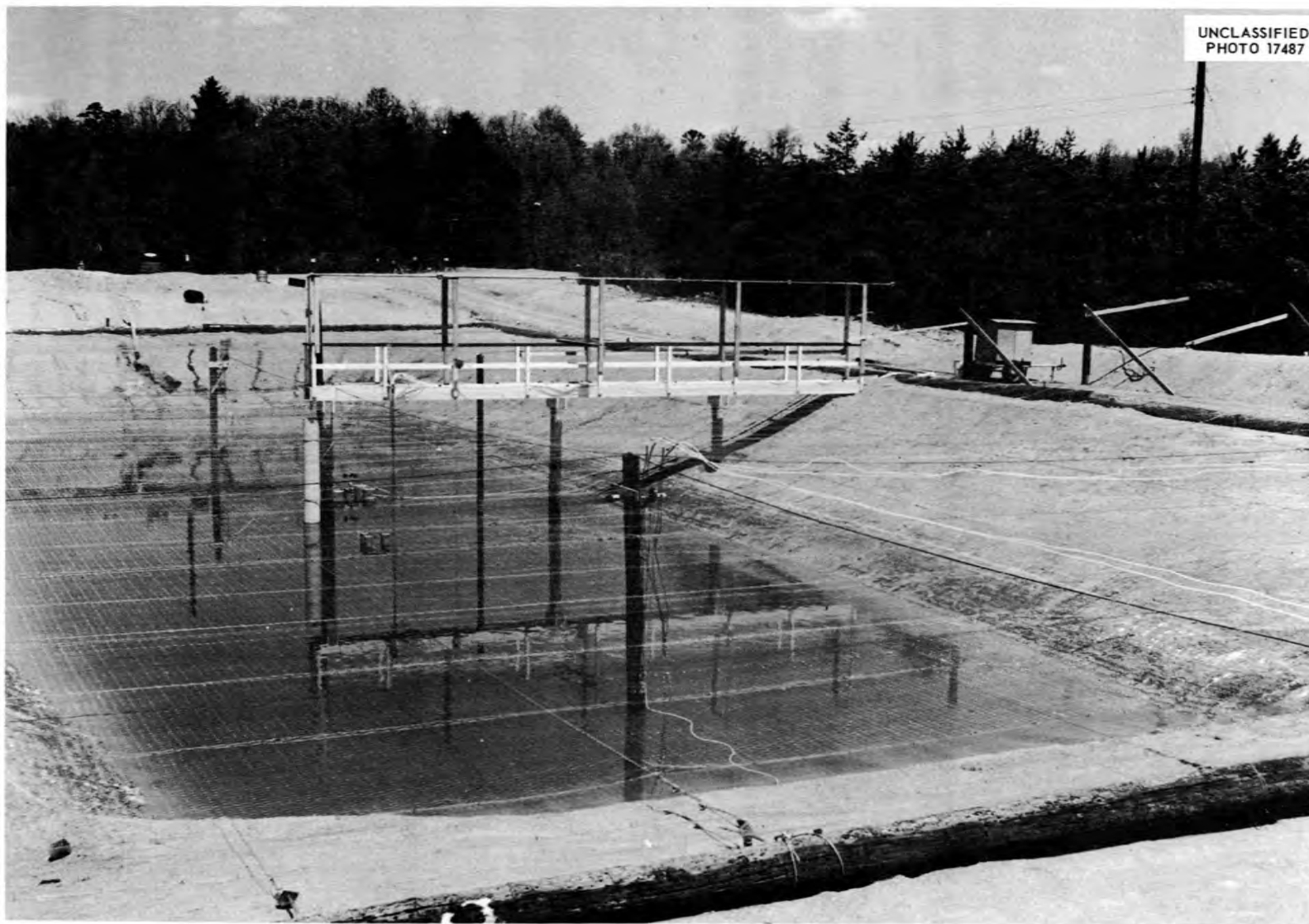


Fig. 27. View of Waste Pit No. 4.

UNCLASSIFIED  
ORNL-LR-DWG 15480A

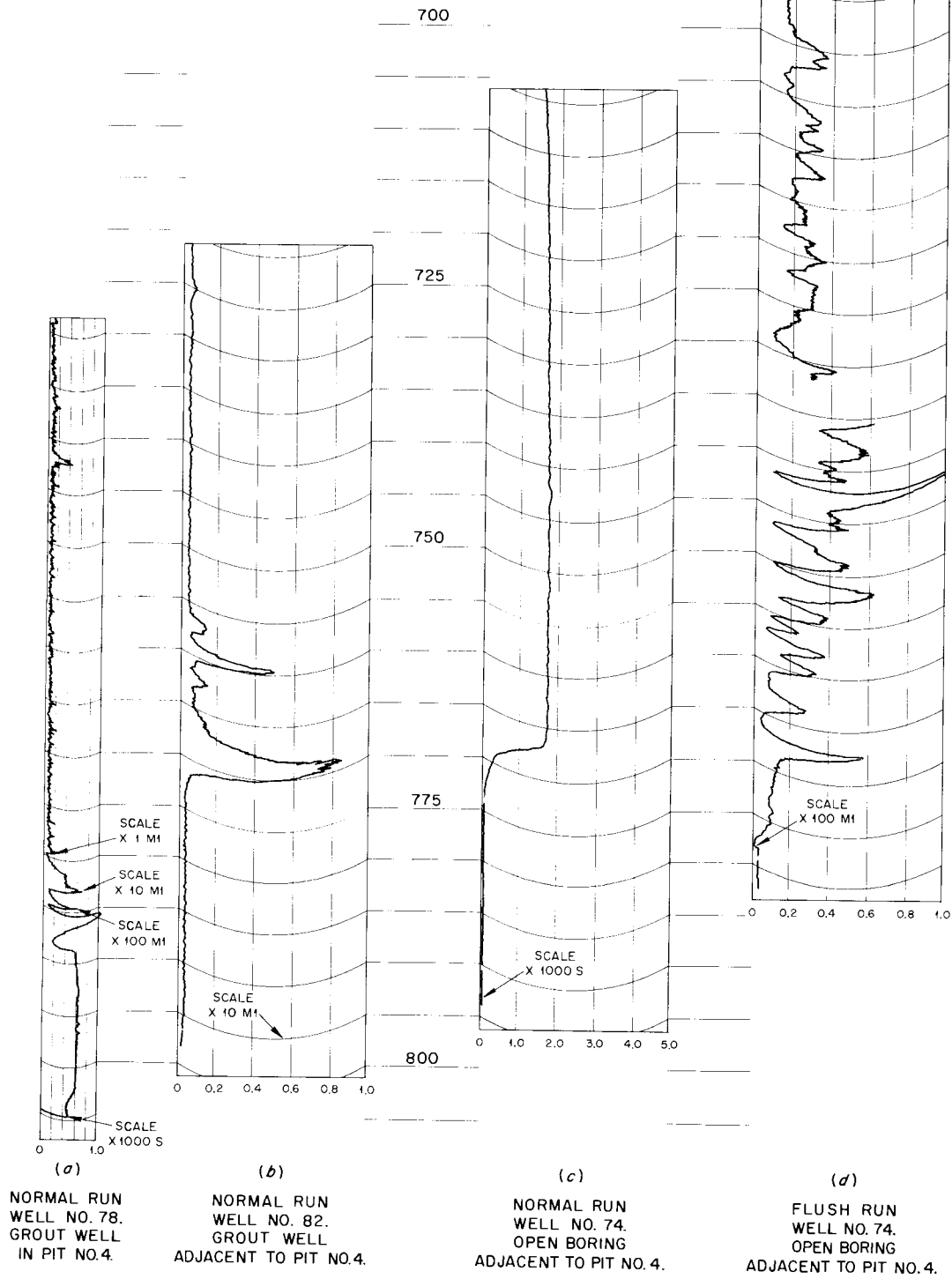


Fig. 28. Radiolog Charts of Pits in or Adjacent to Pilot Pit No. 4.

studied was the Ottawa standard testing sand, ASTM designation C-190. The aerosol size for maximum penetration is in the 0.3 to 0.4  $\mu$  radius range. At a superficial velocity of 0.109 cm/sec through a 7.8-cm-thick bed the aerosol penetration was 13.0% for aerosols flowing up the column and 3.6% for aerosols flowing down the column at the aerosol size for maximum penetration. Complete data are shown in Fig. 29.

The variation of aerosol penetration as a function of velocity is shown in Fig. 30.

#### CHEMISTRY AND SOILS ENGINEERING

G. G. Robeck (USPHS)	H. L. Krieger (USPHS)
B. Kahn (USPHS)	W. J. Lacy (ERDL)
A. Rudnick (USPHS)	M/Sgt. R. R. Rollins
E. R. Eastwood	(ERDL)
M. I. Goldman (USPHS)	

#### Radiochemistry

Precipitation methods for the determination of low levels of radioactive cesium, zirconium, and niobium in water ( $\sim 10^{-8}$   $\mu\text{C}/\text{ml}$ ) have been developed. Cesium is precipitated (from liter volumes)

as cesium ammonium phosphomolybdate or is coprecipitated with sodium potassium cobaltinitrite, the empirical formulas being  $\text{Cs}_{1.8}(\text{NH}_4)_{1.2}\text{PO}_4 \cdot 12\text{MoO}_3$  and  $\text{Cs}_{0.2}\text{K}_{1.9}\text{Na}_{0.9}\text{Co}(\text{NO}_2)_6$ , respectively. The cesium perchlorate precipitate finally obtained from the phosphomolybdate method contains less than 0.01 mg of sodium, phosphorus, molybdenum, or lead – the major probable contaminants – per 10 mg of cesium. The sole significant contaminant found in the final precipitate was potassium, and then only if large amounts of potassium were present in the original solution (see Table 7). The only significant contaminating ion in the perchlorate precipitate obtained from the cobaltinitrite method was potassium, which constituted 4% of the total weight.

The two procedures for the determination of low activities of cesium were tested by having several water samples analyzed by an experienced technician, in the Analytical Chemistry Division, who was previously unacquainted with the procedures. The results summarized in Table 8 indicate that the two methods are equally good.

TABLE 7. POTASSIUM CONTAMINATION IN CESIUM AMMONIUM PHOSPHOMOLBYDATE PROCEDURE

Weight of $\text{K}^+$ in Sample, Added as Chloride (mg)	Weight of $\text{K}^+$ , Recovered as Perchlorate (mg)	Weight of $\text{Cs}^+$ , Recovered as Perchlorate (mg)
2000	2.0	9.2
1500	0.9	8.8
1000	0.4	7.3
250	0.05	14.4
$\sim 5$	0.02, 0.03, 0.01	11.6, 15.3, 11.1

TABLE 8. ANALYSIS OF WATER FOR LOW LEVELS OF  $\text{Cs}^{137}$

Sample	Cesium Added (counts/min/ml)	Cesium Recovered (counts/min/ml)	
		Phosphomolybdate Method	Cobaltinitrite Method
Clinch River at mouth of Emory River	None	0.009 $\beta$	0.015 $\beta$
Clinch River at Clinton	None	0.003 $\beta$	0.005 $\beta$
Synthetic Wichita water	20.0	18.4 $\gamma$	20.6 $\gamma$
Synthetic Augusta water	20.0	18.7 $\gamma$	19.7 $\gamma$
Oak Ridge tap water	20.0	19.0 $\gamma$	18.7 $\gamma$

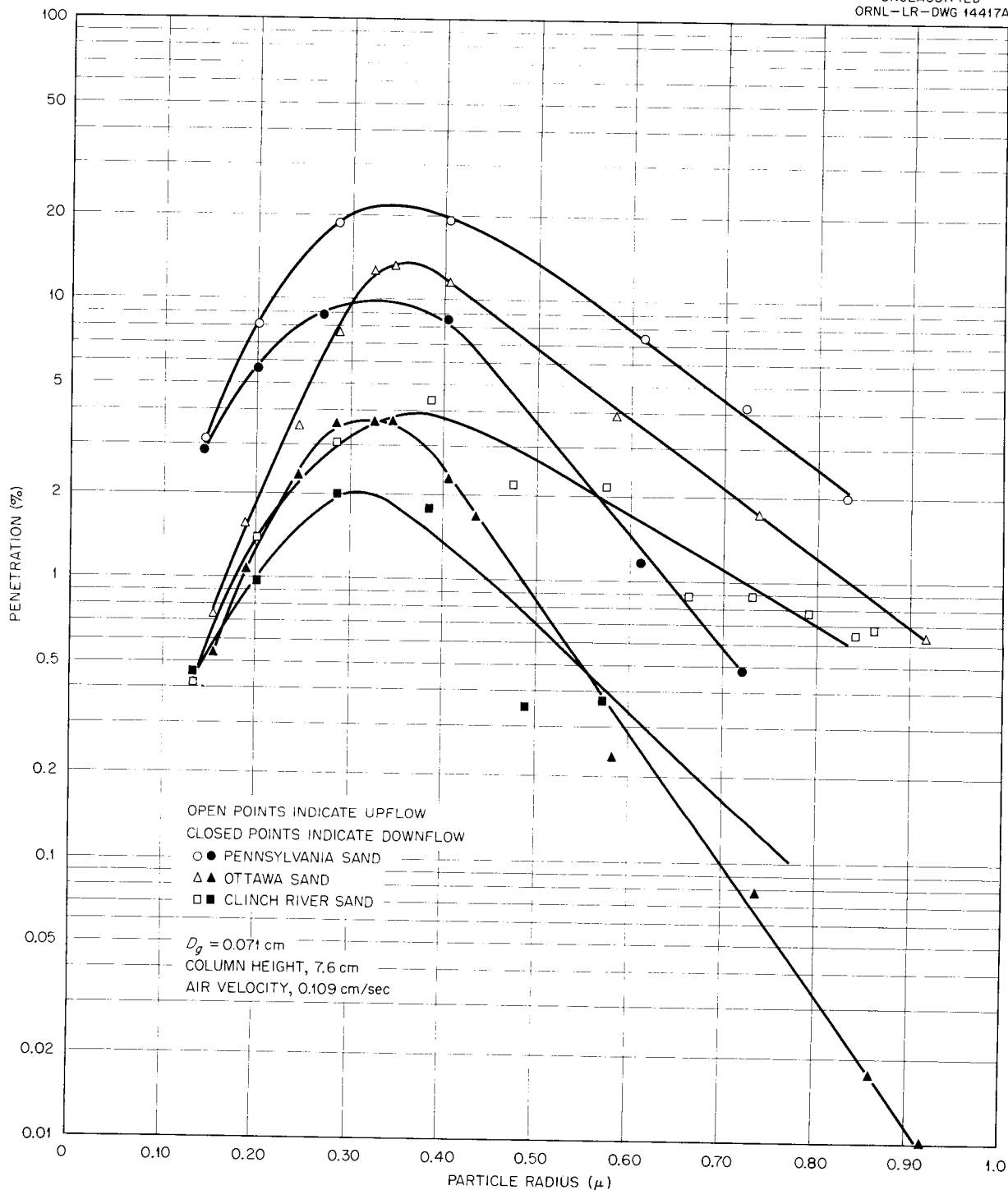


Fig. 29. A Comparison of Filter Sands.

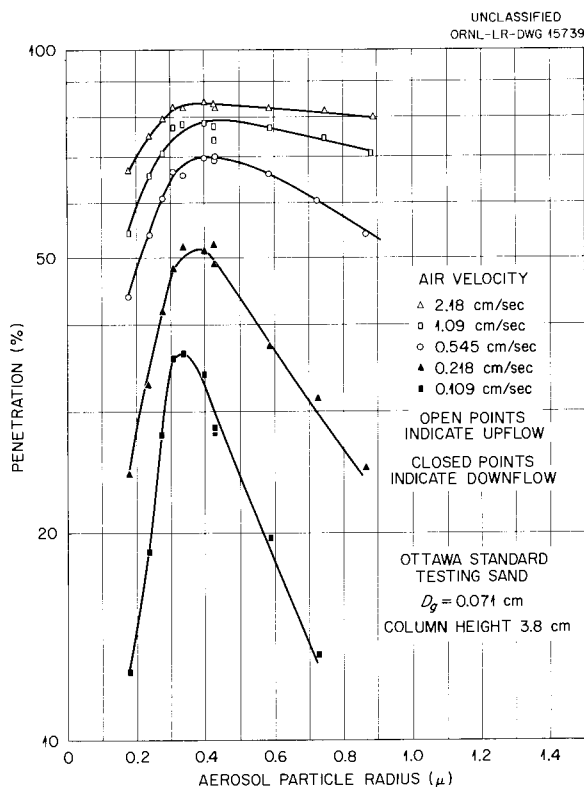


Fig. 30. Filter Performance of Ottawa Standard Testing Sand.

The phosphate precipitation method for zirconium and niobium was tested with other fission products, to determine if satisfactory decontamination of the final zirconium and niobium precipitate could be obtained. Approximately equal amounts of  $Ce^{144}$ ,  $Sr^{90}$ ,  $Y^{90}$ ,  $Cs^{137}$ , and  $Ru^{106}$  were added to water, and the zirconium and niobium precipitation procedure was followed. The average decontamination factors were  $5 \times 10^5$  for the zirconium procedure and  $3 \times 10^5$  for the niobium procedure.

Tap water, to which had been added  $Cs^{137}$  tracer and 20 mg/ml  $Cs^+$  carrier, was passed through a Dowex-50 resin column (50-100 mesh, 85-95% moisture, 5 meq/g dry weight) to determine the feasibility of using ion-exchange resins for concentrating cesium. The minimum amount of resin required per liter of tap water (hardness 90 ppm) acidified with 2 ml of 1 M HCl was 5 g, and 4 g for unacidified water. With an 0.8-cm-dia column and a flow rate of 5 ml/min, at least 99.5% of the cesium in the influent was adsorbed on the column, and more than 99.9% of the adsorbed cesium could

be leached from the column with 10 ml of 6 M HCl.

A sample of soil taken from White Oak Lake in 1955 and analyzed radiochemically at that time was counted on a gamma scintillation spectrometer in order to determine the feasibility of identifying (with that instrument) the radionuclides present. The  $Cs^{137}$  gamma ray (0.66 Mev) and the two  $Co^{60}$  gamma rays (1.17 and 1.33 Mev) could be identified readily and measured in a 10-g sample of the soil, while the 0.13-Mev gamma ray of  $Ce^{144}$  barely could be identified, being only slightly above background.

### Chemical Decontamination of Radioactive Liquid Wastes

Because of the small fraction of  $Sr^{89}$  extracted with tributyl phosphate (TBP) from the "Hope" solution (see Table 10), the composition of this solution was varied in an attempt to increase the extraction. A number of 10-ml aqueous volumes containing 0.01 mg/ml of  $Sr^{++}$  and  $Sr^{89}$  activity were shaken with equal volumes of TBP. The average distribution factor

$$\left( \frac{Sr^{89} \text{ in organic phase}}{Sr^{89} \text{ in aqueous phase}} \right)$$

for 4 consecutive passes listed in Table 9 indicate that extraction of strontium increased with the concentration of  $Al(NO_3)_3$ , but is not large, even from saturated  $Al(NO_3)_3$  solutions.

TABLE 9. DISTRIBUTION FACTOR OF  $Sr^{89}$  BETWEEN AQUEOUS AND TRIBUTYL PHOSPHATE (TBP) PHASES

Aqueous Phase	Distribution Factor Average per Pass
1.0 M $Al(NO_3)_3$	0.06
1.6 M $Al(NO_3)_3$	0.16
2.5 M $Al(NO_3)_3$	0.26
2.5 M $Al(NO_3)_3$ over zinc pellets	0.15
2.5 M $Al(NO_3)_3$ + 1 mg/ml $Sr^{++}$ carrier	0.30
2.5 M $Al(NO_3)_3$ + $Al^{+++}$ → 2.96 M $Al^{+++}$	0.35
3.0 M dibasic aluminum nitrate	0.066
9 M $NH_4NO_3$ in 0.1 M $HNO_3$	0.050
9 M $NH_4NO_3$ in $H_2O$	0.014
9 M $NH_4NO_3$ in 1.0 M $HNO_3$	0.013

HEALTH PHYSICS PROGRESS REPORT

Several other solutions similar to those in Table 9 were investigated but the distribution factors were very nearly zero. These solutions were: 1.6 M  $\text{Al}_2(\text{SO}_4)_3 \cdot 18\text{H}_2\text{O}$ ; 1.6 M  $\text{Fe}(\text{NO}_3)_3 \cdot 9\text{H}_2\text{O}$ ; 1.6 M  $\text{SnCl}_4 \cdot 5\text{H}_2\text{O}$ ; 5 M  $\text{NaNO}_3$ ; 3.5 M  $\text{Ca}(\text{NO}_3)_2$ ; and 3.0 m  $\text{Mg}(\text{NO}_3)_2$ .

Studies on the removal of fission products from the acid  $\text{Al}(\text{NO}_3)_3$  solution with TBP were completed, and results were obtained for four consecutive passes on 50 ml of 1.6 M  $\text{Al}(\text{NO}_3)_3$  plus all carriers with 5 ml of equilibrated TBP, at room temperature, followed by 15 min of shaking are summarized in Table 10.

It was found that the extraction of fresh ruthenium could be enhanced by heating the solution with iron, magnesium, or zinc, while the extraction of zirconium and niobium was improved by the presence of cupferron. Hence, the above procedure was modified by adding 0.1 ml of 6% cupferron to 5 ml of TBP for the first two passes, and heating the aqueous solution with 10 mg of iron before the third and fifth passes. The results of this extraction are given in Table 11.

To recover the solvent for possible re-use and to concentrate further the fission products, back-extractions of the activity were made from 10 ml of TBP by consecutive passes of concentrated  $\text{HNO}_3$ , 0.1 M  $\text{HNO}_3$ , 0.1 M HF in 0.1 M  $\text{HNO}_3$ , and distilled water. The results given in Table 12 indicate good back extraction.

Preliminary to a pilot plant coprecipitation study to be performed jointly with C. D. Watson (Chemical Technology Division), additional tests were made

TABLE 10. PER CENT ACTIVITY REMOVED (CUMULATIVE) FROM ACID ALUMINUM NITRATE SOLUTION BY EXTRACTION INTO 100% TBP

Tracer	1st Pass	2nd Pass	3rd Pass	4th Pass
Aged Ru <sup>106</sup>	60.8	82.4	89.8	92.4
Fresh Ru <sup>106</sup>	3.1	13.3	23.1	27.3
Zr <sup>95</sup> -Nb <sup>95</sup>	72.4	87.2	88.7	88.7
Y <sup>91</sup>	91.2	99.3	99.8	99.96
Sr <sup>89</sup>	5.1	7.7	9.3	10.1
Ce <sup>144</sup> -Pr <sup>144</sup>	86.3	99.0	99.9	99.93

TABLE 11. PER CENT ACTIVITY REMOVED (CUMULATIVE) FROM ACID ALUMINUM NITRATE SOLUTION BY MODIFIED EXTRACTION INTO 100% TBP

Tracer	1st Pass	2nd Pass	3rd Pass	4th Pass	5th Pass	6th Pass
Aged Ru <sup>106</sup>	63.7	83.3	95.8	97.1	97.8	98.1
Fresh Ru <sup>106</sup>	11.7	27.5	90.8	86.5	98.8	99.4
Zr <sup>95</sup> -Nb <sup>95</sup>	91.7	94.5	95.9	96.2	96.2	96.3
Y <sup>91</sup>	90.0	99.2	99.7	99.8	99.9	99.9
Sr <sup>89</sup>	6.1	7.2	7.7	8.2	8.4	8.5
Ce <sup>144</sup> -Pr <sup>144</sup>	84.3	99.0	99.8	99.9	99.92	99.93

TABLE 12. BACK-EXTRACTION OF FISSION PRODUCTS FROM 100% TBP INTO AQUEOUS SOLUTIONS

Tracer	Activity Back-Extracted (%)				Total Activity Back-Extracted (%)
	Concentrated $\text{HNO}_3$	0.1 M $\text{HNO}_3$	0.1 M HF in 0.1 M $\text{HNO}_3$	$\text{H}_2\text{O}$	
Ce <sup>144</sup> -Pr <sup>144</sup>	91.4	8.5	0	0.09	99.99
Y <sup>91</sup>	27.7	67.3	0	5.0	99.99
Ru <sup>106</sup>	96.2	1.1	0	0.1	97.4
Zr <sup>95</sup> -Nb <sup>95</sup>	27.2	17.4	53.8	0.4	98.8

of the removal of fission products from the acid aluminum nitrate solution. Decontamination by means of ammonium phosphomolybdate and zirconium molybdate plus barium sulfate was studied, all removals being listed in Table 13. The procedure consisted of boiling 50 ml of solution with 200 mg ammonium molybdate and 8 mg  $Zr^{4+}$  for 10 min and then filtering. Then 4.4 g of  $(NH_4)_2 SO_4$ , 1.9 g of  $Ba(NO_3)_2$ , 0.05 ml of  $H_3PO_4$ , and an additional 200 mg ammonium molybdate were added to the solution, which was then boiled 30 min and filtered.

TABLE 13. REMOVAL OF FISSION PRODUCTS FROM ACID ALUMINUM NITRATE SOLUTION BY COPRECIPITATION

Radionuclide	Cumulative Removal (%)	
	Molybdate	Sulfate
$Cs^{137}$	19	96
$Sr^{89}$	14	94
$Y^{91}$	10	94
$Ce^{144}$	7	99.94
$Ru^{106}$ (fresh)	70	75
$Ru^{106}$ (old)	10	25
$Zr-Nb^{95}$	98	99

#### Soil Exchange Studies

Column tests with Conasauga shale were initiated in order to develop a method of determining cation exchange capacity (CEC) by using radioactive  $Cs^{137}$  as tracer, and to note the effect, if any, of aggregate size on the CEC. Considerable effort was expended in setting up instruments to measure and record continuously effluent activity and to improve reproducibility. Some question had been raised about differences in exchange capacity determined by using initially dry columns and those in which the voids are originally filled with water, so comparison studies were made on both dry and "wet" columns.

The CEC was determined in these tests by calculating the difference between the activity of the applied solution and the mean activity of the effluent. This was done both graphically from the recorder charts and by sampling aliquots of the raw and effluent solutions. For the "initially

water-saturated" series, instrumentation of questionable reliability was used. With one exception, the exchange capacity was never saturated. In general, the ratio of effluent to initial activity increased to about 0.95, as measured by the continuous monitor, and then remained constant. Perhaps this was due to continued  $Ba^{137}$  adsorption in the column after cesium saturation had been reached. This belief has been tentatively supported by measurements made on aliquots of several effluents by using a G-M counter and a scintillation counter.

The results are summarized in Table 14. The listed CEC was calculated at the volume at which the maximum per cent was first achieved. The solution used was 0.05 M CsCl, pH 7.0, tagged with  $Cs^{137}$ ; 10 g of soil was used, and the superficial flow rate was 0.5 ml/min. The cation-exchange capacities of duplicate 10-20 and 40-80 mesh portions of Conasauga shale and of a special sample submitted by the USGS were determined by the standard ammonium-acetate method. The results are summarized in the following:

	Cation Exchange Capacity (meq/100 g)
Conasauga shale, 10-20 mesh	20.0-20.0
Conasauga shale, 40-80 mesh	20.6-20.8
Special soil sample, ungraded	8.0-8.4

It can be seen by comparing these values with those in Table 14 that the CEC as determined by the cesium method is less than the standard value by a factor of almost 2.

Several of the columns used in the method-development study were eluted to determine if additional uptake occurred on standing for a period of about two months. The feed solution was eluted with benzene, the volume and activity of the aqueous eluant were measured, and the additional sorption was calculated. Anomalous results were obtained.

A status report was prepared which summarized the work on the development of a method for determining soil-cation-exchange capacity by using tracers.

Additional uptake studies have been initiated by using aqueous fission product solution and Conasauga shale to evaluate column parameters developed in the earlier series of uptake studies in

TABLE 14. RESULTS OF PRELIMINARY TESTS TO DETERMINE EFFECT OF AGGREGATE SIZE ON CEC OF CONASAUGA SHALE

Aggregate Size			Maximum Passing Obtained (%)*				Volume to Achieve Maximum Value of Per Cent Pass (ml)				CEC (meq/100 g)			
Pass Sieve No.	Retained on Sieve No.	Log Mean Size (mm)	Dry Run		Wet Run		Dry Run		Wet Run		Dry Run		Wet Run	
			a	b	c	d	a	b	c	d	a	b	c	d
6	8	2.82	94	95	96.5	89	100	135	120	75	11.2	11.5	12.0	11.0
10	20	1.3	95	95	99	100	60	70	75	110	12.0	12.0	11.5	12.0
20	40	0.59	95	96.5	94	94	80	60	65	75	13.0	12.5	11.8	13.0
40	80	0.282	95	95	95	90	50	70	70	75	13.0	13.0	13.8	11.0

$$*\text{Per Cent Passing} = \frac{\text{instantaneous effluent activity}}{\text{initial activity}} \times 100$$

which a fixed volume of waste solution was passed through soil columns of increasing length. The parameter used was the soil weight contacted per waste volume applied, or gram of soil per milliliter of waste solution. In the latest studies, in which both soil weight and waste volume were varied, the universality of this parameter was tested and found to be not so general as had been formerly thought.

A sample of intermediate-level liquid waste from waste pit No. 2 was passed through 10 g of 40–80 mesh Conasauga shale at a rate of 1 ml/cm<sup>2</sup>/sec in an effort to obtain a quantitative measure of the uptake of cesium by the soil and the nonabsorption of ruthenium, an effect being noted in the field. The Ru<sup>106</sup> appeared immediately in the effluent, together with an unknown flocculent material formed by reaction between the soil and solution. The volume throughput before Cs<sup>137</sup> first appeared in the effluent was about 1.7 liters (or about 170 column volumes) and about 4.4 liters for an activity effluent to activity influent ratio of 0.865.

#### Leaching of Fission Products from Shale by Tap Water

A laboratory test procedure was used to determine the rate and amount of radioactive material that could be leached from contaminated shale by tap water. The leaching results may be applicable to the pit disposal method of waste treatment. An analysis of the shale used in the tests is shown in Table 15. This shale material was chosen

TABLE 15. PROPERTIES OF OAK RIDGE SHALE\*

Conasauga Shale of the Middle Cambrian Age,  
Excavated from Liquid Waste Pit No. 2

Mechanical Composition		
Grain Size (mm)	Description	Per Cent
0.25–0.125	Fine sand	0.23
0.125–0.06	Very fine sand	0.92
0.06–0.002	Silt	86.7
0.002 or less	Clay	12.2
	Loss on acid treatment	19.4
Base Exchange Capacity		
28.6 meq per 100 g		
Electron Microscope Examination		
Mica-type mineral		
Quartz		
Halloysite (small amount)		
Kaolin group mineral (none detectable)		

\*Analysis by Geochemistry and Petrology Branch, Geological Survey, U.S. Dept. of Interior, Washington, D.C.

because it was from the site of the excavation for the second radioactive liquid seepage pit at ORNL.

The shale was initially contaminated by slurring for 90 min 0.5 g of shale with 500 ml of tap water contaminated with the particular radioisotope to be studied. The concentration of activity per gram of

shale was between  $1$  to  $3 \times 10^6$  counts/min. This value was determined from the initial concentration of activity (4000-6000 counts/min/ml) in the tap water and, the per cent removal of radioactivity from the water by clay slurring.

The decontaminated water was decanted from each beaker, after which the clay was allowed to air-dry for 24 hr. It was then added to a 280 ml (10 oz) glass sample bottle containing 250 ml of Oak Ridge tap water. Each bottle was shaken for 2 min daily for 40 days. Triplicate aliquot samples of the supernatant were removed from each bottle from time to time, dried under an infrared lamp, and counted in a gas-flow internal proportional counter. To avoid picking up clay particles during sampling, all samples were taken before the bottles were shaken. The samples were dried in aluminum dishes, and the approximate counting efficiency for the radioisotopes studied was about 50%. The

radioisotopes and their daughter products had reached equilibrium before the samples were counted. The counts per minute per milliliter for the samples were considered significantly different from zero when compared with the values from a 0.95 confidence level nomograph.

The radioactive isotopes studied were  $Ce^{144}$ ,  $Pr^{144}$ ,  $Ba^{140}$ ,  $La^{140}$ ,  $Ru^{106}$ ,  $Rh^{106}$ , and  $Zr^{95}$ - $Nb^{95}$ .

The results obtained are shown in Fig. 31. In discussing the behavior of the radioisotopes in soil it is convenient to treat them in groups - the radioisotopes that behave alike chemically being considered as a group.

*Cerium, Praseodymium, Zirconium, and Niobium.* - In soils that give soil- $H_2O$  solutions in the neutral or alkaline range (pH 6-8.5), these four elements would be fixed as insoluble oxides or hydroxides and, for this reason, would leach or diffuse extremely slow. In acid soils (soil solution pH 4-6),

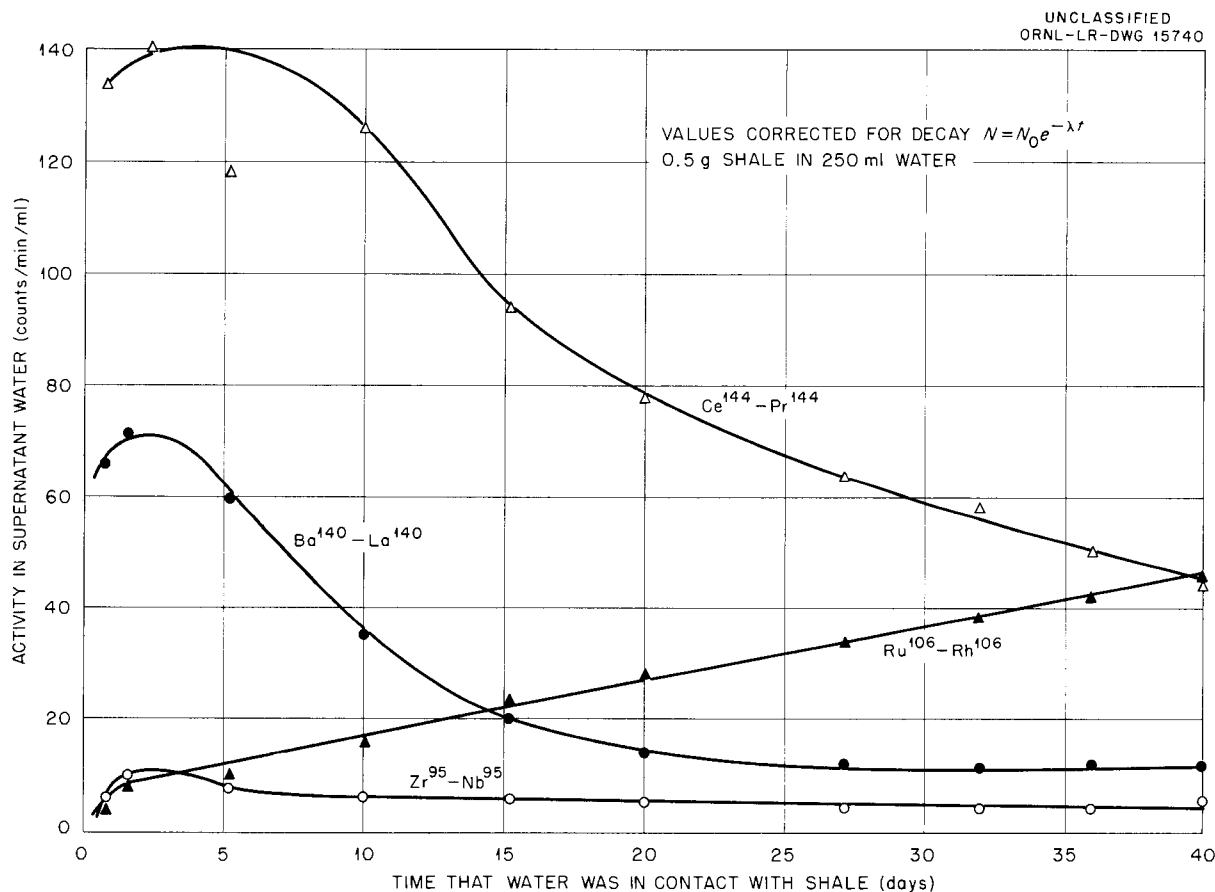


Fig. 31. Leaching Effect of Tap Water on Contaminated Shale.

## HEALTH PHYSICS PROGRESS REPORT

some of the elements similar to these may exist as polyvalent cations, which in general are strongly fixed by clay particles in an immobile form. The results indicate that  $Ce^{144}$ - $Pr^{144}$  gave the highest count rate in the supernatant liquid and  $Zr^{95}$ - $Nb^{95}$  gave the lowest. A possible explanation for the high initial activity of  $Ce^{144}$ - $Pr^{144}$  may be contamination of the tap water during the addition of the shale material.

*Barium and Strontium* (not studied). - These are alkaline earth elements and may be soluble in the soil solution of acid as well as alkaline soils. However, they would be present as divalent cations and would tend to be strongly fixed by the clay particles. For this reason, they would diffuse very slowly.

*Ruthenium*. - It would be expected that this element would be reduced by soil organic matter to the free metal and, as such, not diffuse. However, in varying degrees, this element would exist as an anion in the soil. In general, the  $RuO_4^{--}$  ion is not fixed by clays, and, consequently, it might be expected to be mobile in soil systems. In this study the ruthenium as a cation was adsorbed on to the clay during slurring, from an equilibrium mixture of ruthenium anions and cations. As the graph in Fig. 31 indicates, some of the ruthenium cations are going into solution, probably as the ruthenate anions.

It is evident from the above discussion that the fate of this element in the soil is not completely understood, because of the complex chemistry of ruthenium.

RADIATION DOSIMETRY

G. S. Hurst R. H. Ritchie

EXPERIMENTAL PHYSICS OF DOSIMETRY

R. D. Birkhoff C. C. Sartain  
 T. E. Bortner B. G. Saunders  
 J. S. Cheka W. G. Stone  
 H. H. Hubbell H. P. Yockey

Health Physics Division

F. N. Huffman H. J. Moe  
 R. M. Johnson T. B. Smiley  
 AEC Fellows in Radiological Physics

Electron Attachment in Gas Mixtures Containing O<sub>2</sub>

In the study of electron attachment in gases, new pulse-height data for various partial pressures of O<sub>2</sub> and N<sub>2</sub> have been obtained, and the attachment coefficient of electrons in O<sub>2</sub>-N<sub>2</sub> mixtures have been determined. The curves obtained are very similar to the ones shown in the previous report,<sup>1</sup> except that the new curves were taken for a 9.0-cm

source-to-collector separation, while the previous ones were for a 6.0-cm separation. Even though N<sub>2</sub> is nonattaching, the attachment coefficient  $\alpha$  (probability of attachment per centimeter in the electric field direction and per millimeter of mercury of the attaching gas) for O<sub>2</sub> depends on the partial pressure of O<sub>2</sub> and on the partial pressure of N<sub>2</sub>. Fig. 32 shows  $\alpha$ , for various values of  $E/P$ , as a function of oxygen partial pressure. These data were obtained for 40-cm total pressure and with a 9.0-cm distance of electron travel in the field direction. Very similar data were obtained for the 6.0-cm separation, ruling out the possibility of nonuniform attachment phenomena.

The variation of the attachment coefficient with pressure of N<sub>2</sub> is shown in Fig. 33 for one particu-

<sup>1</sup>G. S. Hurst et al., *HP Semiann. Prog. Rep. Jan. 31, 1956*, ORNL-2049, p 48, Fig. 24.

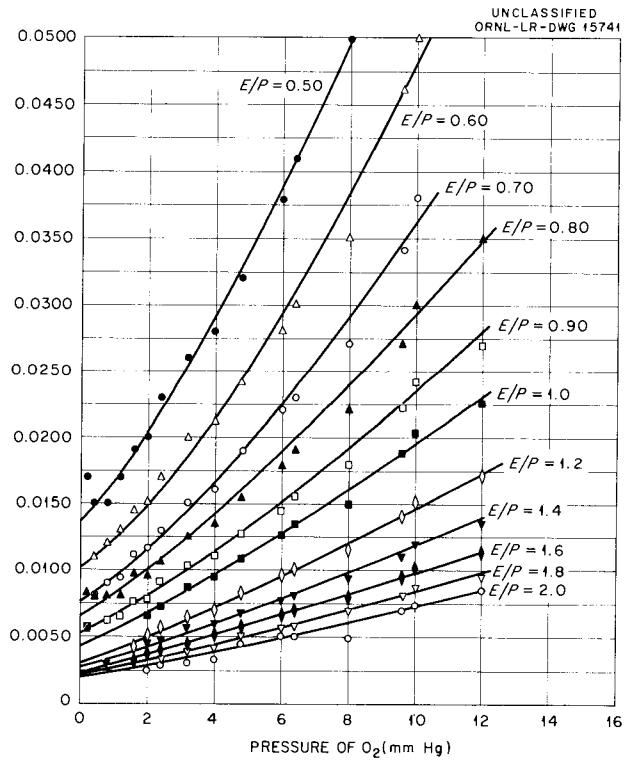
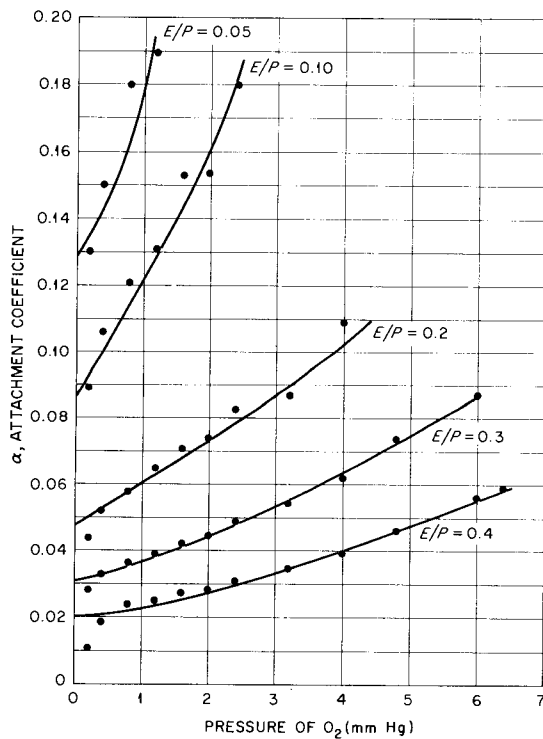


Fig. 32. Variation of  $\alpha$  with Pressure of O<sub>2</sub> for Various Values of  $E/P$ . Pressure of N<sub>2</sub> is 40 cm Hg. Source to collector is 9.0 cm.

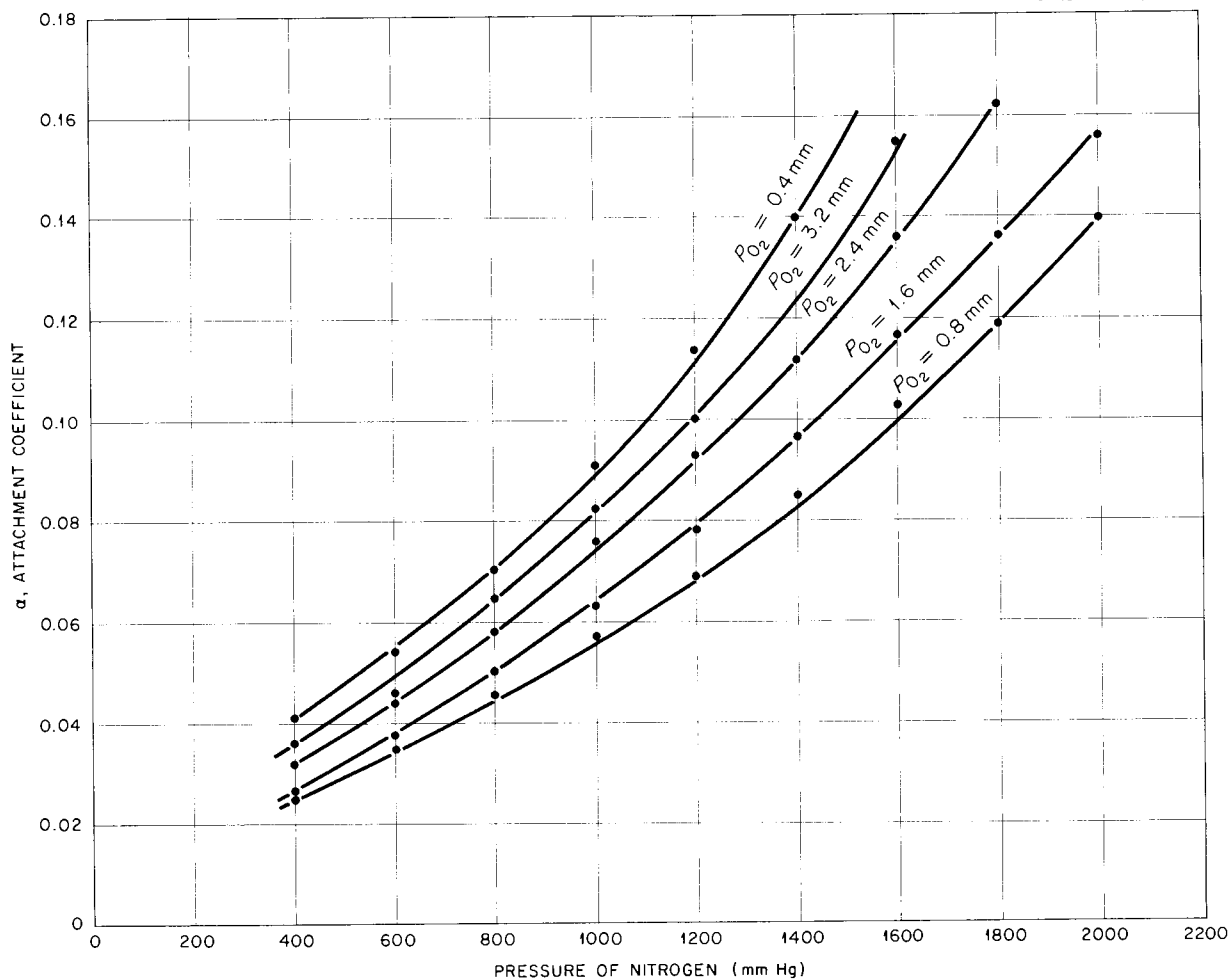


Fig. 33. Variation of  $\alpha$  with Pressure of  $N_2$  for Various Pressures of  $O_2$ .  $E/P = 0.40$ . Source to collector is 9.0 cm.

lar value of  $E/P = 0.4$ , and for various partial pressures of  $O_2$ .

#### Studies of Radiation Effects on Organic Material

A cryostat for bathing samples continuously in liquid nitrogen or other heat-transfer liquids during nuclear-reactor irradiation has been completed and successfully operated. In this low-temperature irradiation facility various cuts of single crystals of piezoelectric substances have been exposed to neutron fluxes from approximately  $3 \times 10^{15}$  neutrons/cm<sup>2</sup> to approximately  $6 \times 10^{16}$  neutrons/cm<sup>2</sup>.

Preliminary results indicate that approximately  $6 \times 10^{16}$  neutrons/cm<sup>2</sup> produce considerable cracking and discoloring of Rochelle salts, ammonium

dihydrogen phosphate, potassium dihydrogen phosphate, and sodium chlorate.

Single crystals of sodium chlorate have been irradiated in a bath of liquid nitrogen. Single crystals of potassium dihydrogen phosphate, which shatter at the temperature of liquid nitrogen, have been irradiated while held in a bath of alcohol at dry-ice temperature. The changes in the crystals caused by radiation are now being measured. Single crystals of ammonium dihydrogen phosphate and Rochelle salts will be studied next. In each case, a sufficient number of cuts of each crystal are irradiated and measured in order to provide the data to calculate all elastic and electrical constants of the substance.

### Ionization in Gas Mixtures by Alpha Particles

There is general interest in the studies of ionization produced by alpha particles in gas mixtures. Radiochemists have special interest in these studies when one of the gas components (for example, acetylene) readily polymerizes due to ionization. For this reason, a study was made of the amount of ionization produced by  $\text{Pu}^{239}$  alpha particles in several gas mixtures, most of which had acetylene as one component. With the exception of one case (to be discussed below) the number of ion pairs per electron volt ( $1/W_m$ ) is given by

$$(1) \quad \frac{1}{W_m} = \left( \frac{1}{W_1} - \frac{1}{W_2} \right) Z + \frac{1}{W_2},$$

where  $Z = P_1/P_1 + aP_2$  and  $W_1$  and  $W_2$  are constants for the two gas components having respective pressures of  $P_1$  and  $P_2$ . The constant  $a$  is determined empirically for each of the mixtures. Table 16 summarizes the data for the mixtures. The straight lines in Figs. 34-42 show the good

agreement between experimental values and the above formula. The other curve in the figures is a plot of the Huber *et al.*<sup>2</sup> formula and shows the

<sup>2</sup>P. Huber, E. Baldinger, and W. Häeberli, *Helv. Phys. Acta.* 23, Supp. 3 (1950).

TABLE 16. CONSTANTS FOR THE GAS-MIXTURE EQUATION

Gas Mixture	$(1/W_1) \times 10^3$	$(1/W_2) \times 10^3$	$a$
$\text{N}_2 + \text{C}_2\text{H}_2$	27.5	36.1	0.265
$\text{CO}_2 + \text{C}_2\text{H}_2$	29.1	36.1	0.927
$\text{CH}_4 + \text{C}_2\text{H}_2$	34.3	36.1	0.386
$\text{N}_2 + \text{CH}_4$	27.5	34.3	0.617
$\text{He} + \text{C}_2\text{H}_2$	33.0	36.1	0.058
$\text{C}_2\text{H}_2 + \text{A}$	36.1	49.3	3.420
$\text{C}_6\text{H}_6 + \text{A}$	36.3	44.8	5.380
$\text{CH}_4 + \text{A}$	34.3	38.8	2.000
$\text{C}_2\text{H}_2 + \text{C}_6\text{H}_6$	36.1	36.2	

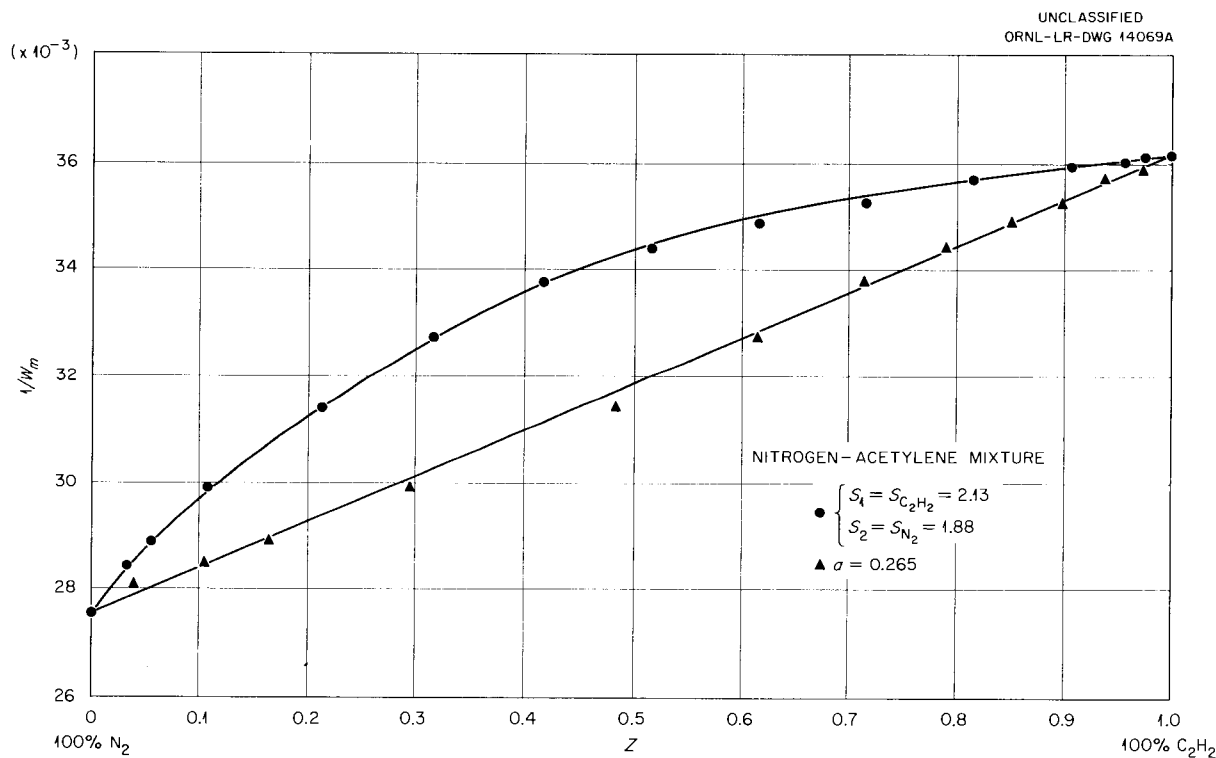


Fig. 34. Relative Ionization ( $1/W_m$ ) Produced by  $\text{Pu}^{239}$  Alpha Particles in Nitrogen-Acetylene Mixtures.

UNCLASSIFIED  
ORNL-LR-DWG 14643A

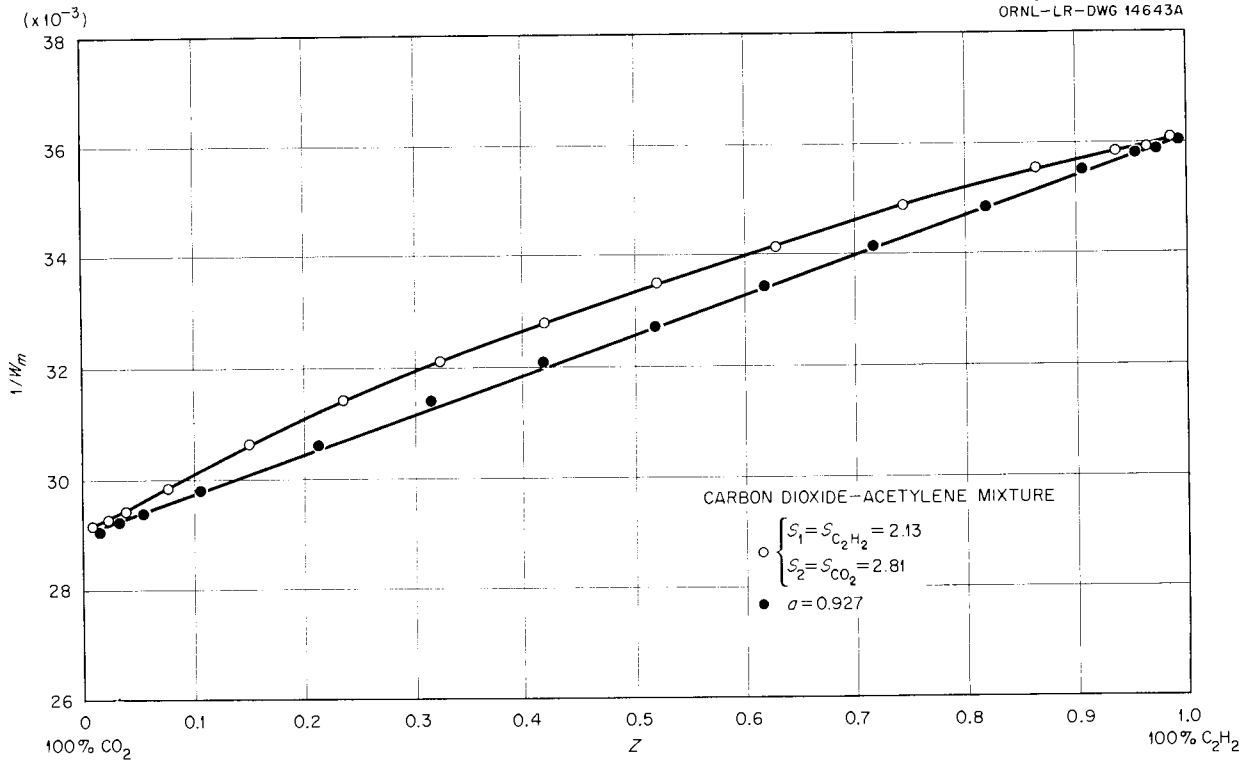


Fig. 35. Relative Ionization ( $1/W_m$ ) Produced by  $Pu^{239}$  Alpha Particles in Carbon Dioxide-Acetylene Mixtures.

UNCLASSIFIED  
ORNL-LR-DWG 14644A

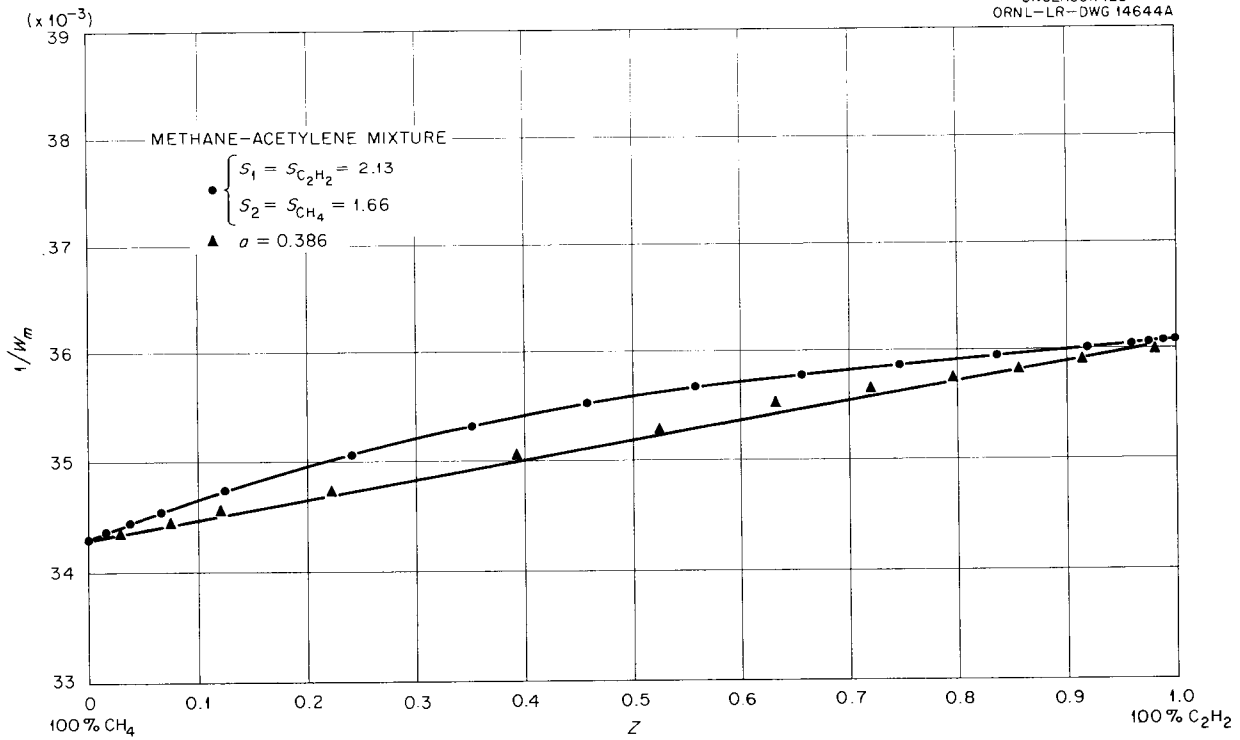


Fig. 36. Relative Ionization ( $1/W_m$ ) Produced by  $Pu^{239}$  Alpha Particles in Methane-Acetylene Mixtures.

UNCLASSIFIED  
ORNL-LR-DWG 14645A

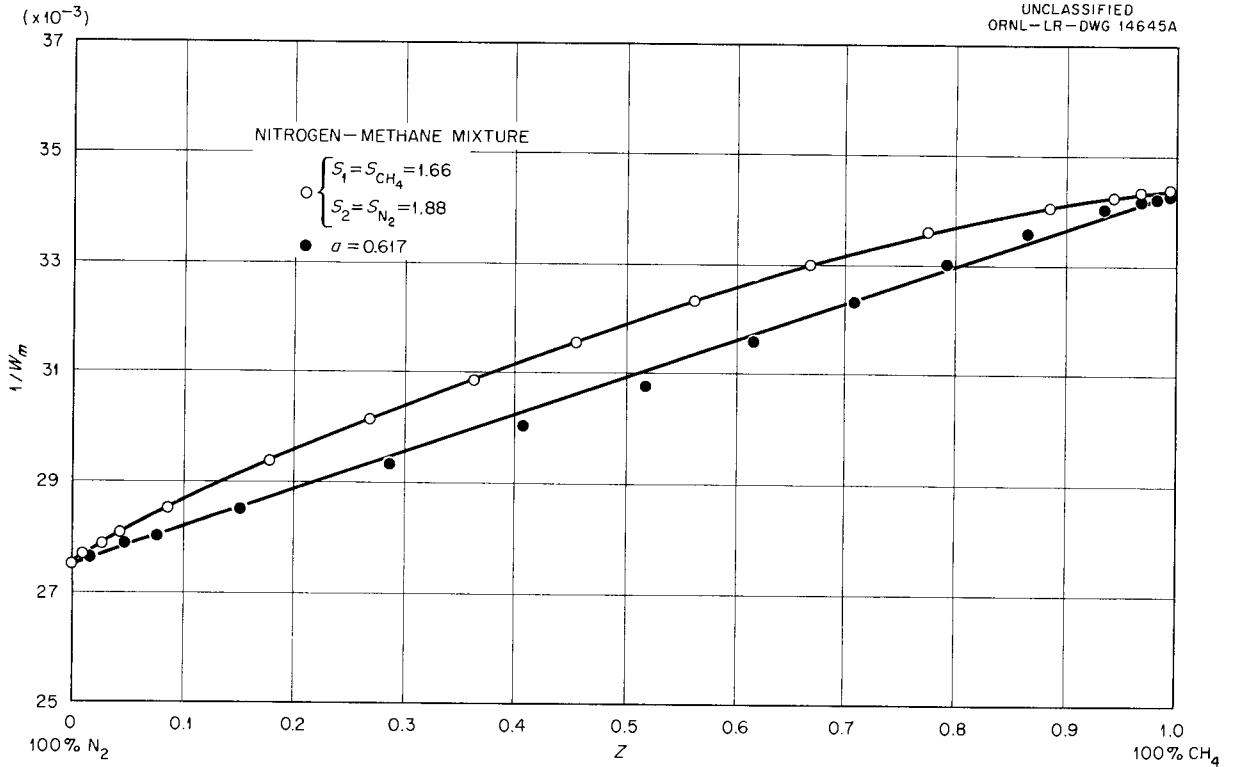


Fig. 37. Relative Ionization ( $1/W_m$ ) Produced by  $\text{Pu}^{239}$  Alpha Particles in Nitrogen-Methane Mixtures.

UNCLASSIFIED  
ORNL-LR-DWG 14646A

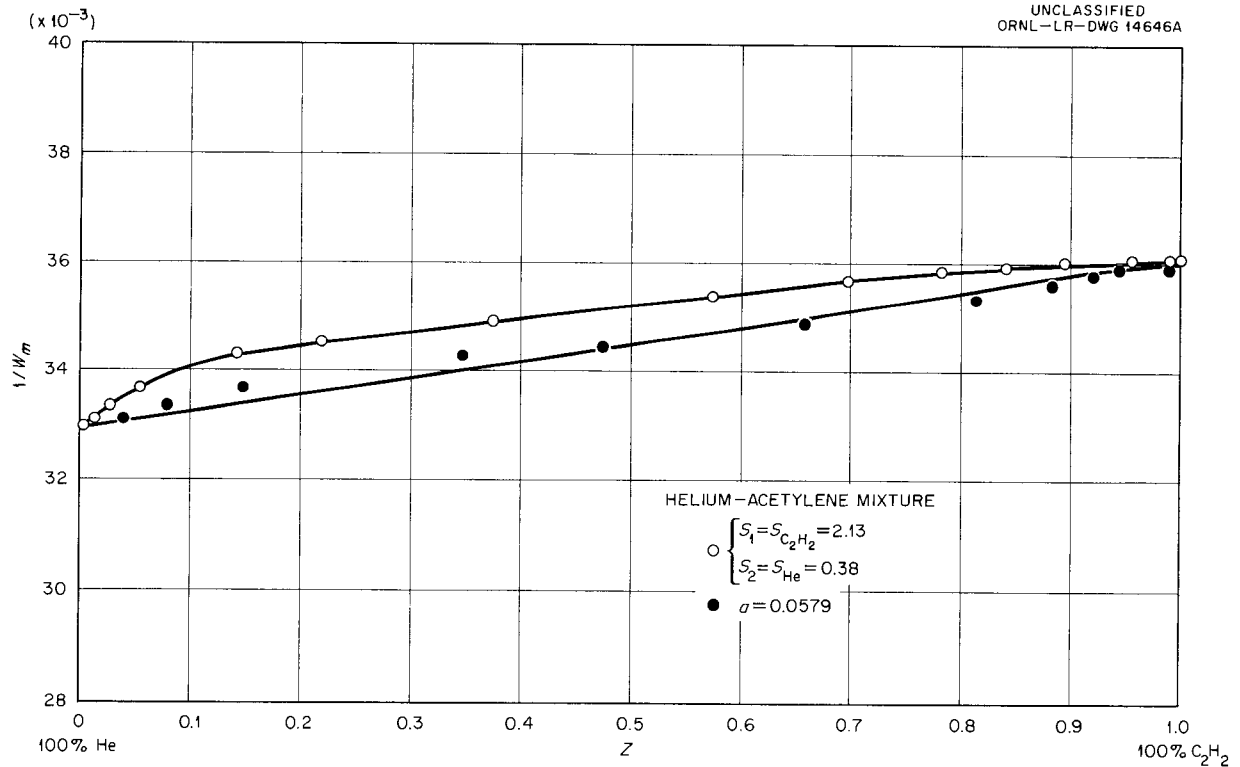


Fig. 38. Relative Ionization ( $1/W_m$ ) Produced by  $\text{Pu}^{239}$  Alpha Particles in Helium-Acetylene Mixtures.

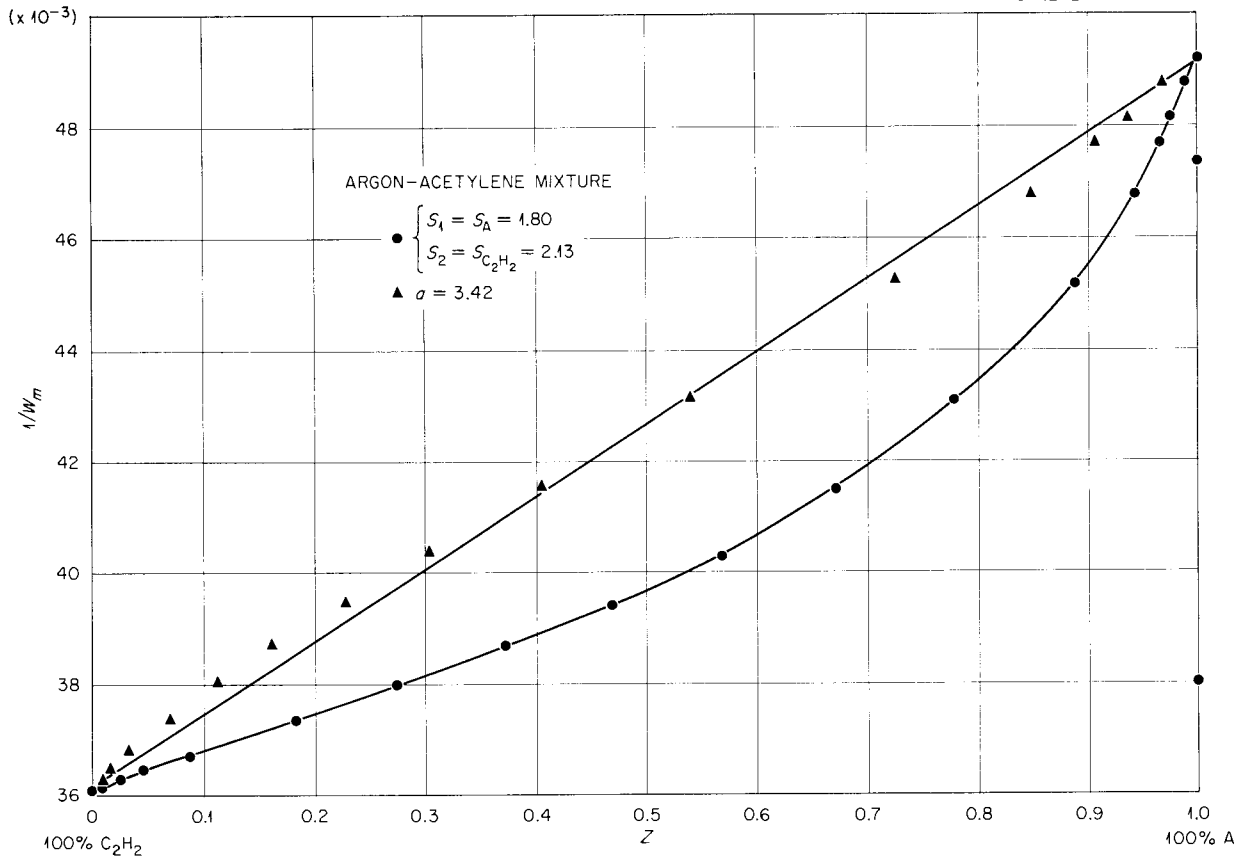


Fig. 39. Relative Ionization ( $1/W_m$ ) Produced by  $Pu^{239}$  Alpha Particles in Argon-Acetylene Mixtures.

discrepancy between experimental data and their formula. Their formula holds when  $a$  is equal to the ratio of stopping powers of the two gases; that is,  $a = S_2/S_1$ .

The data obtained for the mixture  $Ne + C_2H_2$  (Fig. 43) did not fit the above equation (Eq. 1). The sudden decrease in ionization current as the  $C_2H_2$  in the mixture increased to 10%  $C_2H_2$  indicates that some nonionizing process is using the energy of the neon metastable state. Though several possible explanations come to mind, none is offered here until more data have been obtained for neon mixtures.

#### Spatial Distribution of Energy Absorbed from an Electron Beam Penetrating Aluminum

Studies of the absorbed-dose distribution with depth in a solid bombarded with an electron beam have been completed. The beam introduced into an infinite medium is scattered and absorbed as the

electrons slow down, and the ionization produced by the beam in a planar air cavity perpendicular to the initial beam direction is a measure of the spatial rate of energy dissipation at various distances from the plane of incidence. Ions were produced in the layer of air by the passage of forward-scattered electrons and secondaries and were collected by the action of an electrostatic field impressed across the cavity. The layer of air serving as the cavity could be put at various depths in the slab by changing the thickness of a foil which formed the initial absorbing layer. Before striking the foil the beam was directed through a small hole which subtended a small solid angle to minimize the loss of electrons backscattered from the absorbing material. Thus all incident electrons which struck the slab were accounted for, and backscattered electrons could be rescattered into the slab and produce additional ionization. The electron beam was produced by a small

UNCLASSIFIED  
ORNL-LR-DWG 14649A

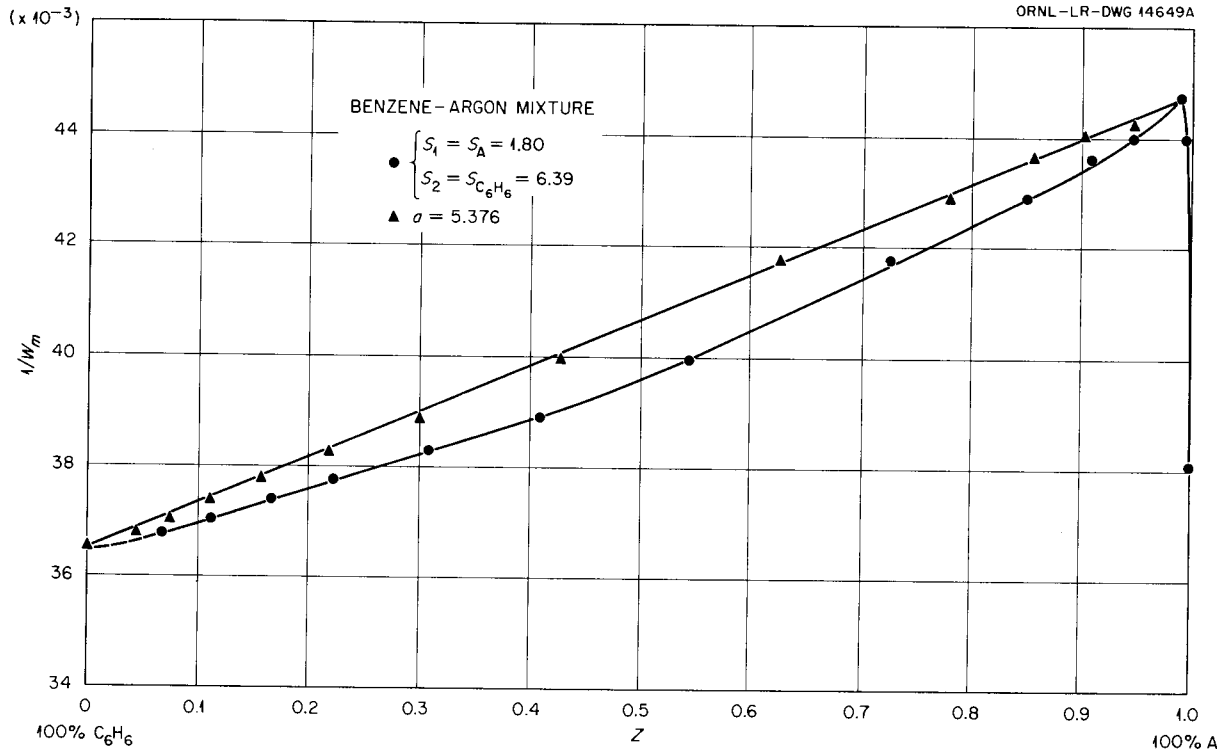


Fig. 40. Relative Ionization ( $1/W_m$ ) Produced by  $Pu^{239}$  Alpha Particles in Benzene-Argon Mixtures.

UNCLASSIFIED  
ORNL-LR-DWG 14650A

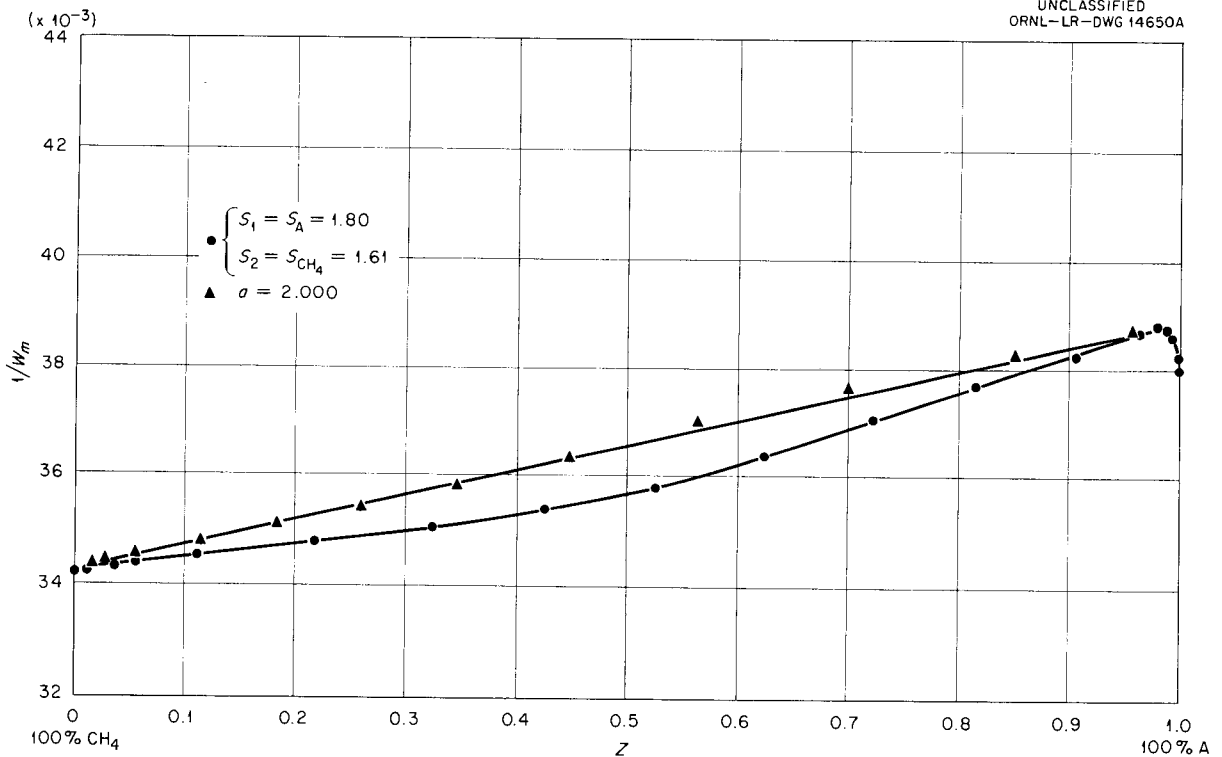


Fig. 41. Relative Ionization ( $1/W_m$ ) Produced by  $Pu^{239}$  Alpha Particles in Argon-Methane Mixtures.

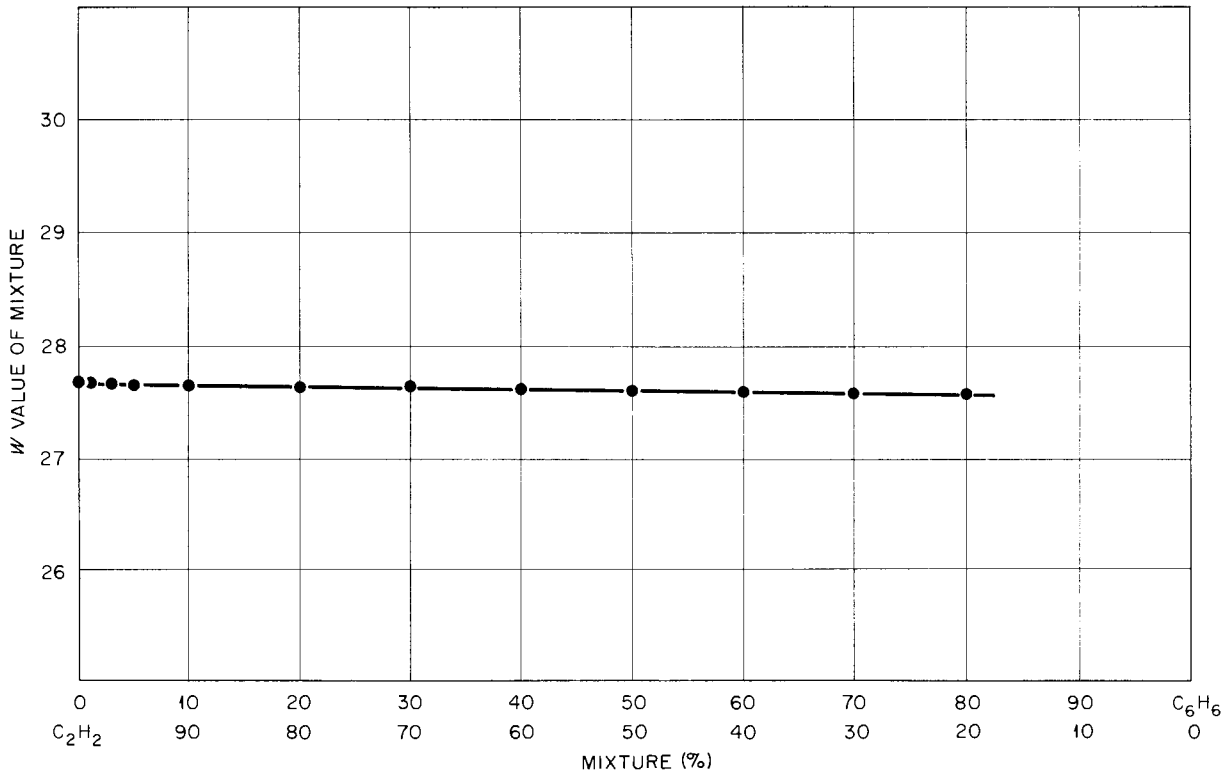


Fig. 42. Graph of  $W$  Value for Acetylene-Benzene Mixtures vs Per Cent Mixture.

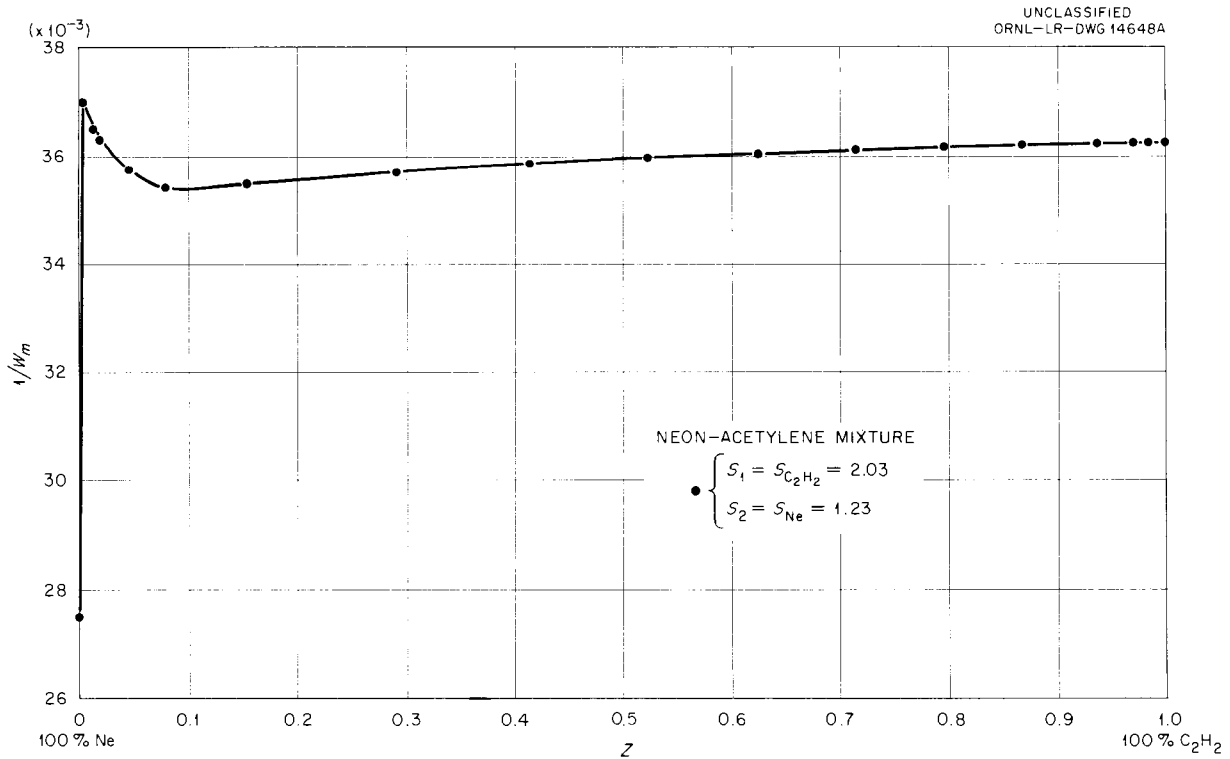


Fig. 43. Relative Ionization ( $1/W_m$ ) Produced by  $Pu^{239}$  Alpha Particles in Neon-Acetylene Mixtures.

electron accelerator which provided a collimated monoenergetic beam at any energy between 0 and 126.5 keV. The experiment yields the ratio of ion current to beam current, and this ratio may be converted to energy dissipated per unit distance by multiplying by various conversion coefficients and the value of  $W$ , the average energy required to create an ion pair. A  $W$  value of 34 eV per ion pair was taken from the data of Jesse and Saudauskis.<sup>3</sup> The converted data are shown in Figs. 44, 45, 46, and 47 for the incident energies of 57, 80, 104, and 126.5 keV, respectively. The points in the graphs are experimental values. Also given (solid line) is the theoretical distribution in each case as calculated from the theory of Spencer.<sup>4</sup>

Agreement is within experimental error except at the deeper penetrations where the experimental

values are consistently below those given by the theory. A possible increase in  $W$  at low electron energies may account for this discrepancy. If the depth-dose distributions at the above energies are combined with those at higher energies, it appears that a universal depth-dose curve can be obtained which will be of use in electron beam therapy and in exposure calculations in Health Physics. The similarity in shape of the depth-dose curves for various incident energies is seen in Fig. 48, where the results of the present work are plotted along with data taken by Frantz<sup>5</sup> (0.5 MeV) and Trump *et al.*<sup>6</sup> A complete account of this investigation appears elsewhere.<sup>7</sup>

<sup>5</sup>F. Frantz, private communication, quoted in L. V. Spencer, *Phys. Rev.* 98, 1597 (1955).

<sup>6</sup>J. G. Trump, K. A. Wright, and A. M. Clarke, *J. Appl. Phys.* 21, 345 (1950).

<sup>7</sup>F. N. Huffman, *Spatial Distribution of Electron Depth Dose in Aluminum*, ORNL-2137 (Aug. 1, 1956).

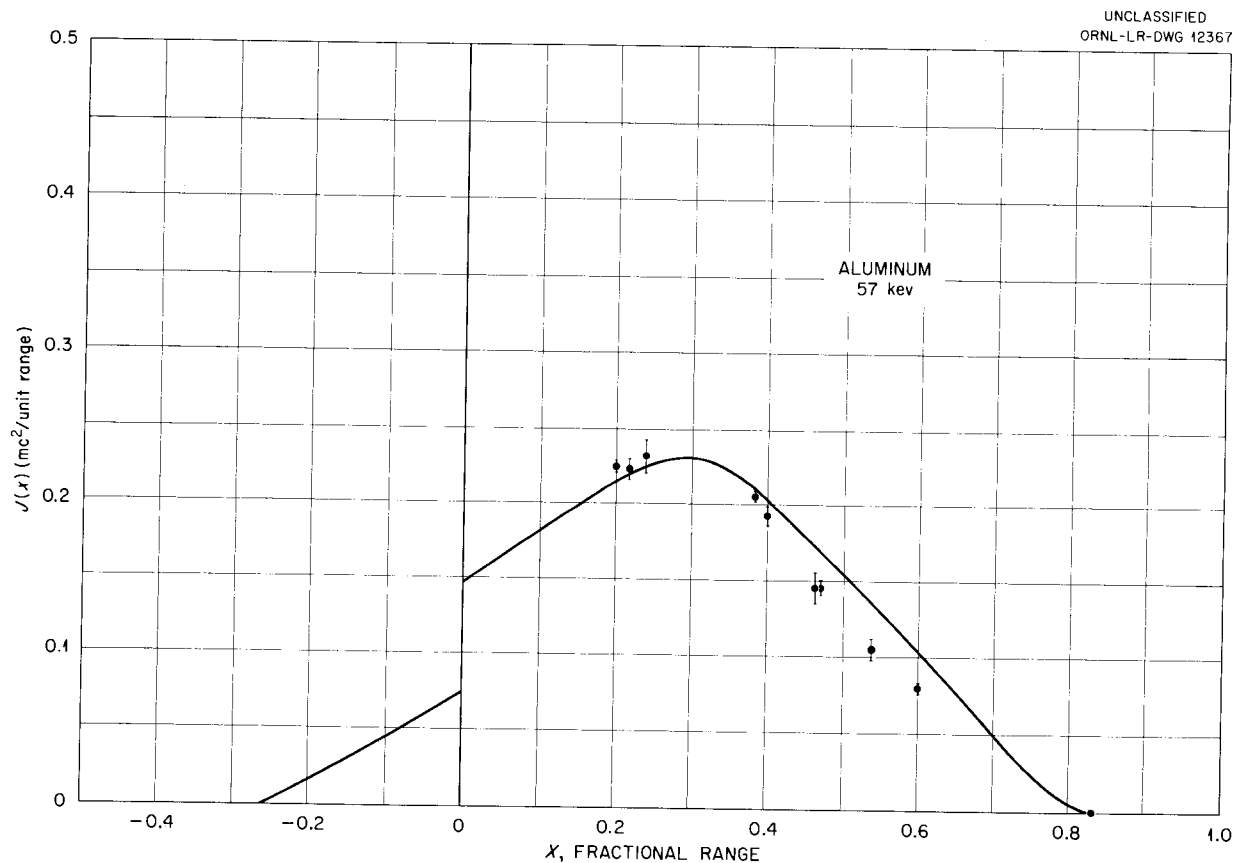


Fig. 44. Spatial Distribution of Dosage as a Function of Penetration Depth (Incident Energy of 57 keV).

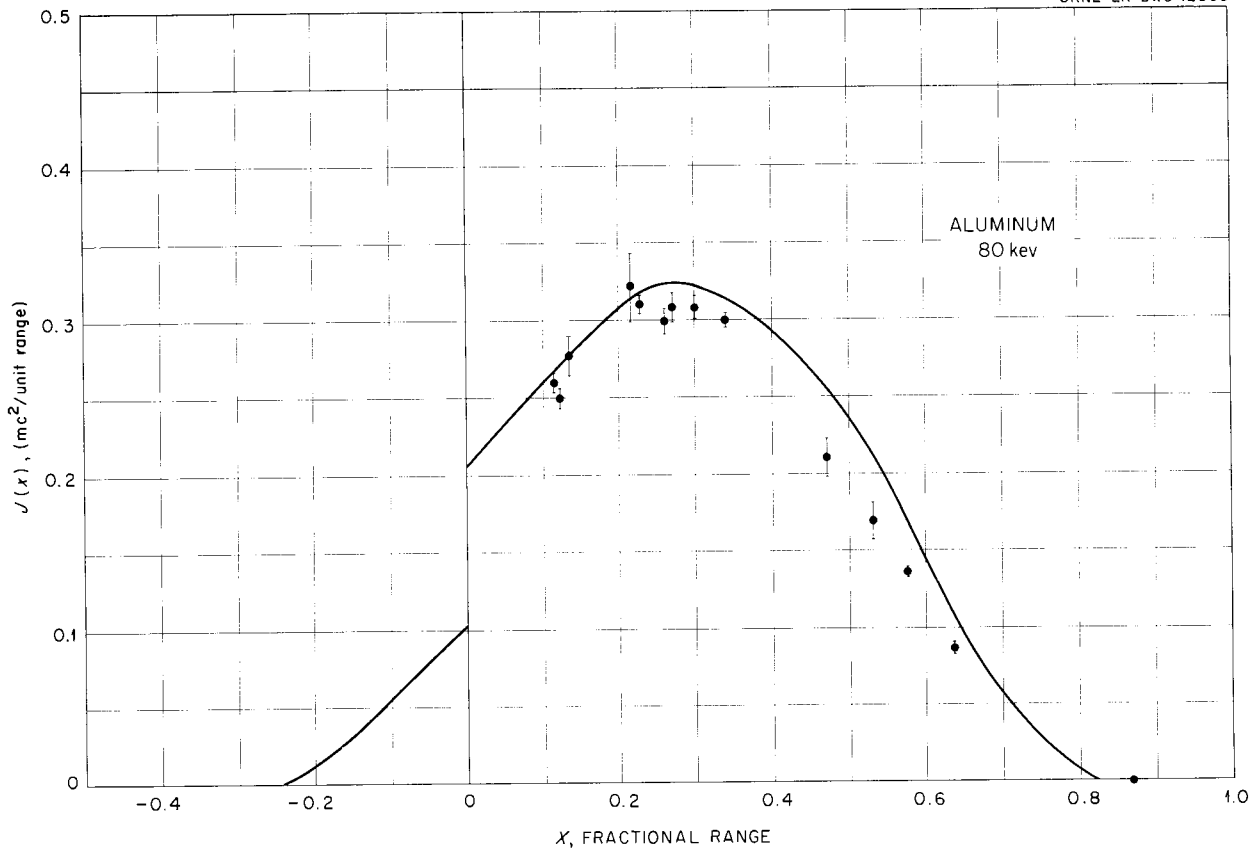


Fig. 45. Spatial Distribution of Dosage as a Function of Penetration Depth (Incident Energy of 80 kev).

#### Measurements of Electron Flux in a Radioactive Medium

One of the problems which arises when an attempt is made to calculate the exposure from an ingested beta-emitting radioisotope is the change in the energy spectrum of the radiation as the radiation is absorbed in the tissue; that is, the nuclear beta spectrum, as might be measured by a beta spectrometer, is altered considerably in shape because the electrons slow down and because they can make violent collisions with atomic electrons of the medium, resulting in the liberation of additional electrons, usually designated as secondaries. The quantity of interest is the distance traveled by both primary and secondary electrons as they go from an energy  $T + \Delta T$  to a lower energy  $T$ . In the medium the track length associated with electrons in a particular energy interval  $\Delta T$  is usually designated as the differential track length, and it is proportional to the electron flux in the same energy

interval; that is, the number of electrons per square centimeter having energies between  $T$  and  $T + \Delta T$ .

In a recent theoretical treatment, Spencer and Fano<sup>8</sup> have reduced the problem to an integral equation. However, the equation is sufficiently complicated to make it desirable that the solution be programmed for the electronic digital computer. It is hoped that such a computing program will be carried out ultimately at ORNL. In the meantime several calculations have been made by using a simplified theory given by Spencer and Attix.<sup>9</sup> The results of these approximate calculations have already proved useful in the calibration of the beta dosimeter described elsewhere in this report. The spectral distribution of electron flux in a water

<sup>8</sup>L. V. Spencer and U. Fano, *Phys. Rev.* 93, 1172 (1954).

<sup>9</sup>L. V. Spencer and F. H. Attix, *Radiation Research* 3, 239 (1955).

UNCLASSIFIED  
ORNL-LR-DWG 12365

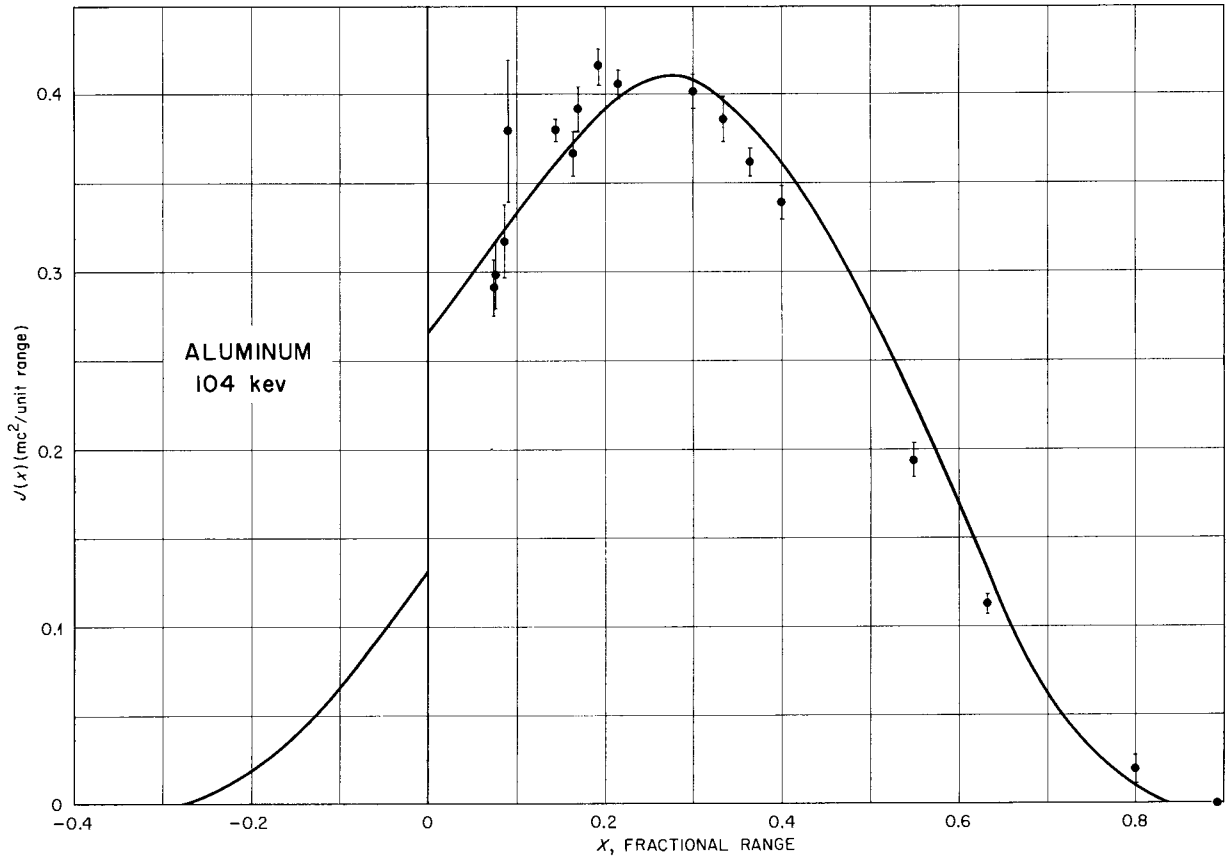


Fig. 46. Spatial Distribution of Dosage as a Function of Penetration Depth (Incident Energy of 104 kev).

medium has been determined thus far for the isotopes  $Ca^{45}$ ,  $W^{185}$ ,  $Ag^{111}$ ,  $Y^{90}$ ,  $P^{32}$ ,  $Tl^{204}$ , and  $S^{35}$ .

A brief outline of the physical basis for such calculations is given as follows: If  $y(T) dT$  represents the number of centimeters traveled by electrons having energy between  $T$  and  $T + dT$ , then

$$y(T) = \frac{1}{\frac{dT}{dx}(T)} \left\{ \int_T^{T_0} N(T') dT' + \int_{2T}^{T_0} K(T', T) y(T') dT' \right\},$$

with  $N(T')$  as the nuclear beta spectrum and  $K(T', T)$  representing the probability per unit path that an electron of energy  $T'$  will have a collision such that a secondary electron will be born with energy less than  $T'/2$  but greater than  $T$ . The function  $K(T', T)$  is an integral of the Möller electron-electron scattering cross section  $k_M$ :

$$K(T', T) = \int_{T'-T}^{T_0} k_M(T', \tau) d\tau$$

$$\approx \frac{2\pi N_e r_0^2}{(\beta')^2} [T^{-1} - (T' - T)^{-1}].$$

The energy diagram shown in Fig. 49 gives the relationships among the various energies.

The hatched region represents the energy interval into which primary electrons at energy  $T'$  may contribute secondaries with energies above  $T$ . Thus the right hand integral in the first equation is

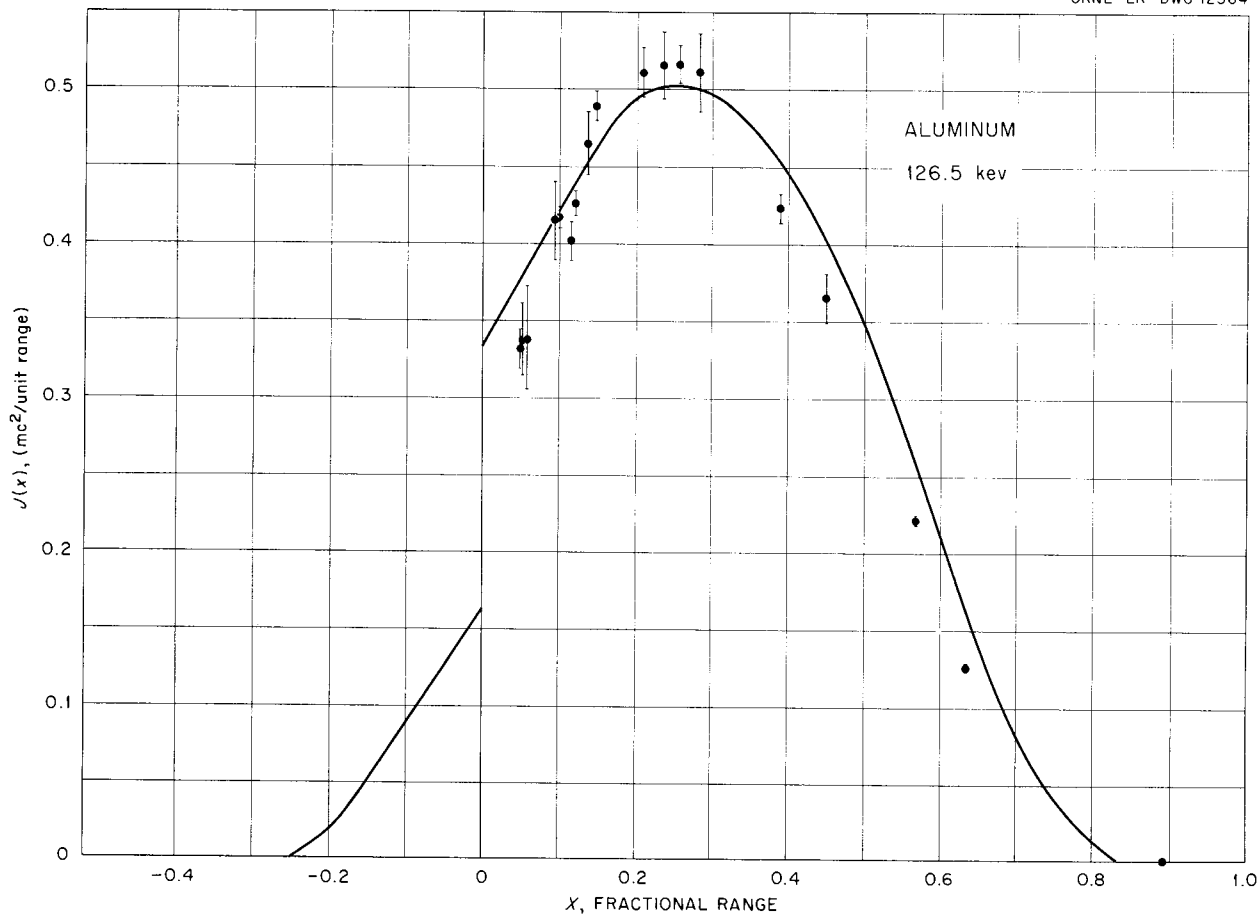


Fig. 47. Spatial Distribution of Dosage as a Function of Penetration Depth (Incident Energy of 126.5 keV).

the total number of secondaries in the medium with energies above  $T$  and the left hand integral is the number of primaries with energies above  $T$ . The total number of electrons above  $T$  divided by the stopping power  $dT/dx$  at energy  $T$  is then the differential track length in the medium caused by electrons of energy between  $T$  and  $T + dT$ , and this differential track length is proportional to the flux in the same energy interval. Here  $T_0$  is the maximum beta energy. The solution of this integral equation may be carried out readily by numerical methods.

An interesting result of the calculation for any beta spectrum is the prediction of a large flux of secondary electrons with energies below 10 keV, which exceeds the flux at higher energies by a factor of approximately two at about 1 keV and may be considerably larger at lower energies although no theoretical calculation can be made because of

uncertainties as to the validity of the stopping-power formula and the Möller cross sections at low energies.

Experimental determinations of the electron flux have been carried out for  $\text{P}^{32}$  in Bakelite by a method suggested by Spencer and Fano.<sup>8</sup> In this method a vacuum cavity in the medium communicates with a beta spectrometer by a channel cut through the radioactive material. The flux from the cavity is assumed to be the difference between that from cavity and channel and that from the channel alone. The flux thus obtained agrees well with that given by the theory for energies above 0.4 MeV. Below this energy the flux appears to be a few per cent less than that given by the theory. It is possible that the discrepancy may be attributed to the approximation to the integrated Möller formula which was used or to inaccuracies in the Möller formula itself, which has been found by several

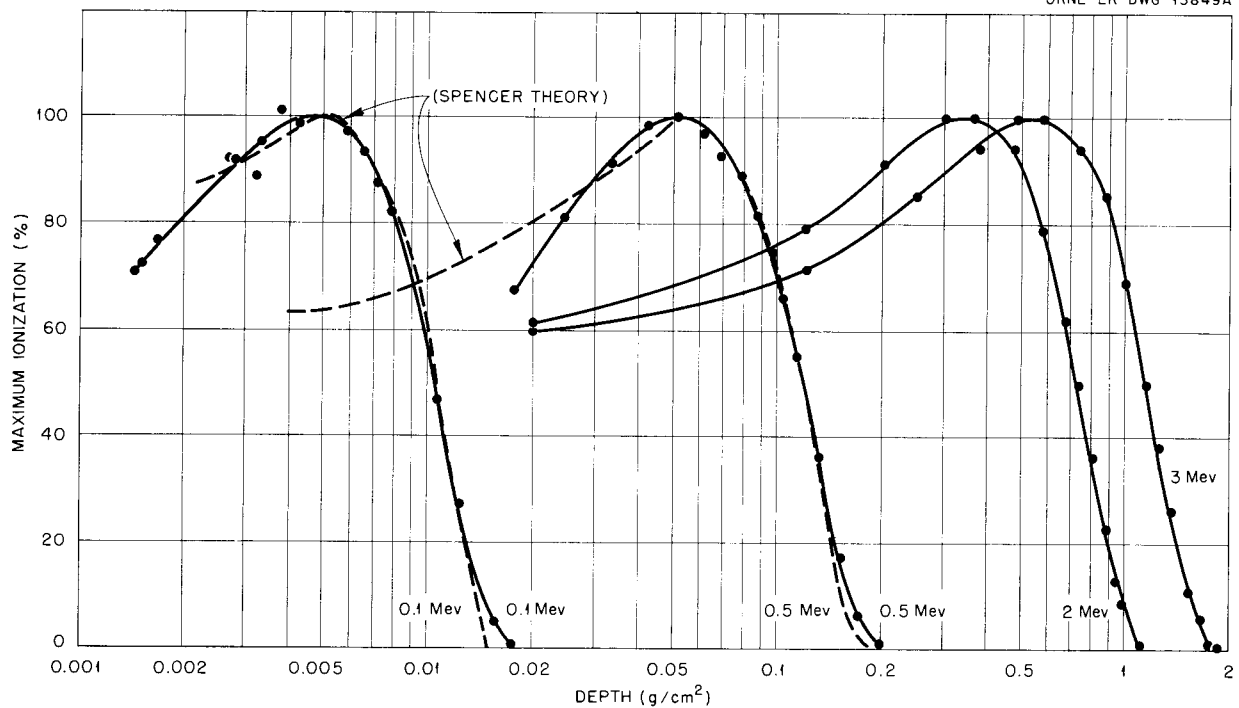


Fig. 48. Per Cent Maximum Ionization vs Depth in  $\text{g}/\text{cm}^2$  Aluminum Curves.

observers to overestimate slightly the electron-electron cross section.

Measurements of the number of electrons of each energy in water have been made with the magnetic spectrometer down to an energy of 50 keV, as shown in Fig. 50. Below 0.2 MeV the data have been corrected for loss of transmission in the spectrometer. The beta spectrum of  $\text{P}^{32}$  is included for comparison.

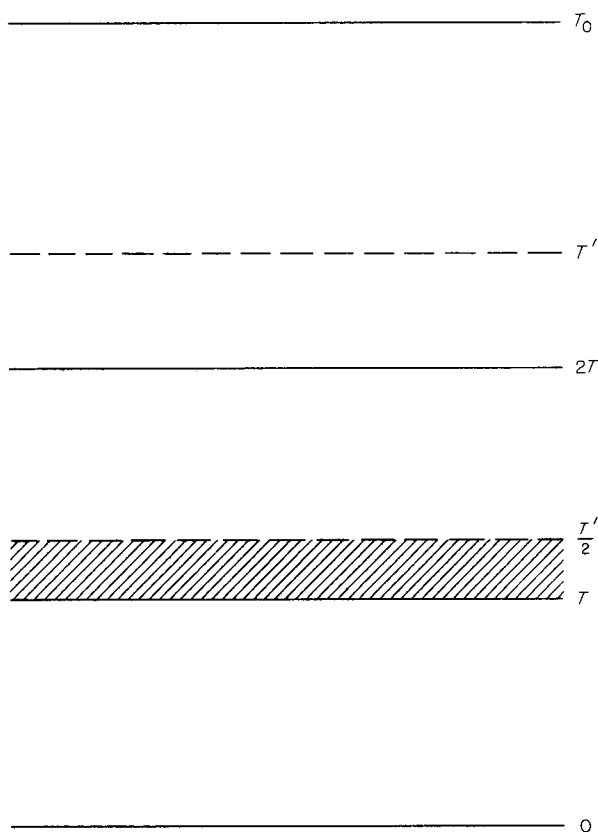
In order to extend the measurements to lower energies, a low-energy electrostatic spectrometer is being developed. The scintillation detector has been constructed and is currently under test.

#### The Design and Calibration of Pocket Dosimeters for Beta Radiation

Several practical pocket ionization chambers have been developed which, in conjunction with the standard Victoreen chamber, permit the measurement of an absorbed beta ray dose. The chambers consist of an ion-collecting volume of the same size as the standard chamber and have a wall of conducting paper  $7 \text{ mg}/\text{cm}^2$  thick, equivalent to the minimum thickness of the human epidermis, so that beta rays which can penetrate the skin can enter

the chamber. The inner region is given mechanical strength by an outer perforated cylinder made of thin aluminum or magnesium or of drilled plastic so that the complete unit has the same outside dimensions as the standard chamber and can be charged and read on the same minometer. Figure 51 shows the standard chamber and the various experimental models. Drawings of the perforated aluminum chambers and drilled plastic chambers are given in Figs. 52 and 53, respectively.

The response of the beta chambers to gamma rays and heavily filtered x rays which have effective energies from 21 to 700 keV is as nearly energy-independent under most field conditions as the standard type. The chambers are calibrated by placing them in a cavity, which has walls with  $1 \text{ mg}$  of aluminum-coated Mylar per square centimeter, within a tank containing dilute water solutions of several beta-emitting isotopes. The arrangement is shown in Fig. 54. A dilute solution of a radioisotope is run into the cell from the reservoir. The upper hose connection is then pinched off and the reservoir lowered a few inches below the cell to create a partial vacuum and expand the walls of the cavity. An electrometer head

UNCLASSIFIED  
ORNL-LR-DWG 45743

**Fig. 49. Energy Level Diagram for Production of Secondary Electrons.**

and electrode is used to measure the ionization in the cavity.

The dose rate is calculated from the known beta energy spectrum and the measured specific activity of the solutions by using the Bragg-Gray principle. The mean energy of the beta rays traversing the cavity is calculated from the Spencer-Fano-Attix theory of the electron-slowning-down spectrum. With a 1 mg/cm<sup>2</sup> Mylar foil separating the cavity from the solution, ionization varied from 75% of the calculated value for S<sup>35</sup> (mean energy of 55 kev) to 100% for P<sup>32</sup> (493 kev). A chamber with a 7 mg/cm<sup>2</sup> conducting paper wall inserted into the cavity had a response varying from 10 to 95% of the calculated values for mean energies of the betas in the cavity

from 55 kev to 654 kev. The practical personnel dosimeters described above had a response in this cavity of 50% or more of that of the paper chamber. The other calibration sources used were Ca<sup>45</sup>, W<sup>185</sup>, Tl<sup>204</sup>, and Ag<sup>111</sup>. The results are shown in Fig. 55.

If a person wears both a new chamber and a standard one, the new chamber will read the total dose received, and the standard chamber will read only the gamma dose. Hence the beta-ray dose may be obtained by subtraction. However, the maximum permissible skin exposure to soft radiation is twice that for hard gamma; hence the new chamber reads, in the most unfavorable case, 50% of the beta dose, and its reading can be interpreted directly as percentage of maximum permissible exposure.

Sample chambers are now being field tested by the Applied Health Physics Section.

#### Neutron Films (NTA)

The NTA film packet was modified in 1954 to make the film a dosimeter.<sup>10</sup> The 30- $\mu$  emulsion then specified was tested with monoenergetic neutrons and found to read low at low energies. It was thought that the effect was due to failure to detect wrongly oriented short tracks, so the specifications were changed to a 40- $\mu$  emulsion thickness.

Recently, deviations appeared in routine calibration. When the exposures to monoenergetic neutron beams, of energies between 0.6 and 5.4 Mev, were repeated on the 40- $\mu$  emulsions, the readings were consistently high, particularly at the lower energies.

It now appears that the variation in readings is caused by change of moisture content of the emulsion, the gelatin of which tends to come to equilibrium with atmospheric moisture. The original calculations were made on the basis of 50% atmospheric relative humidity. Recently, the relative humidity has been quite high in this area; in particular, during the time these last tests were made, the relative humidity was at least 85%.

Differences in emulsion response to neutrons were calculated with respect to change in moisture content. When the number of tracks were related to the dose by using the earlier ratio of tracks per neutron to reps per neutron under 50% relative humidity, the measured dose was too high; however, it agreed to within 6% with the response

<sup>10</sup>J. S. Cheka, *Nucleonics* 12(6), 40 (1954).

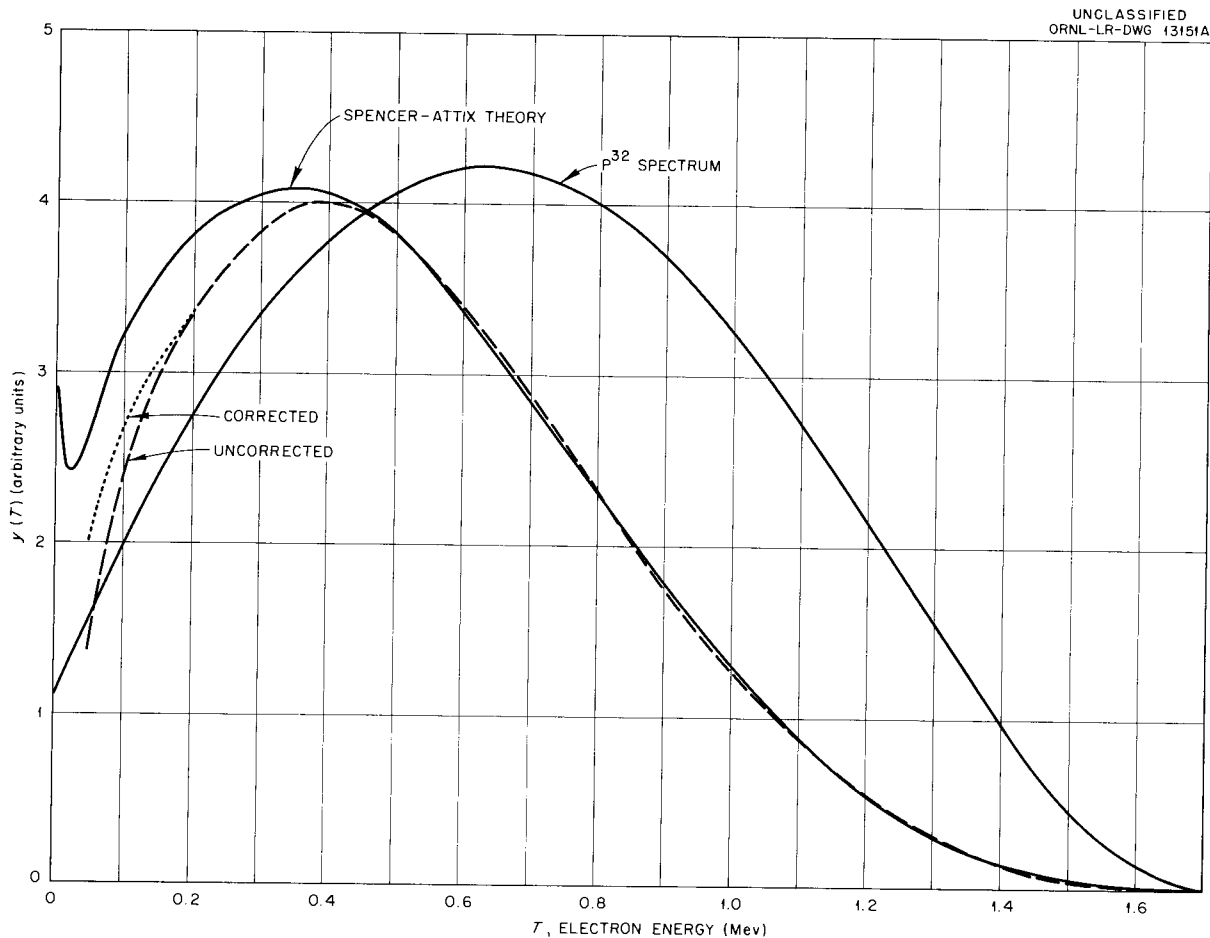


Fig. 50. Spectral Distribution of Electrons from  $P^{32}$  Absorbed in Bakelite.

curve calculated for an emulsion in equilibrium with air at 85% relative humidity.

The consequence of the above findings is that, unless the films are packaged in a moisture-proof wrapper and the original moisture content of the emulsion is known, there is an uncertainty of approximately  $\pm 25\%$  in the film response to neutrons. Several materials are being investigated with the purpose of finding a light, effective, and serviceable moisture-proof envelope.

If low-moisture-content films are sealed in such an envelope, the additional advantage that accrues is that the latent image is stabilized, thereby enabling longer monitoring periods. Such longer periods have the twofold advantage of both lower costs through less frequent processing and greater statistical accuracy because a larger integrated dose is measured.

#### THEORETICAL PHYSICS OF DOSIMETRY

J. Neufeld      R. H. Ritchie  
W. S. Snyder

#### Dependence of the Average Charge of an Ion on the Density of the Surrounding Medium

This investigation is concerned with the effect of the surrounding medium on a heavy ion and is a continuation of recent work on a similar problem involving light ions.<sup>11</sup> Recent experiments revealed the existence of two "density effects." One of these effects expresses a dependence of the average charge of an incident heavy ion on the media at low pressure and is designated as the "pressure effect." The other effect expresses the dependence of the charge of the heavy ion on the

<sup>11</sup>J. Neufeld, *Phys. Rev.* 96, 1470 (1954).

UNCLASSIFIED  
PHOTO 17172



**Fig. 51. Standard Victoreen Pocket Ionization Chamber and Various Beta-Ray-Sensitive Chambers.** At the top is half of a standard chamber cut open and the two types of center electrodes used. Counter-clockwise, from upper left, the chambers shown are: aluminum screen wall, stainless steel screen wall, perforated magnesium wall, drilled plastic wall, perforated aluminum wall, paper wall, and standard Victoreen.

UNCLASSIFIED  
ORNL-LR-DWG 15744

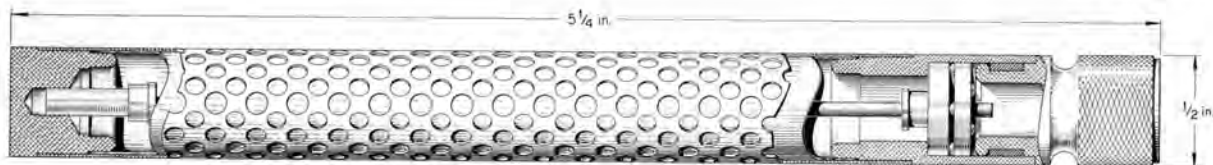


**Fig. 52. Perforated Aluminum Wall Chamber.** The model as constructed has a conductive paper cylinder inside to define the ionization chamber, whose diameter is that of the holes in the end plug and adapter, 0.3125 in.

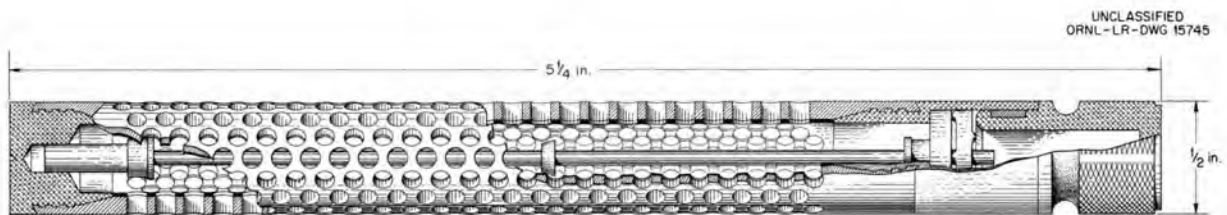


Fig. 53. Drilled Plastic Chamber.



Fig. 54. Calibration Cell for Beta-Ray-Sensitive Pocket Chambers. Cell with its reservoir, S, is shown at left; disassembled cell is shown at right; in front are the electrometer head and electrode.

state of condensation of the medium. According to Bohr and Lindhard<sup>12</sup> these two effects are phenomenologically analogous, since they involve a relationship between the times separating successive collisions of the incident ion and the times required for the excited orbital electrons to re-adjust themselves either by radiation or by redistribution of their excitation energy. It is suggested that these two effects are phenomenologically different, since the average charge of the ion in a condensed medium may be determined, not by the time relationship involving the redistribution of the excitation energy of the ion, but by a polarizing

<sup>12</sup>N. Bohr and J. Lindhard, *Kgl. Danske. Videnskab. Selskab., Mat-fys. Medd.* 28(7), (1954).

field caused by the reaction of the perturbed medium on the moving ion.<sup>11</sup> This field causes spontaneous emission of electrons carried by the ion. A relationship has been established between various values of the polarizing field and the corresponding average charge of an incident heavy ion, in which the orbital electrons are continually maintained in an excited state because of the recurrent collisions with the atoms in the surrounding medium. The value of the polarizing field has been determined from theoretical estimates and from the measurements of ranges of fission fragments in gold. A program has been prepared for the Oracle which computes the average charge of a fission fragment for various values of the polarizing field.

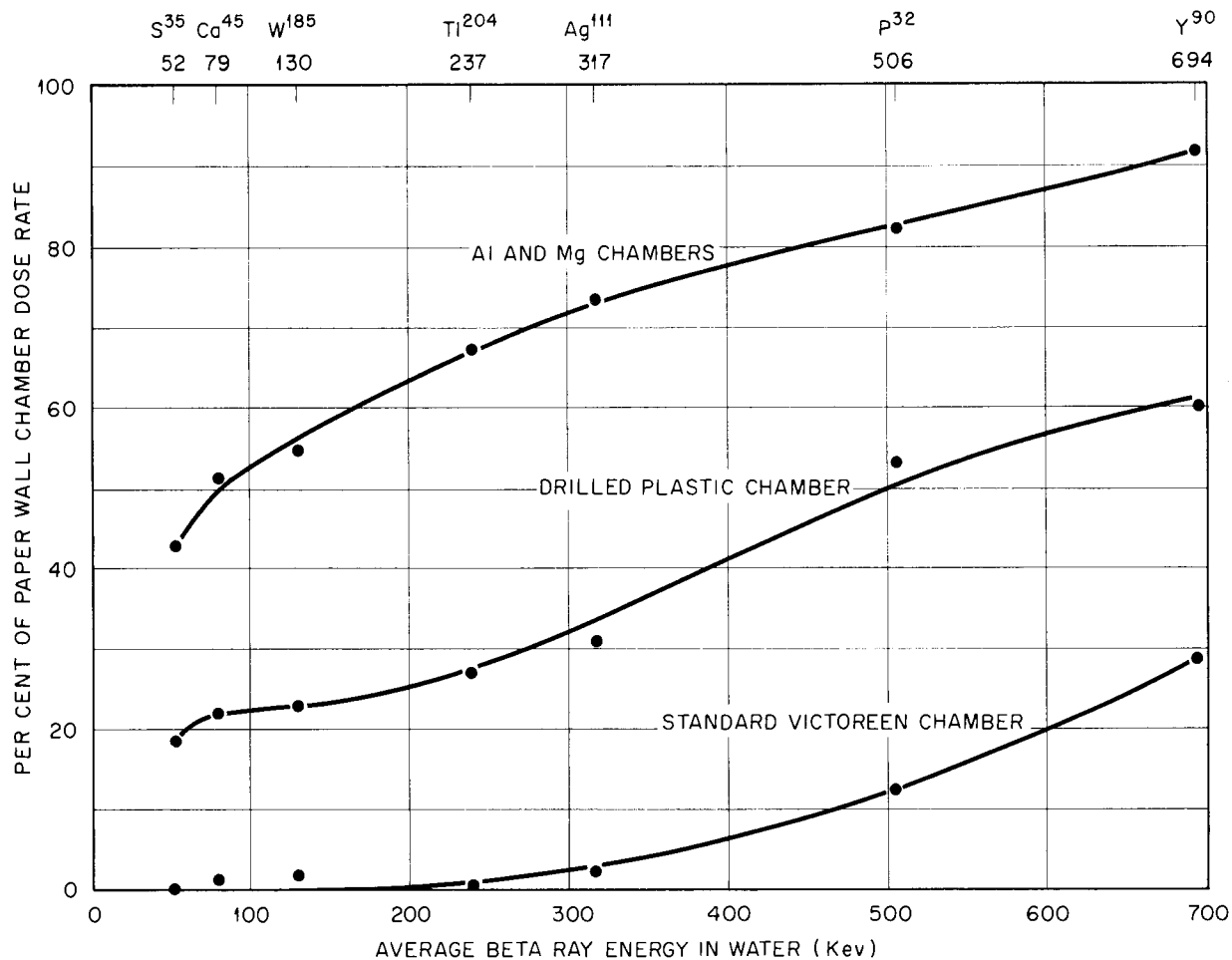


Fig. 55. Response of Beta-Sensitive Pocket Chambers Expressed as Percentages of the Dose to the Dermis. This dose is assumed to be measured correctly by a chamber having paper walls of surface density 7 mg/cm<sup>2</sup>.

**Relative Biological Effectiveness for Heavy Particles**

If  $\Delta E$  is a small increment of energy lost by an incident particle in a gram of tissue while its energy is between  $E$  and  $E + dE$  (Mev), then the biological damage is estimated in rems as  $1.6 \times 10^{-8} \Delta E \cdot R(E)$ , where  $R(E)$  is the relative biological effectiveness assigned by the National Committee on Radiation Protection<sup>13</sup> for a linear

energy transfer (LET) value equal to that of the particle. The total biological damage along the entire track of the ion of energy  $E_0$  is thus given by

$$D = 1.6 \times 10^{-8} \int_0^{E_0} R(E) dE ,$$

and it has been computed for protons, alpha particles, and carbon, nitrogen, and oxygen ions by using LET values calculated elsewhere.<sup>14</sup> The results are shown in Figs. 56, 57, and 58.

<sup>13</sup>U.S. National Bureau of Standards, *Permissible Dose from External Sources of Ionizing Radiation*, Handbook 59 (1954), Superintendent of Documents, Washington 25, D.C.

<sup>14</sup>W. J. Snyder and J. Neufeld, *On the Energy Dissipation of Moving Ions in Tissue*, ORNL-1083 (Nov. 14, 1951).

UNCLASSIFIED  
ORNL-LR-DWG 12537A

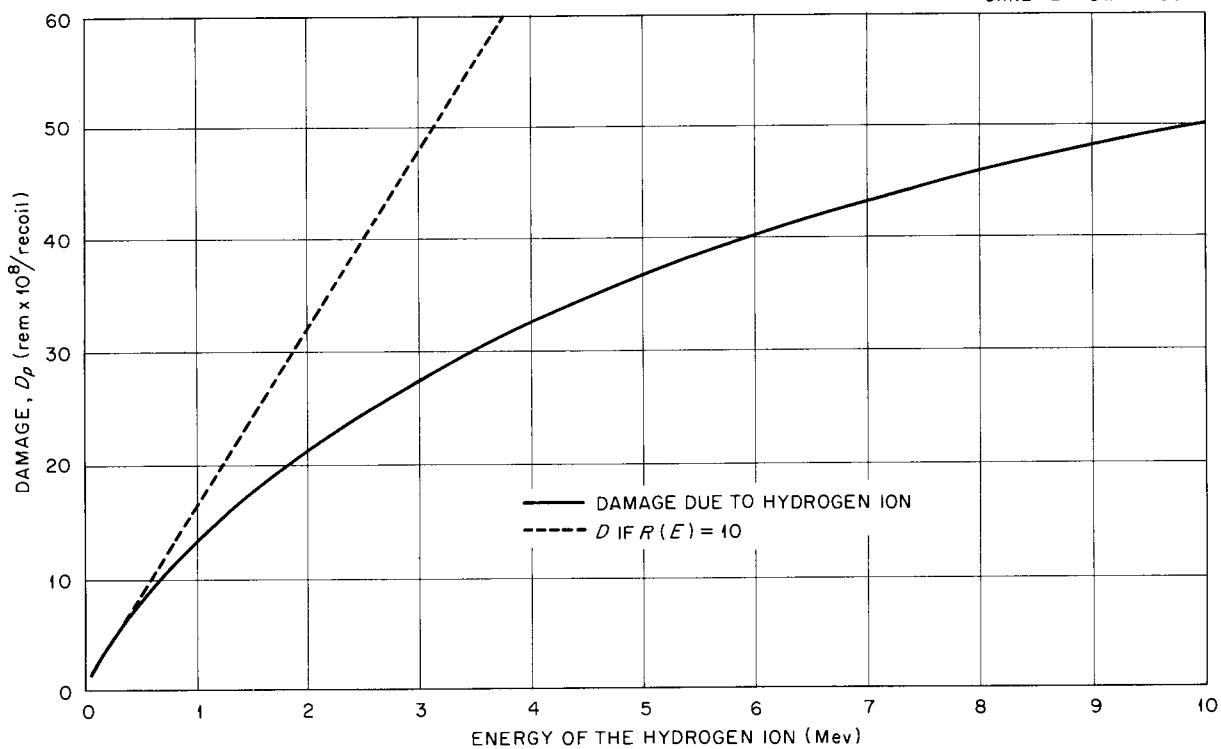


Fig. 56. Damage Produced in Tissue by a Moving Hydrogen Ion.

UNCLASSIFIED  
ORNL-LR-DWG 12538A

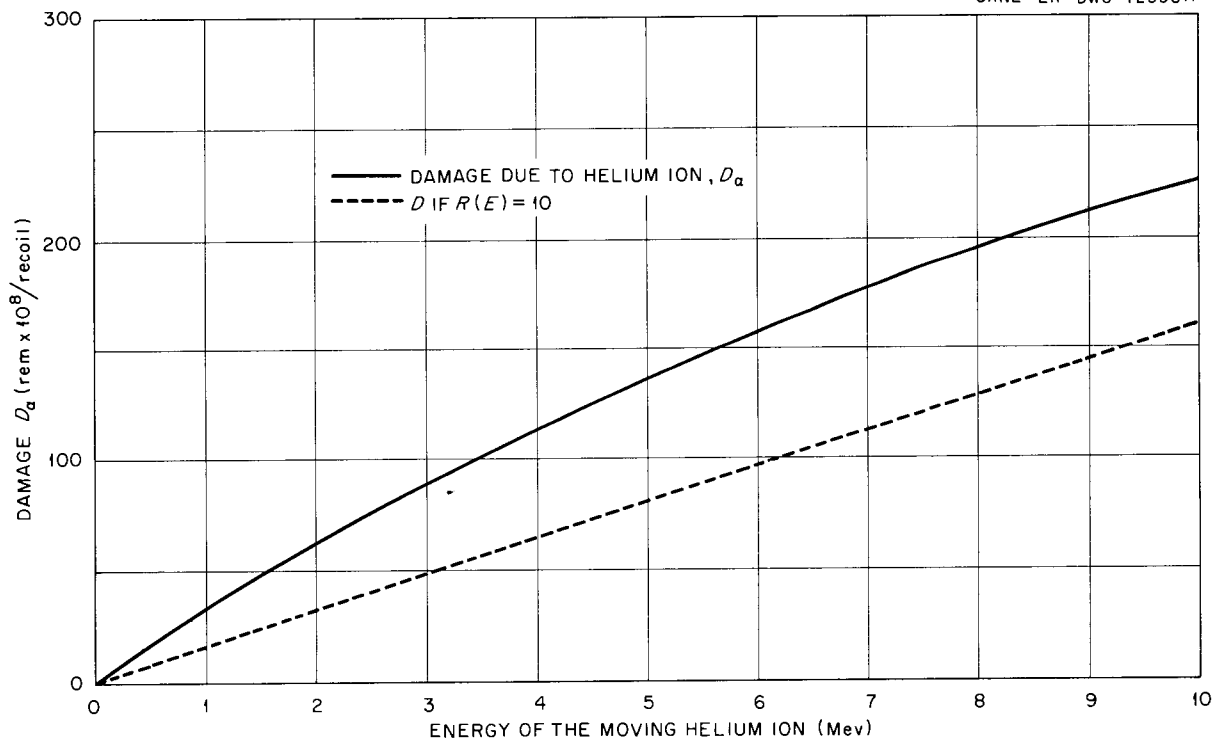


Fig. 57. Damage Produced in Tissue by a Moving Helium Ion.

UNCLASSIFIED  
ORNL-LR-DWG 12539A

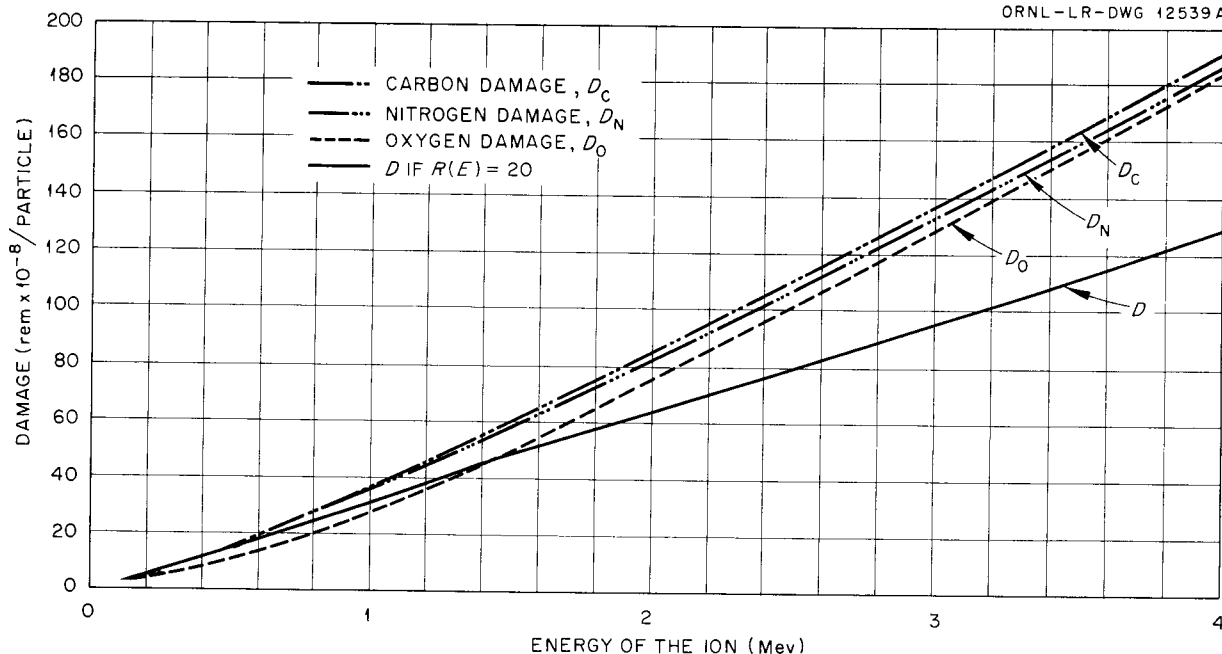


Fig. 58. Damage Produced in Tissue by a Moving Ion of Carbon, Nitrogen, and Oxygen.

**Plasma Losses by Fast Electrons in Thin Films**

The response of electrons in the conduction band of metals to fast electrons may be described in terms of a quantum dielectric constant which is a function of both the frequency and the wave vector of the electromagnetic disturbance in the metal.<sup>15,16</sup> The angle-energy distribution of fast electrons losing energy in thick metal foils has been derived by assuming that the fast electrons undergo only small fractional energy and momentum changes and that the conduction electrons form a Fermi-Dirac gas. The derived distribution exhibits characteristics of both collective interaction and individual interaction and is more general than the result of Ferrell.<sup>17</sup> The angular distribution of electrons undergoing losses to plasma oscillations is given by

where  $\omega_p$  is the plasma frequency,  $v$  is the velocity of the fast electrons,  $\omega_e = (mv^2/2\hbar)$ ,  $\omega_0 = (mv_F^2/2\hbar)$ , and  $v_F$  is the maximum velocity in the Fermi-Dirac distribution.

The energy-angle distribution of a fast electron losing energy in a thin foil has also been treated. It has been shown that the boundary effect is such as to reduce the probability of loss at the plasma frequency and to cause additional loss at lower frequencies. The probability of loss at the plasma frequency decreases by an amount given by

$$P = \frac{2e^2}{bv} t \int_0^\infty \frac{x^2 dx}{(x^2 + t^2)^2} \frac{\cosh x - \cos t}{\sinh x}$$

$$P(\theta)d = \frac{\omega_p^2 e^2}{2\pi\hbar v^2} \frac{1}{\left(\omega_p^2 + \frac{6}{5}\omega_0\omega_e^2\theta^2 + \omega_e^2\theta^4\right)^{1/2}} \frac{d\Omega}{\theta^2 + \left(\frac{\omega_p}{2}\omega_e\right)^2}$$

<sup>15</sup>J. Lindhard, *Kgl. Danske. Videnskab. Selskab. Met.-fys. Medd.* 28(8), (1954).

<sup>16</sup>J. Hubbard, *Proc. Phys. Soc.* 68A, 976 (1955).

<sup>17</sup>R. A. Ferrell, *Phys. Rev.* 101, 554 (1956).

where  $t = (a\omega_p/v)$  and  $a$  is the foil thickness. The quantity

$$-\frac{\hbar v}{te^2} P_{b_1}(t)$$

is plotted in Fig. 59 as a function of  $t$ .

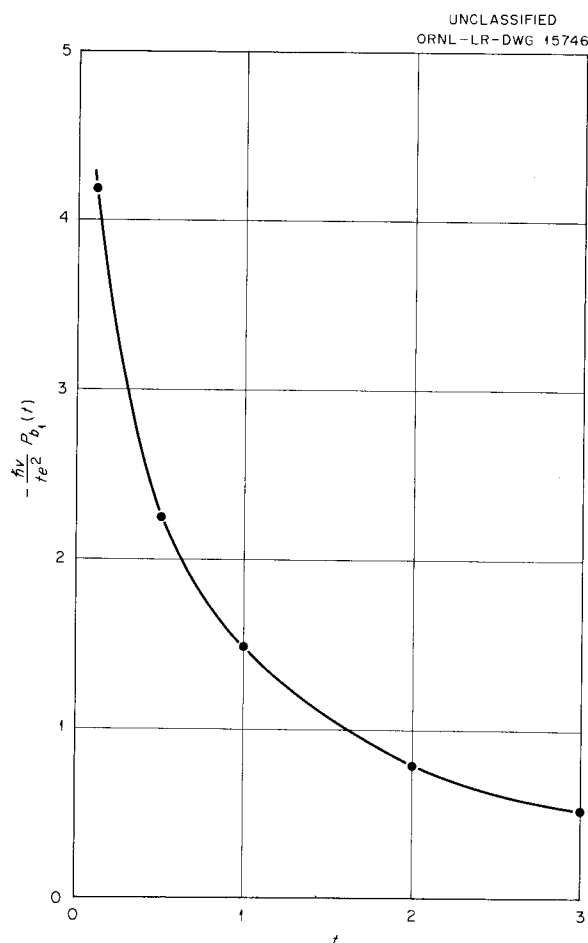


Fig. 59. Probability for Plasma Loss in a Film vs Thickness of the Film.

The magnitude of both the reduction at plasma frequency and the increase at lower frequencies increases as the foil thickness decreases. It is suggested that experimental observation of losses in very thin films will serve to distinguish the losses to plasma oscillations from the losses resulting in interband transitions.

### Vacancies and Displacements in a Solid Resulting from Heavy Corpuscular Radiation

In a study of the vacancies and displacements in a solid resulting from heavy corpuscular radiation, let  $D(E)$  be the number of atoms displaced in a monoatomic solid by a free atom of energy  $E$ , and let  $V(E)$  be the number of vacancies produced by the same atom. When a struck atom has received energy  $y$ ,  $p(y)$  denotes the probability that it is displaced, and, if displacement has occurred, the probability that the striking atom replaces it is taken as  $q(E - y)$ . Assume that a minimum amount of energy  $\alpha$  is necessary to displace an atom and that the struck atom loses this amount of energy in breaking away from its lattice site. If  $K(E, y)$  is the scattering kernel, then  $D(E)$  and  $V(E)$  are solutions of the equation

$$f(E) = \int_0^E dy K(E, y) \{ p(y) [f(y - \alpha) + 1] \theta q(E - y) \} + [1 - p(E - y) q(y)] f(y) \}$$

where  $f(E) = 0$  for  $E < \alpha$ , with  $\theta = 0$  for displacements and  $\theta = 1$  for vacancies. This equation has been solved for some representative cases of  $p(y)$  and  $q(y)$ . The functions  $p(y)$  and  $q(y)$  can be chosen to fit experimental estimates of either  $D(E)$  or  $V(E)$  singly but indicate a fundamental discrepancy in the joint estimates. The discrepancy, if not due to inaccuracy in the interpretation of experimental results, suggests that a mathematical model based on individual collisions is inadequate.

### The Variation of Neutron Dose with Neutron Energy and Geometry

Earlier studies<sup>18</sup> showed that the ratio of maximum dose to first-collision dose cannot exceed 2 in any convex body irradiated by a broad beam of neutrons. A program of computation is under way to determine more precisely the variation of this ratio with the size and geometry of the irradiated body. The aim is to determine a maximum body size for which the ratio does not exceed 1.05, 1.1, etc. Only preliminary results are available at the present time.

<sup>18</sup>J. Neufeld, R. H. Ritchie, and W. S. Snyder, *HP Semiann. Prog. Rep.* July 31, 1955, ORNL-1942, p 20, esp. 24.

### Depth-Dose Curves for Neutrons with RBE as a Function of LET

Depth-dose curves for monoenergetic beams of neutrons normally incident on a 30-cm slab of tissue have been computed for neutron energies of 10, 7.5, 5, 2.5, 1, 0.5, 0.1, 0.02, 0.005, 0.0001, and  $2.5 \times 10^{-8}$  Mev. The accompanying graphs (Figs. 60-81) show the depth dose in soft tissue in rads per neutron (rad = 100 ergs/g) and rems per neutron (rem = rad  $\times$  RBE). The rem curves were computed by using the functional relation of RBE to linear energy transfer (LET) recommended by the National Committee on Radiation Protection.<sup>19</sup> The maximum permissible flux necessary to deliver a dose not exceeding 0.3 rem in the slab during 40 hr is also shown (Fig. 82). These results are to appear in a forthcoming handbook of the National Committee on Radiation Protection, and a more detailed account of the calculation and the results is being prepared for publication.

#### DOSIMETRY APPLICATIONS

F. J. Davis	J. A. Harter
J. A. Auxier	E. B. Wagner
G. S. Hurst	T. D. Strickler

#### Neutron-Insensitive Gamma Dosimetry

The development of a gamma dosimeter that is insensitive to fast neutrons represents a significant advance in the dosimetry of mixed radiation. The technique involves the use of a miniature counter, Fig. 83, conforming to the Bragg-Gray conditions and with walls and gas of atomic number near carbon and oxygen. The dimensions are so small ( $0.5 \times 0.5$  cm right cylinder) and the gas pressure is so low (1 mm Hg) that the probability of energetic electrons producing an ion pair while traversing the chamber is 1/10 or less. For an isotropic distribution of electrons, the mean distance for traversing the cavity is  $4/3r$  (where  $r$  is radius of cylinder), a distance of 3 mm (refs 20 and 21). If the probability of a fast electron producing one ion pair in crossing the counter is sufficiently small, the probability of forming more than one pair can be neglected, and, if pulses

initiated by one ion pair can be counted, a summation of counts is tantamount to a summation of the absorbed energy, or to the absorbed dose, assuming that the chamber volume and the energy to produce one ion pair are known.

However, the fast neutrons that will deposit a tissue rad will deposit only about 1/10 of a  $\text{CO}_2$  rad, and the energy deposited in the counter materials will be by recoil atoms which produce a specific ionization at least 100 times that of electrons. Since the energy is determined by counting pulses, and the average number of ion pairs per pulse is 1 for electrons and 100 or more for recoil atoms, the ratio of count rate to energy absorption rate is reduced by another factor of 100 or more. Therefore, the linear relation of counts to energy deposited, which holds for gamma radiation, will not hold for fast neutrons. The over-all efficiency of the counter for one tissue rad of fast neutrons is at most 1/1000 ( $1/10 \times 1/100$ ) that for one tissue rad of gamma radiation, and, in general, the counter response to neutrons can be neglected even for high neutron/gamma dose-rate ratios. Figure 84 is a block diagram of the apparatus, and Fig. 85 is a typical pulse-height distribution for the proper counting parameters. Pulse-height distributions as a function of counter voltage are shown in Fig. 86. If the counter is operated at an insufficiently high voltage, the gamma cutoff may be so low that occasional neutron-initiated pulses decrease the slope of the pulse-height distribution, as shown in Fig. 87, to such an extent that the neutron response cannot be neglected. Therefore, the counter is operated at as high a voltage as long-term stability will permit. Electronic gain of about 100,000 is used. Carbon dioxide and carbon disulfide work well as filling gases, but  $\text{CO}_2$  is used because of its lower effective atomic number. The walls have been made of various materials, but colloidal-graphite-coated fluorothene is used, since it machines well, has no hydrogen, and has a relatively low effective atomic number.

Energy independence for the dosimeter (when the Bragg-Gray conditions for wall thickness are satisfied) has been verified for gamma rays from  $\text{Ce}^{144}$ ,  $\text{Cs}^{137}$ , and  $\text{Co}^{60}$ , an energy range from less than 0.1 to 1.2 Mev. Count rates as a function of distance from a small  $\text{Co}^{60}$  source are plotted in Fig. 88.

<sup>19</sup>U.S. National Bureau of Standards, *Permissible Dose from External Sources of Ionizing Radiation*, Handbook 59 (1954), Superintendent of Documents, Washington 25, D.C.

<sup>20</sup>F. H. Murray, CP-2922, p 13 (April 6, 1945). (Secret)

<sup>21</sup>S. I. Tomkeieff, *Nature* 155, 24 (1945).

UNCLASSIFIED  
ORNL-LR-DWG 11206

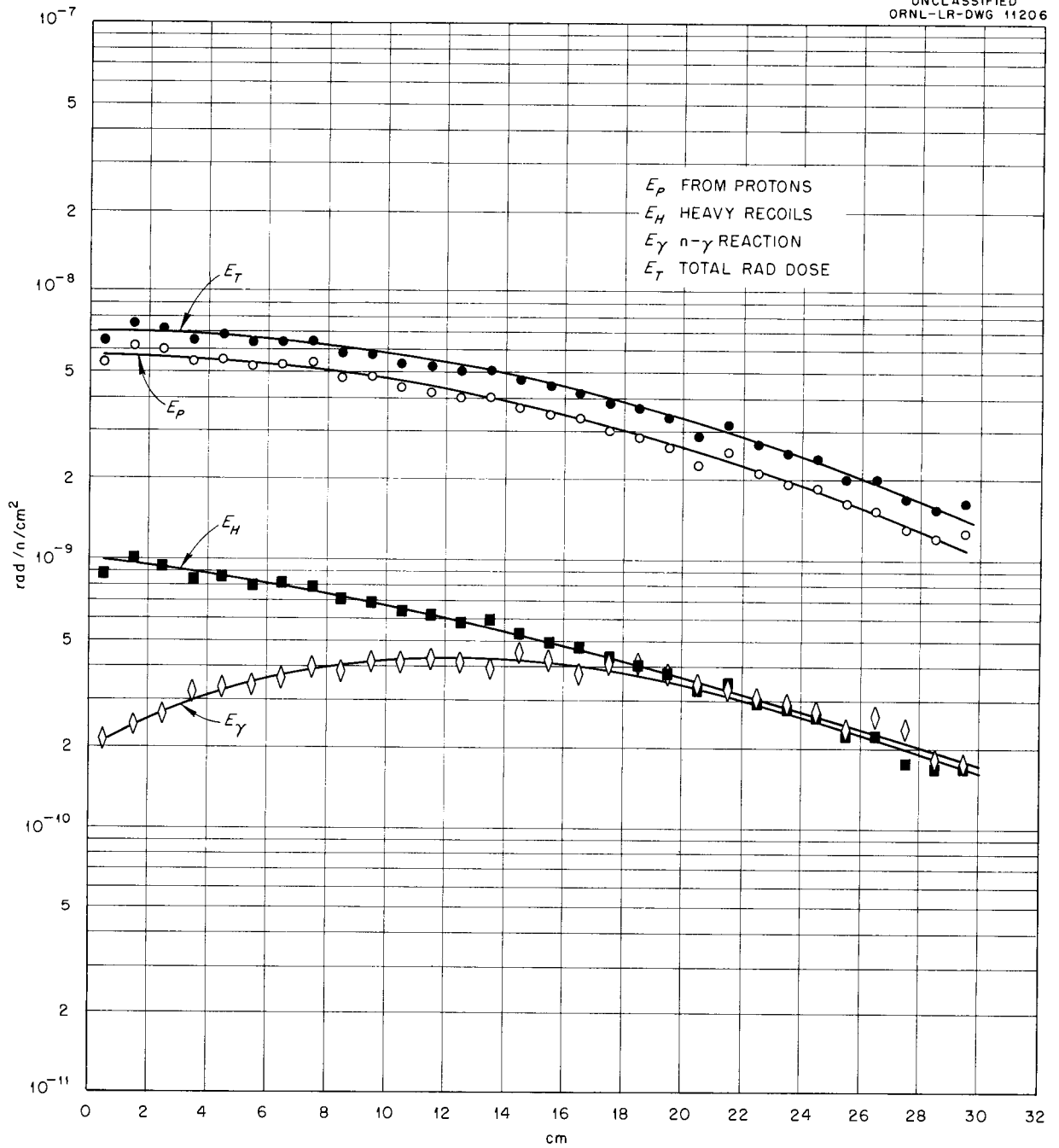


Fig. 60. Absorbed Dose from 10-Mev Neutron Beam.

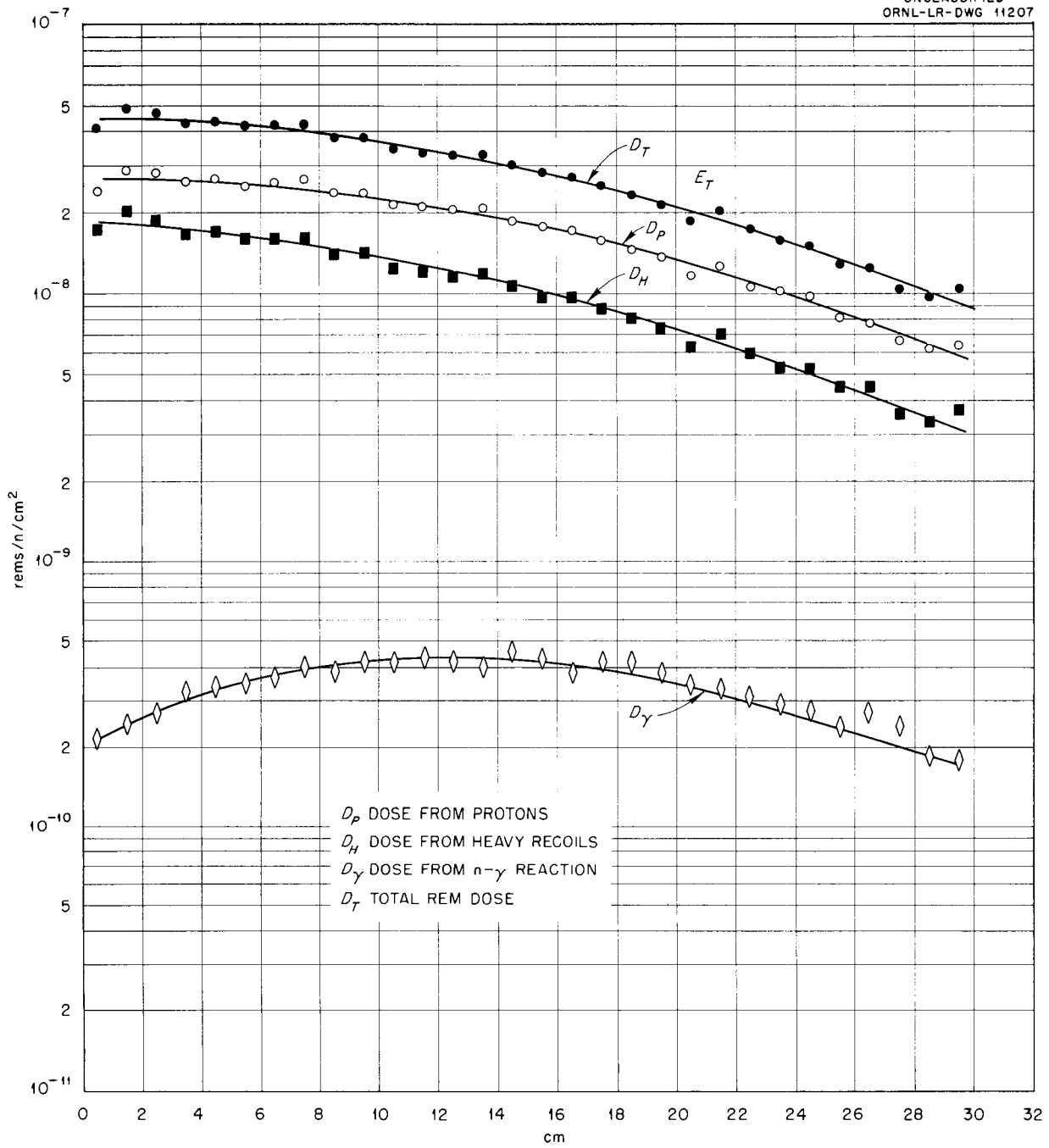


Fig. 61. Biological Dose from 10-Mev Neutron Beam.

UNCLASSIFIED  
ORNL-LR-DWG 11209

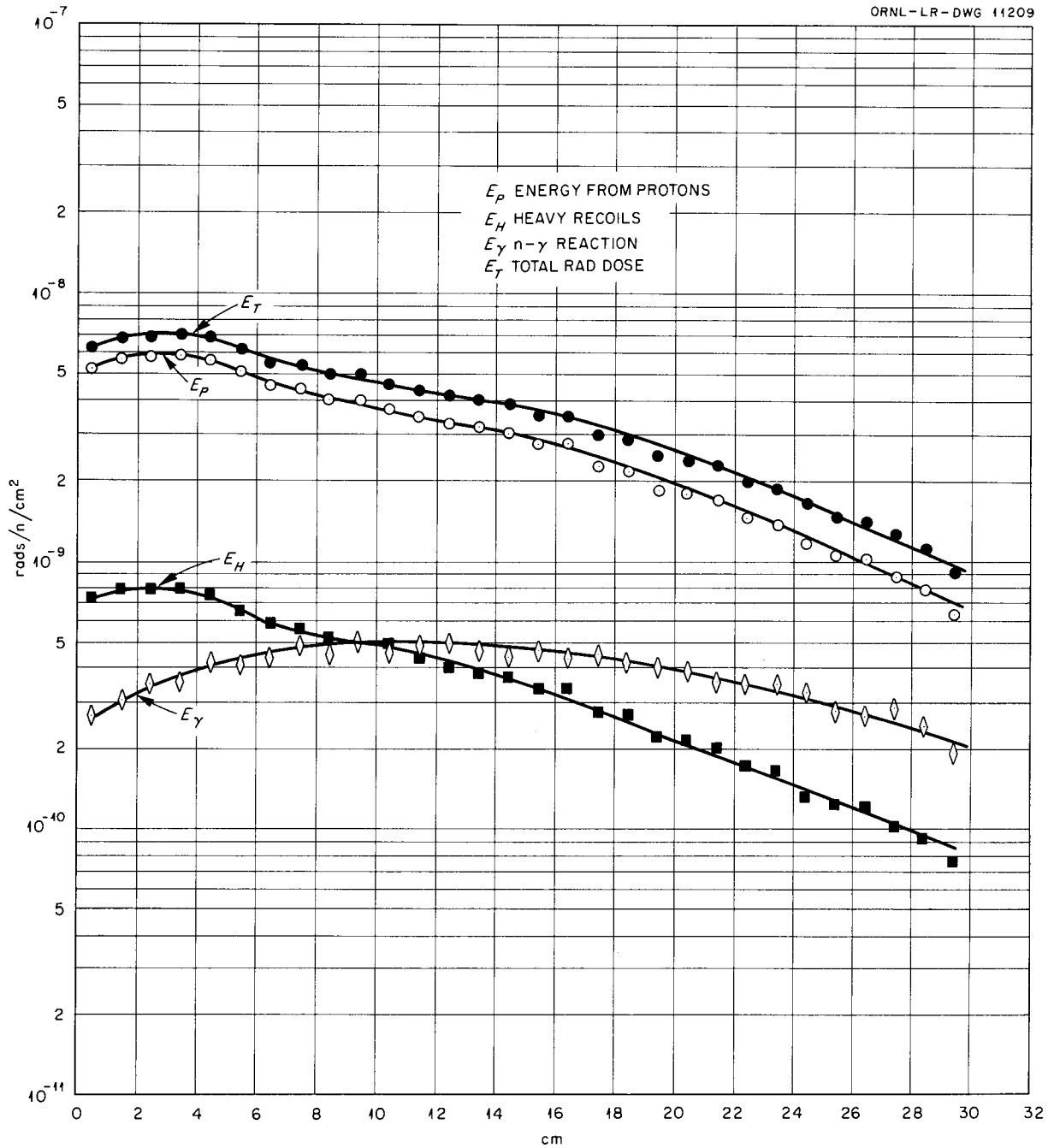


Fig. 62. Absorbed Dose from 7.5-Mev Neutron Beam.

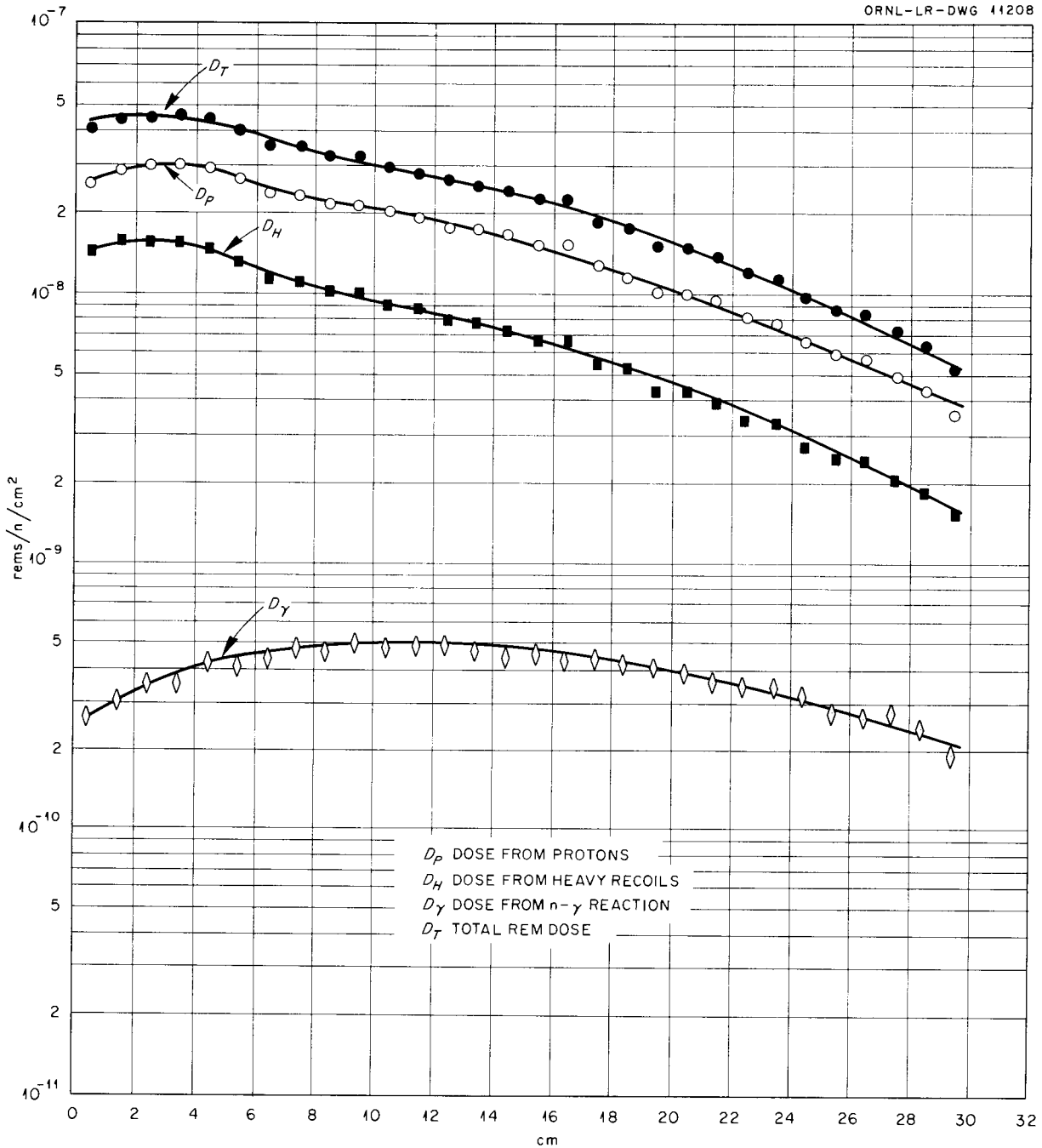


Fig. 63. Biological Dose from 7.5-Mev Neutron Beam.

UNCLASSIFIED  
ORNL-LR-DWG 41210

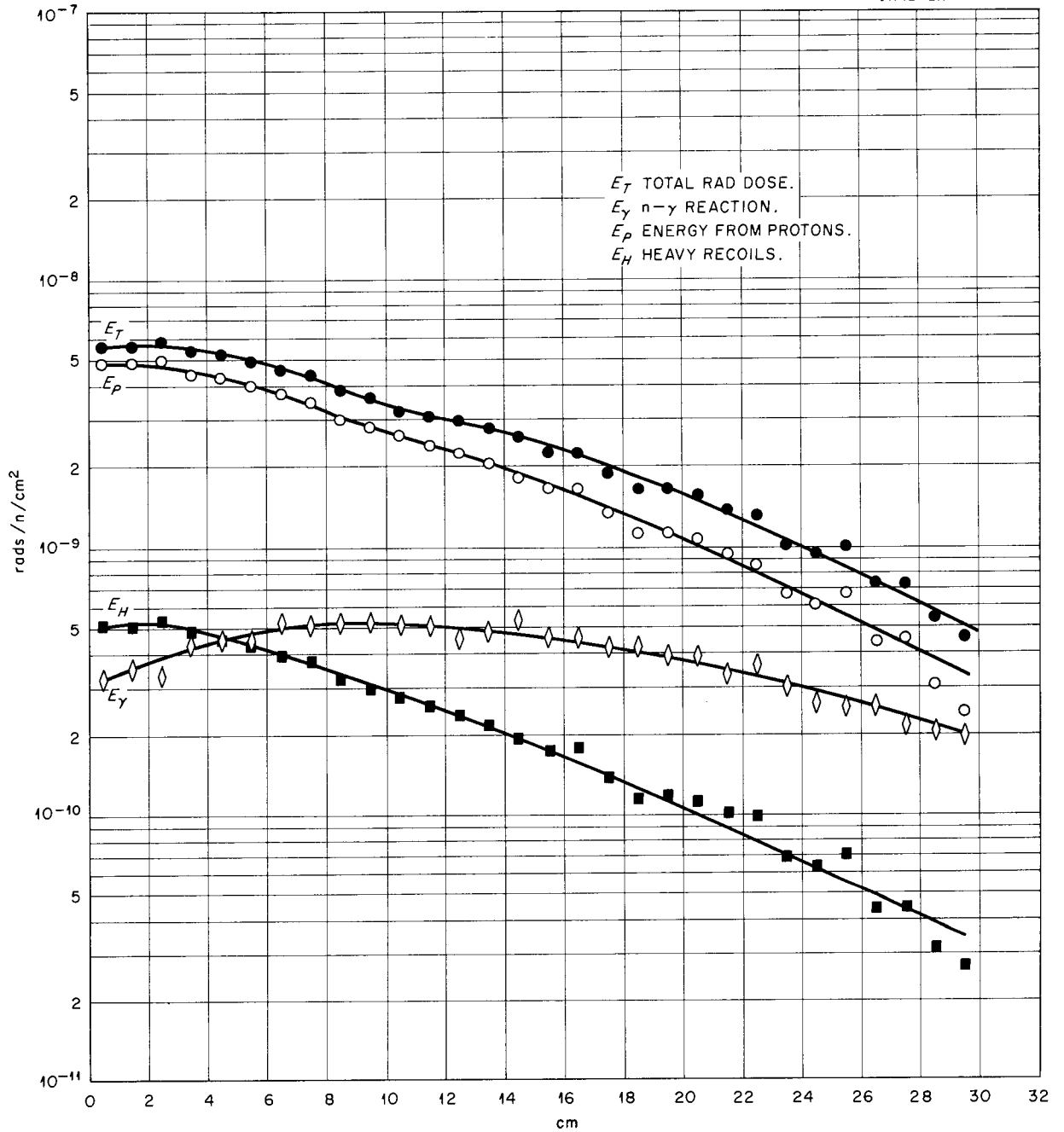


Fig. 64. Absorbed Dose from 5-Mev Neutron Beam.

UNCLASSIFIED  
ORNL-LR-DWG 41244

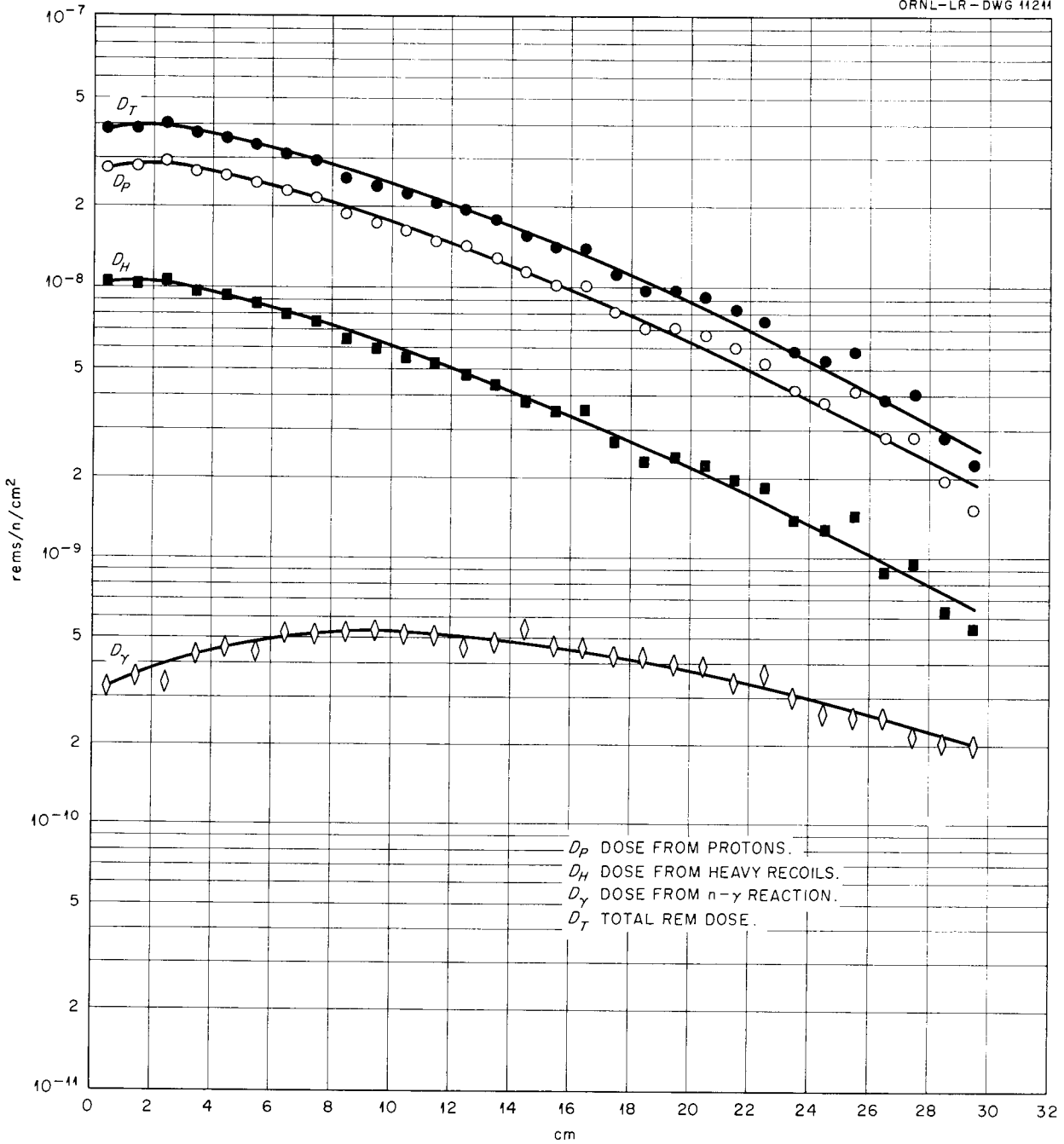


Fig. 65. Biological Dose from 5-Mev Neutron Beam.

UNCLASSIFIED  
ORNL-LR-DWG 11212

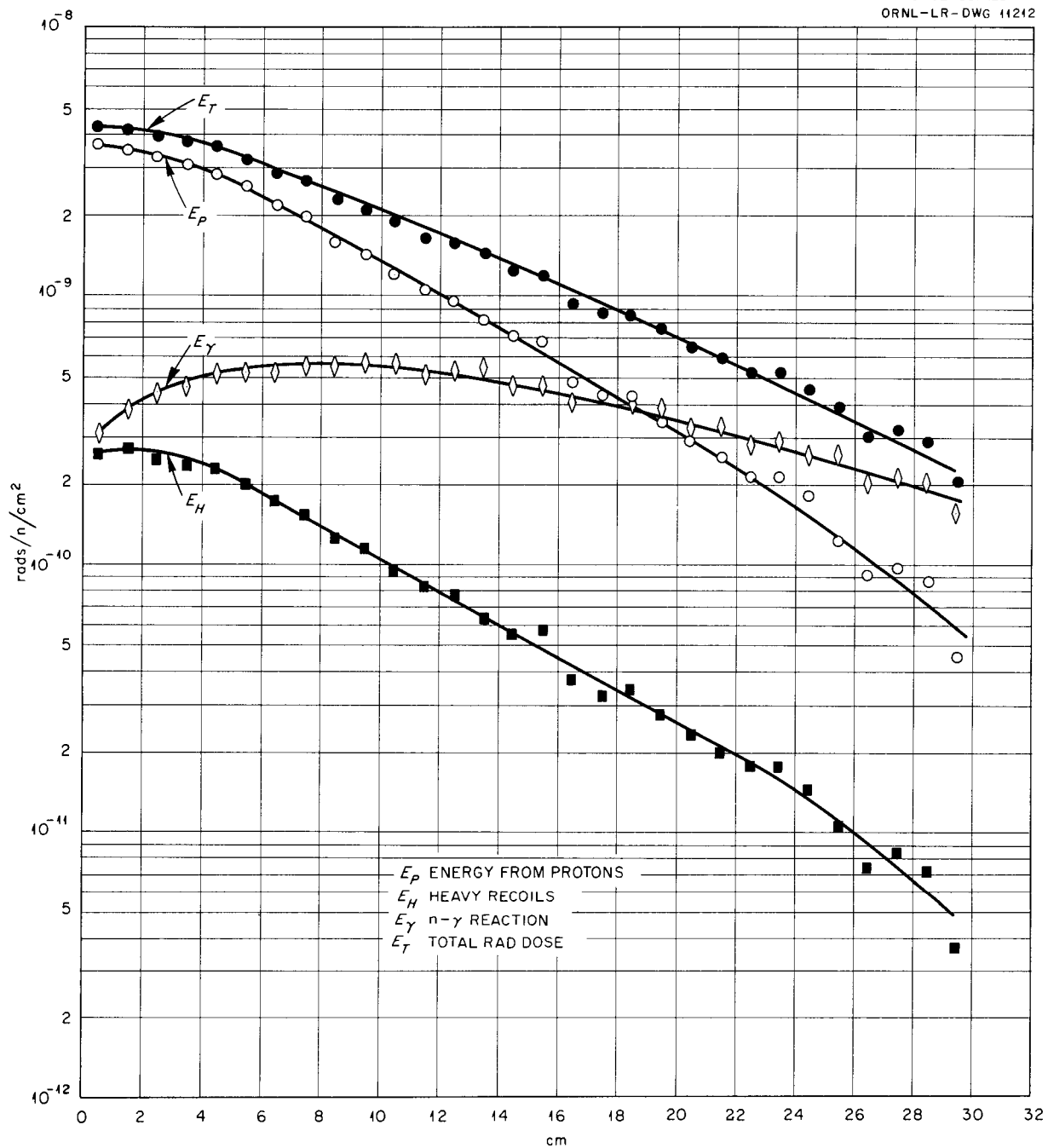


Fig. 66. Absorbed Dose from 2.5-Mev Neutron Beam.

UNCLASSIFIED  
ORNL-LR-DWG 11213

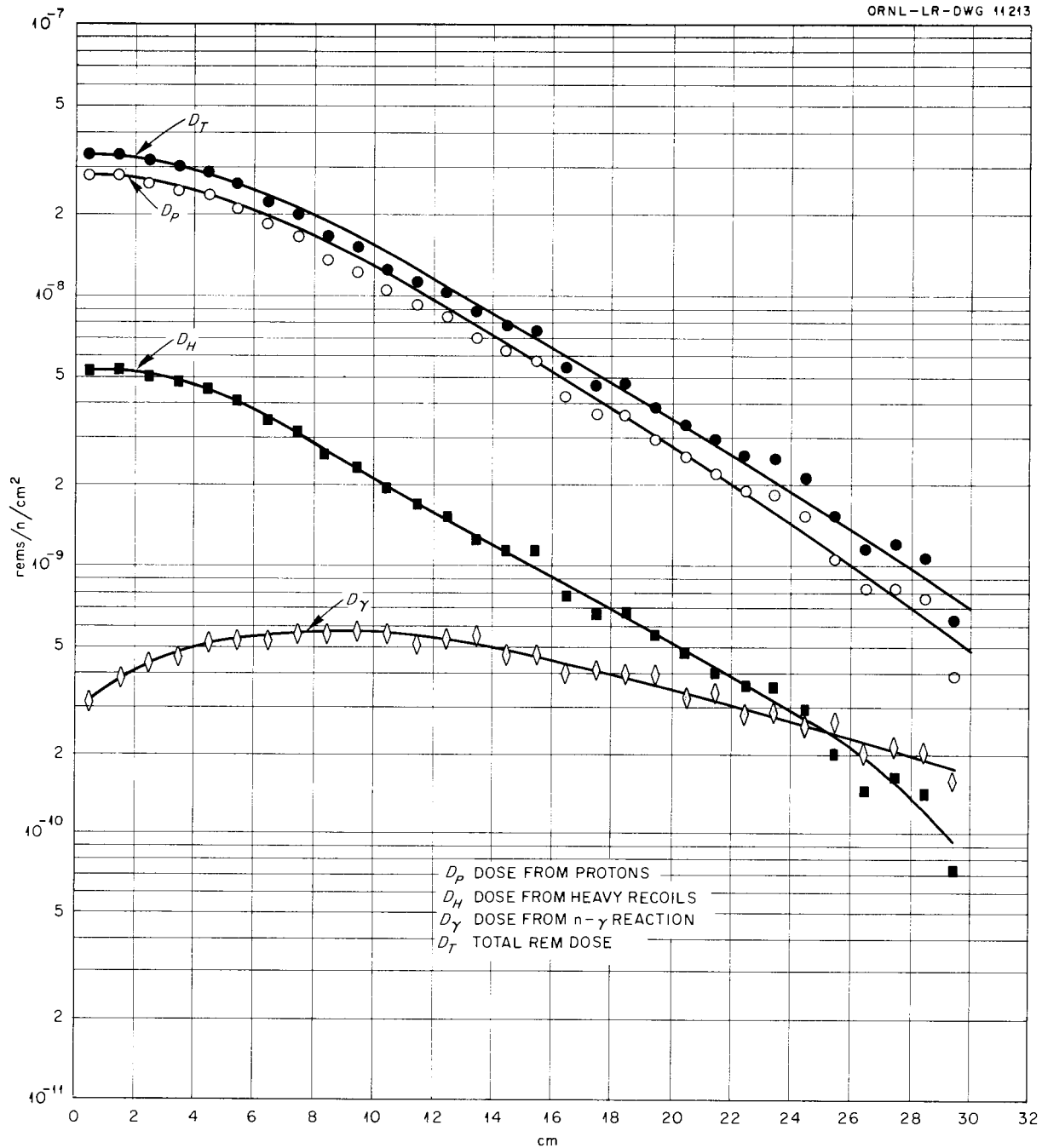


Fig. 67. Biological Dose from 2.5-Mev Neutron Beam.

UNCLASSIFIED  
ORNL-LR-DWG 11192

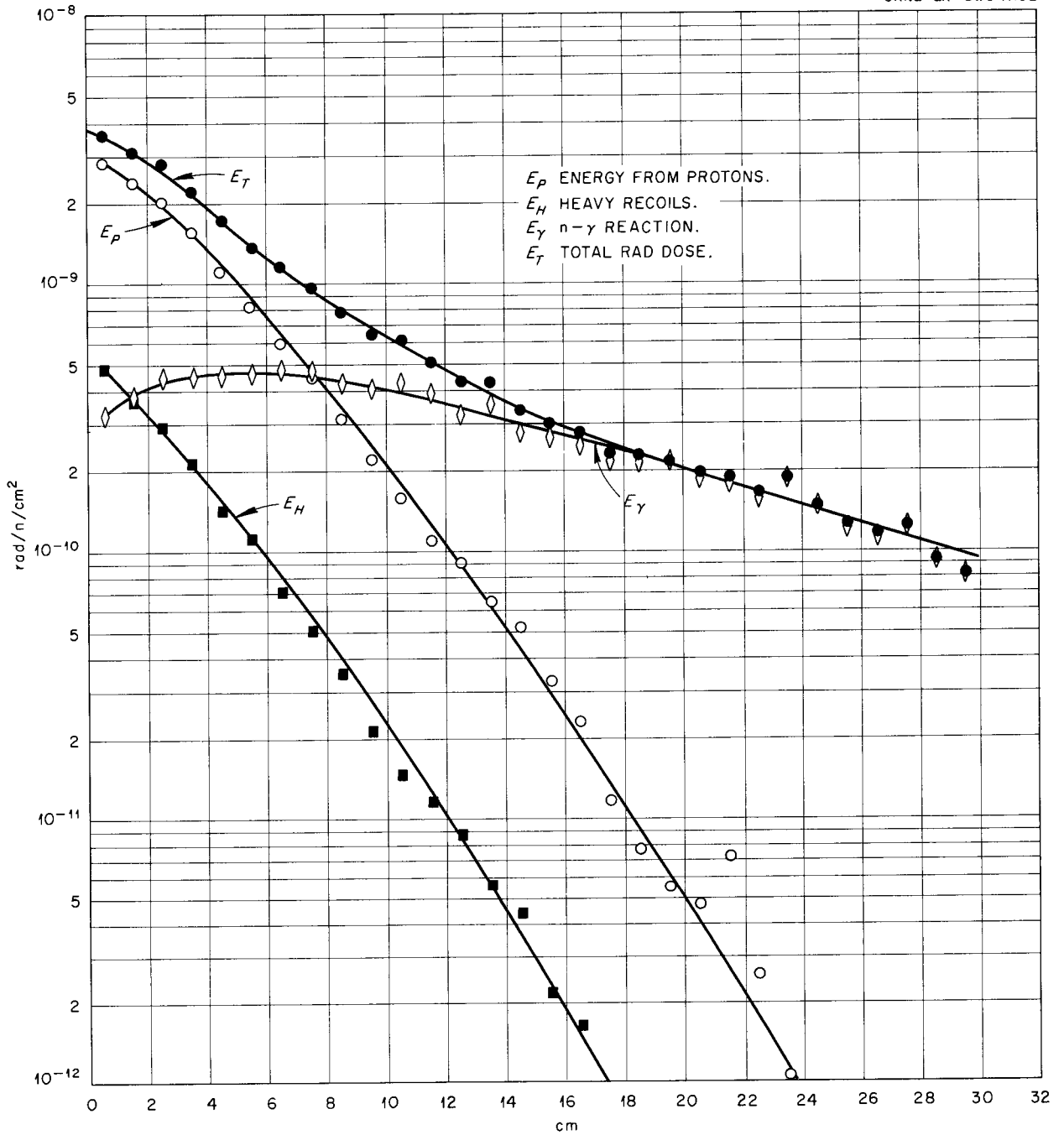


Fig. 68. Absorbed Dose from 1-Mev Neutron Beam.

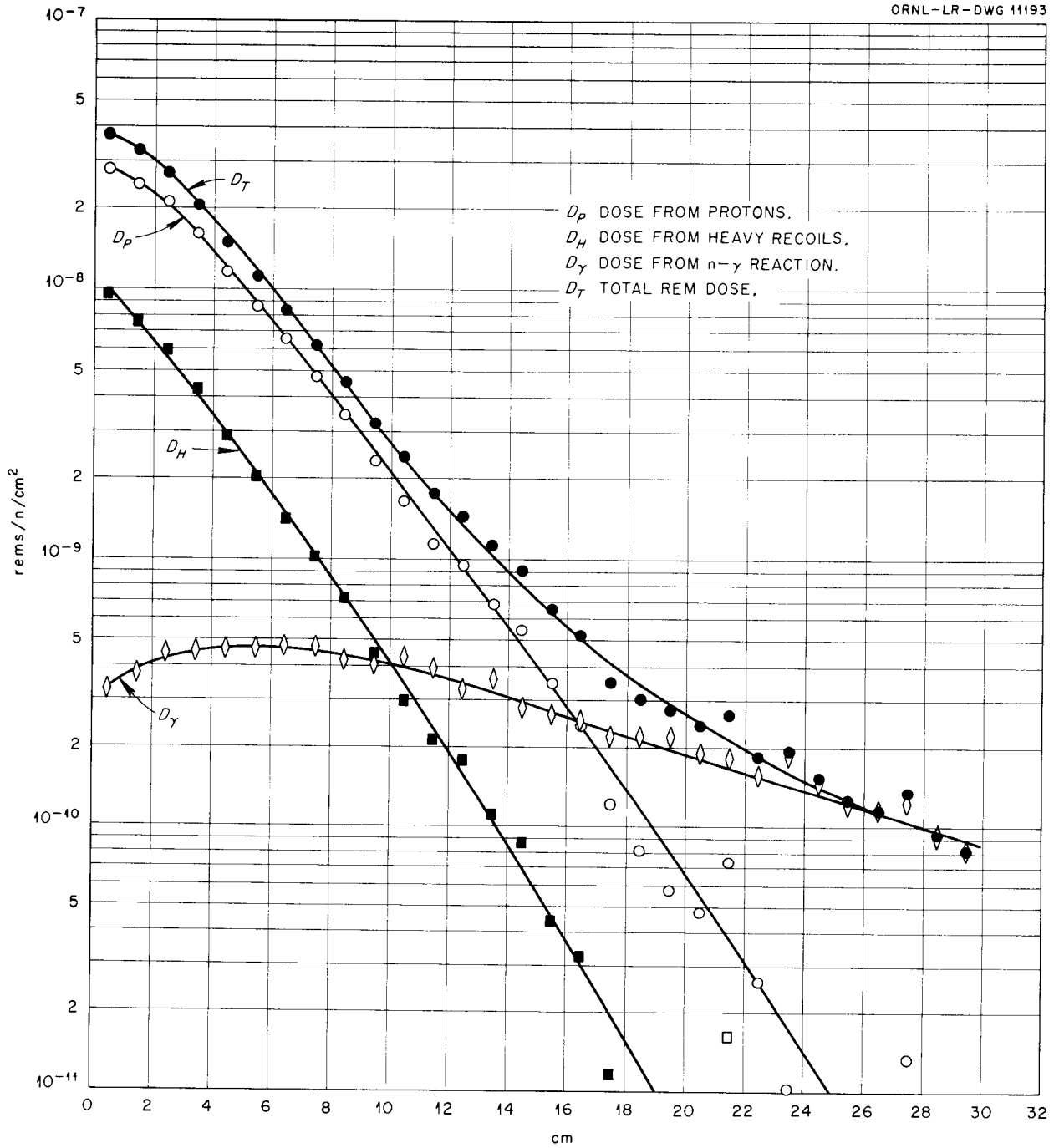


Fig. 69. Biological Dose from 1-Mev Neutron Beam.

UNCLASSIFIED  
ORNL-LR-DWG 11194

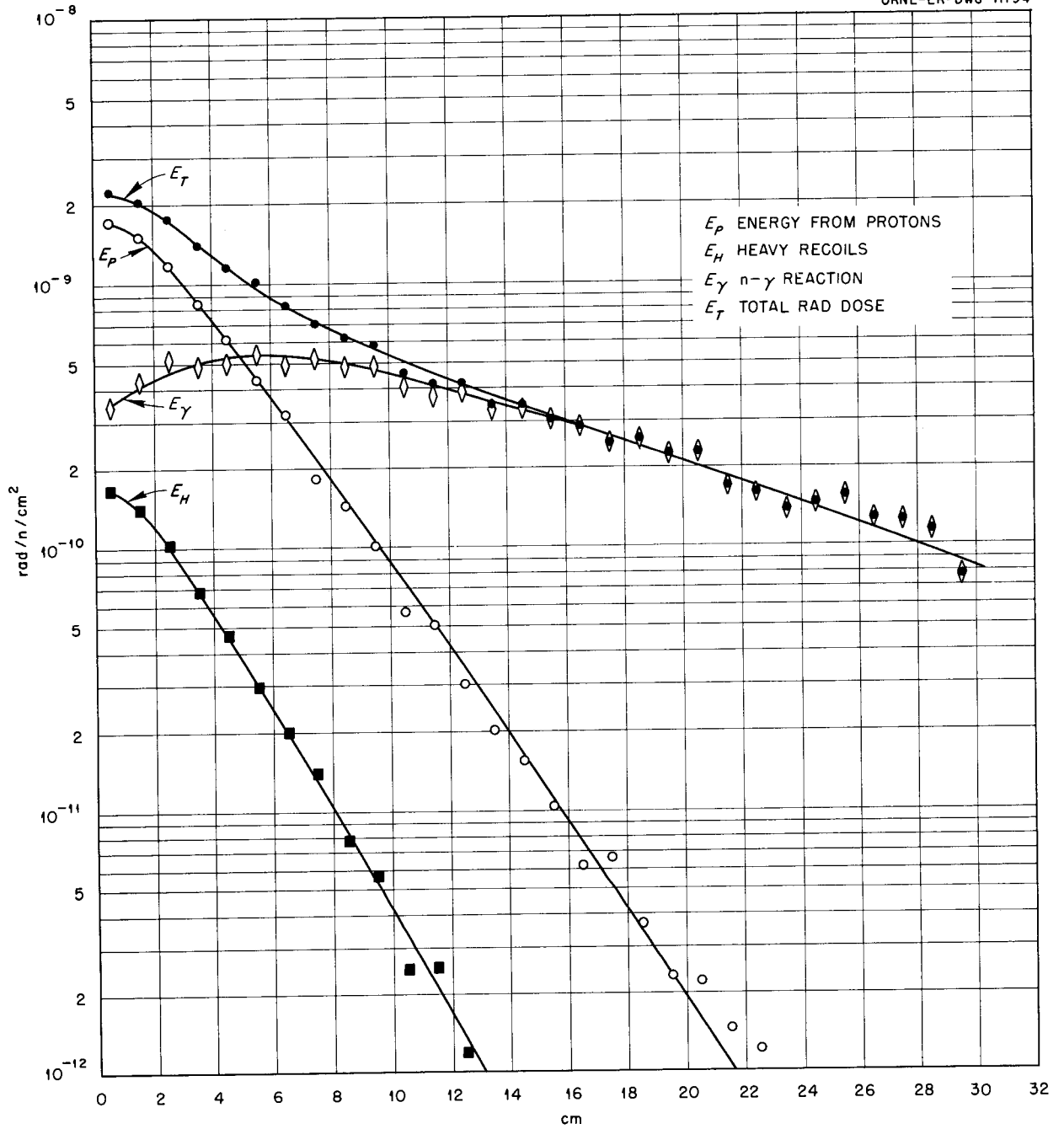


Fig. 70. Absorbed Dose from 0.5-Mev Neutron Beam.

UNCLASSIFIED  
ORNL-LR-DWG 11195

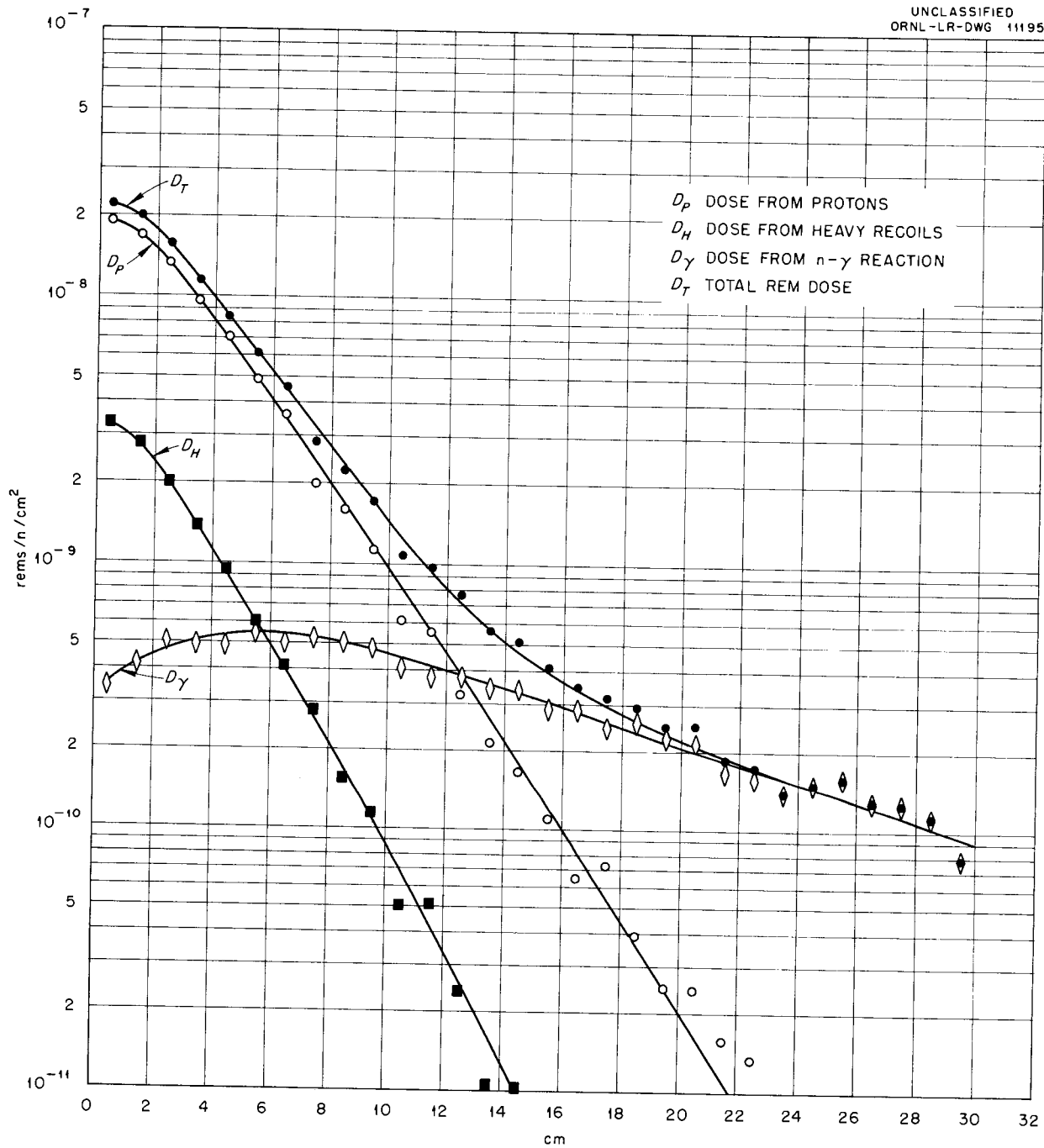


Fig. 71. Biological Dose from 0.5-Mev Neutron Beam.

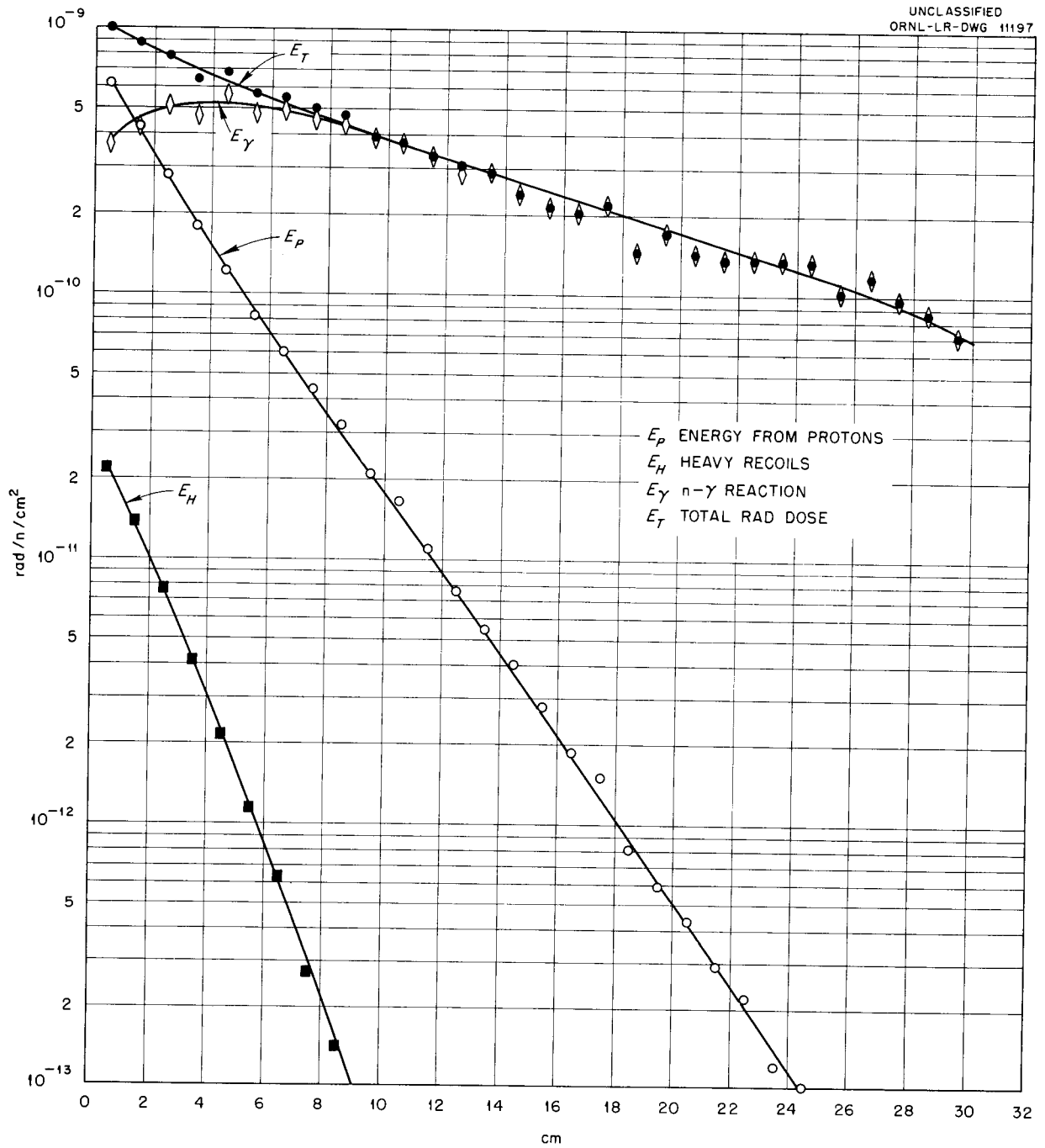


Fig. 72. Absorbed Dose from 0.1-Mev Neutron Beam.

UNCLASSIFIED  
ORNL-LR-DWG 11196

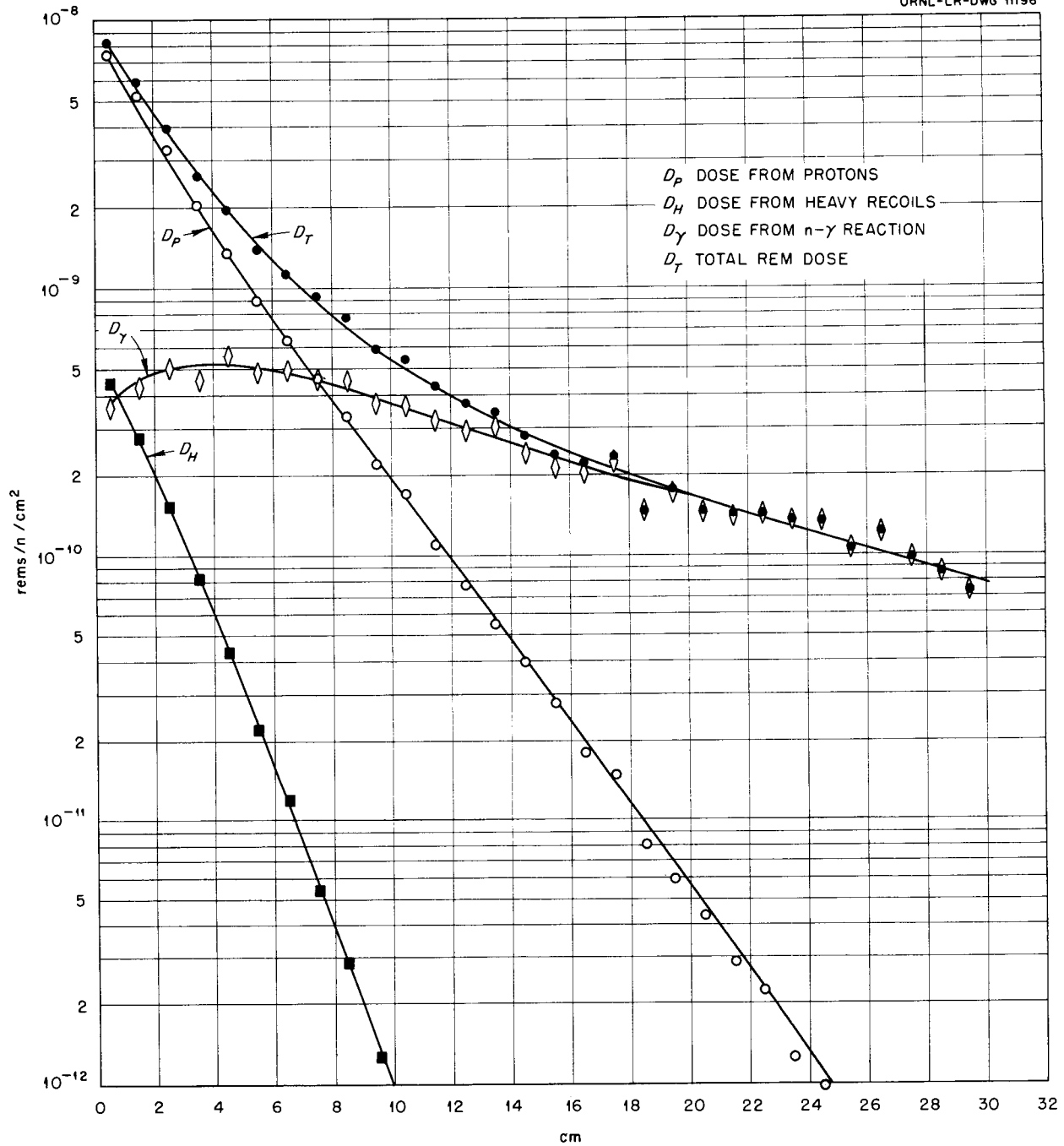


Fig. 73. Biological Dose from 0.1-Mev Neutron Beam.

UNCLASSIFIED  
ORNL-LR-DWG 44198

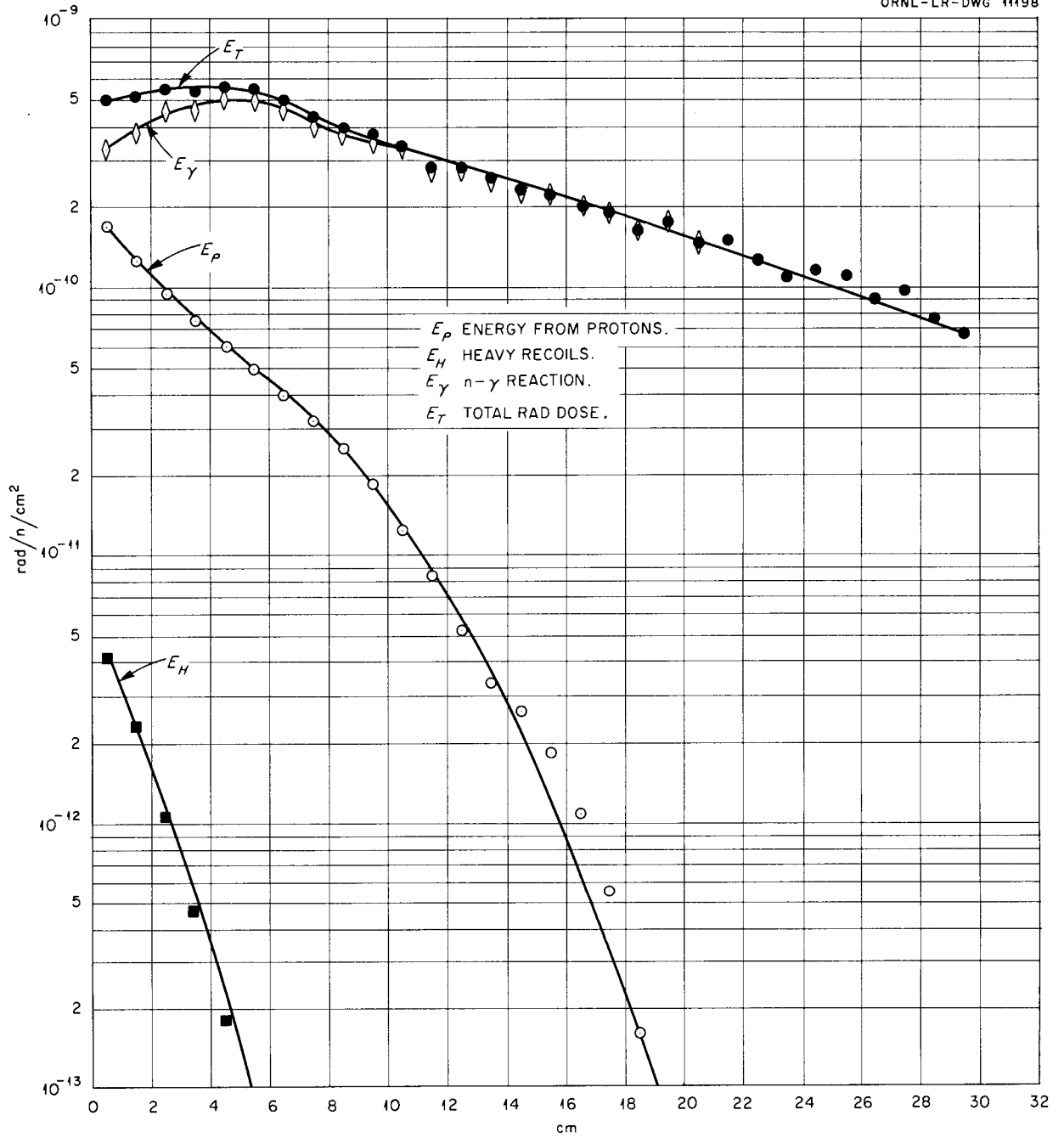


Fig. 74. Absorbed Dose from 0.02-Mev Neutron Beam.

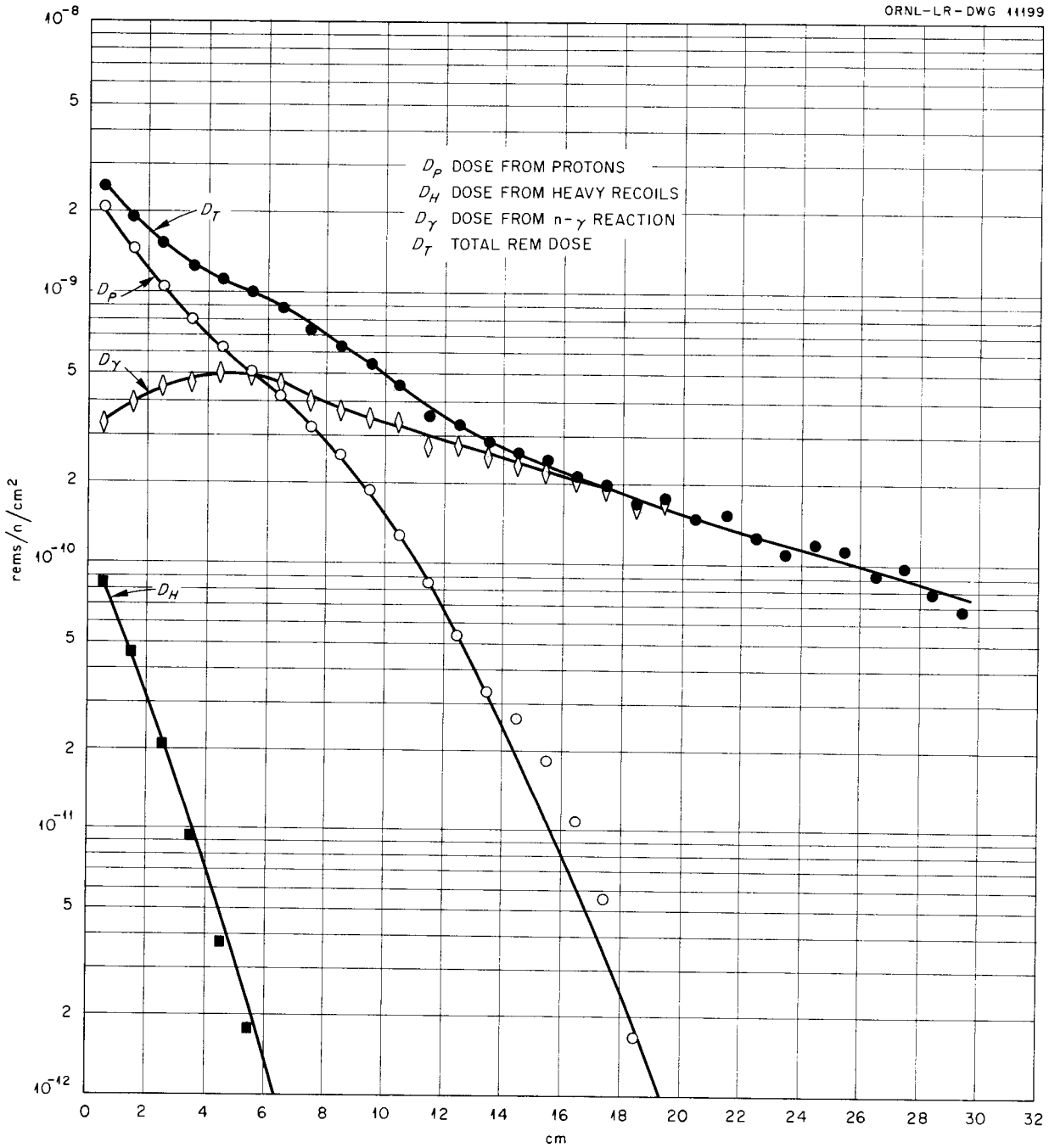


Fig. 75. Biological Dose from 0.02-Mev Neutron Beam.

UNCLASSIFIED  
ORNL-LR-DWG 11200

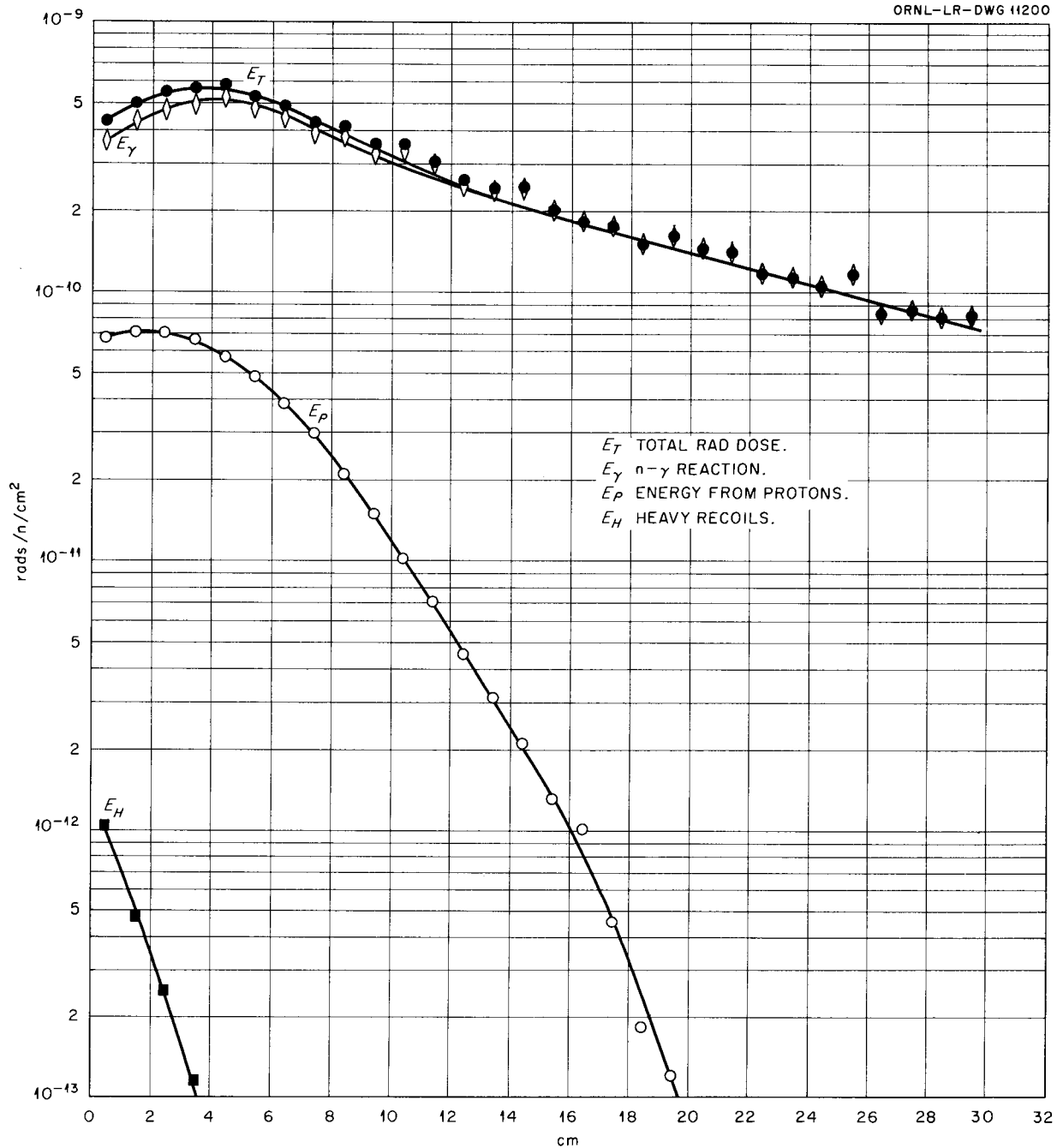


Fig. 76. Absorbed Dose from 0.005-Mev Neutron Beam.

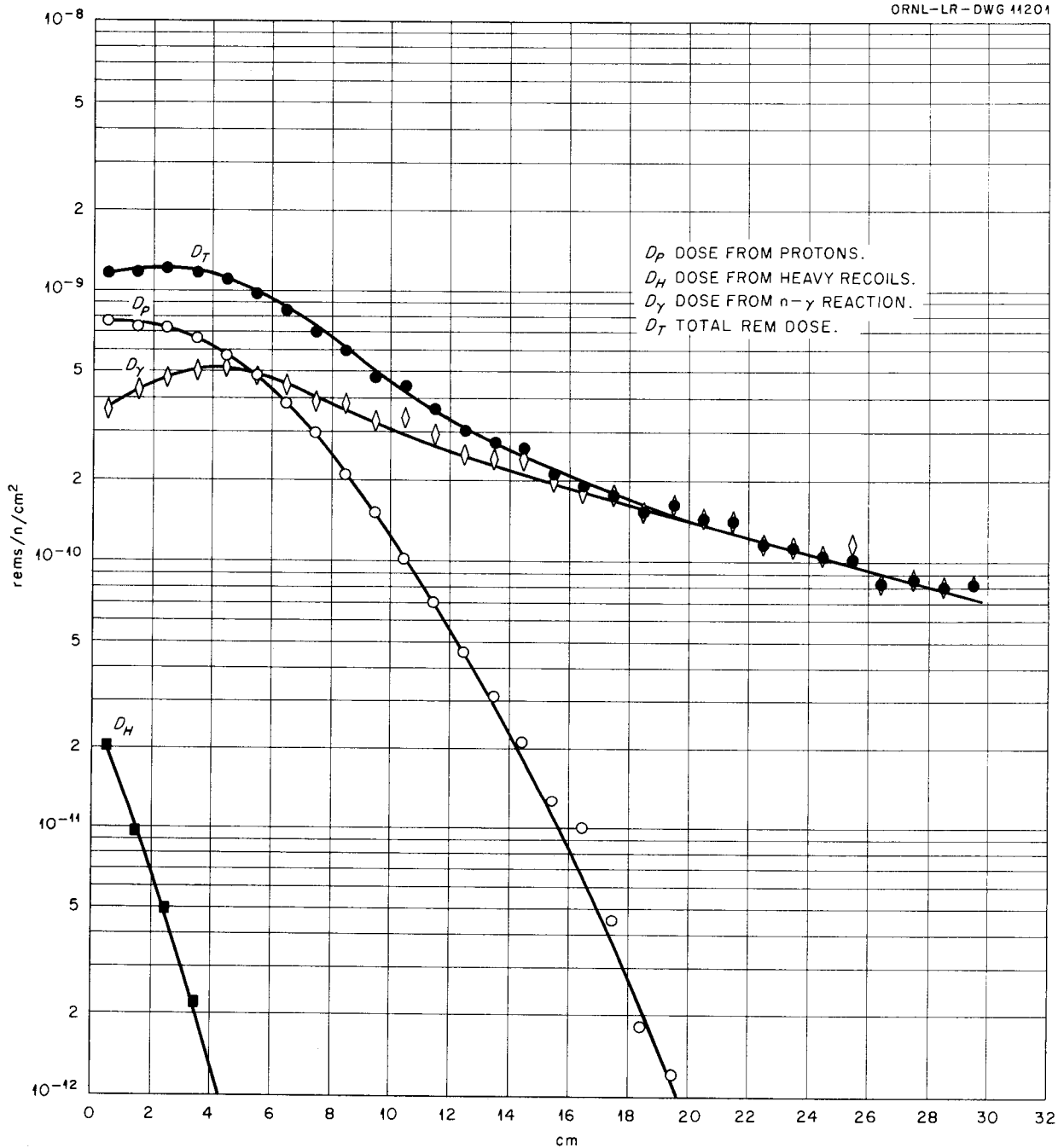


Fig. 77. Biological Dose from 0.005-Mev Neutron Beam.

UNCLASSIFIED  
ORNL-LR-DWG 41203

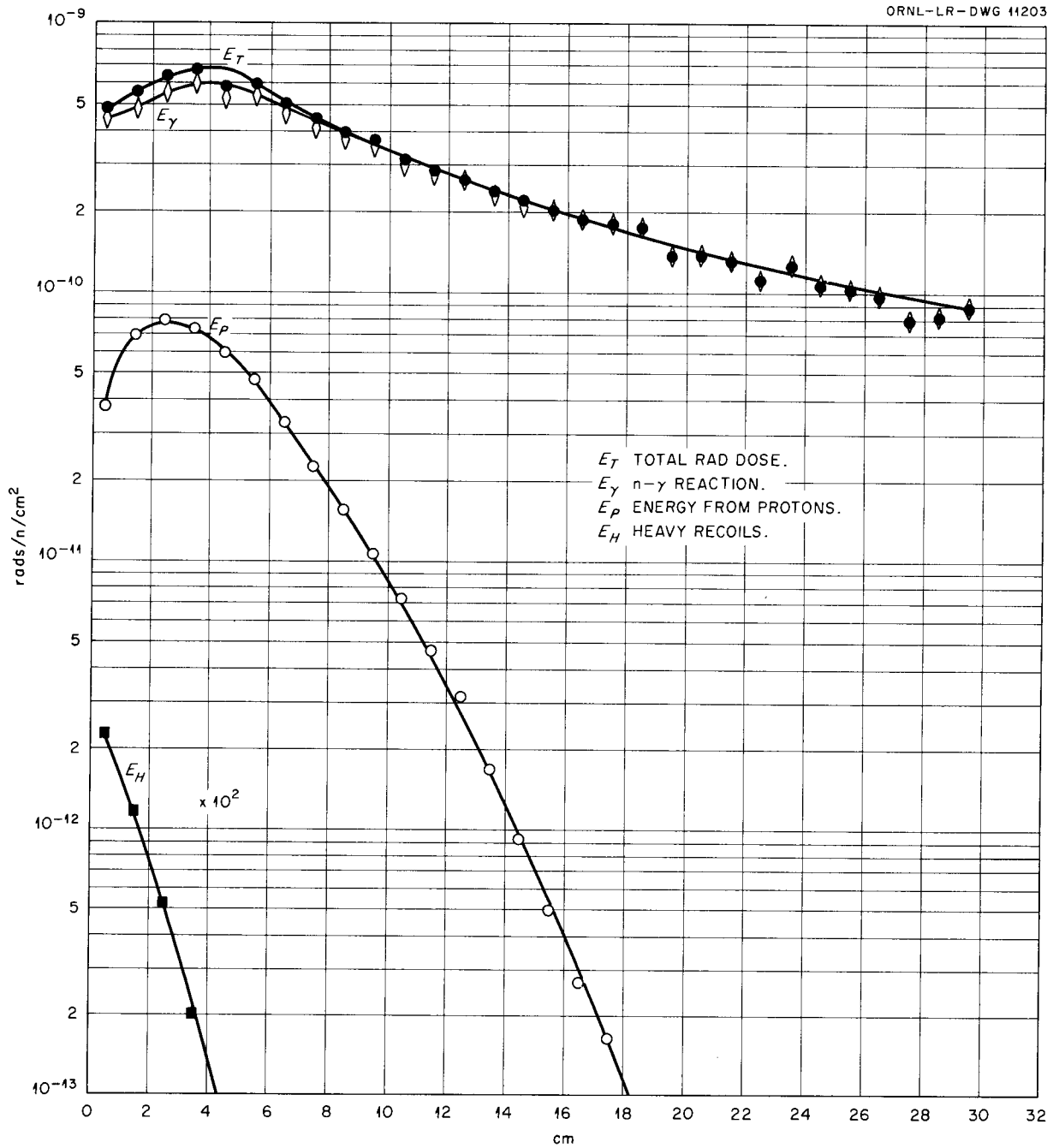


Fig. 78. Absorbed Dose from 0.0001-Mev Neutron Beam.

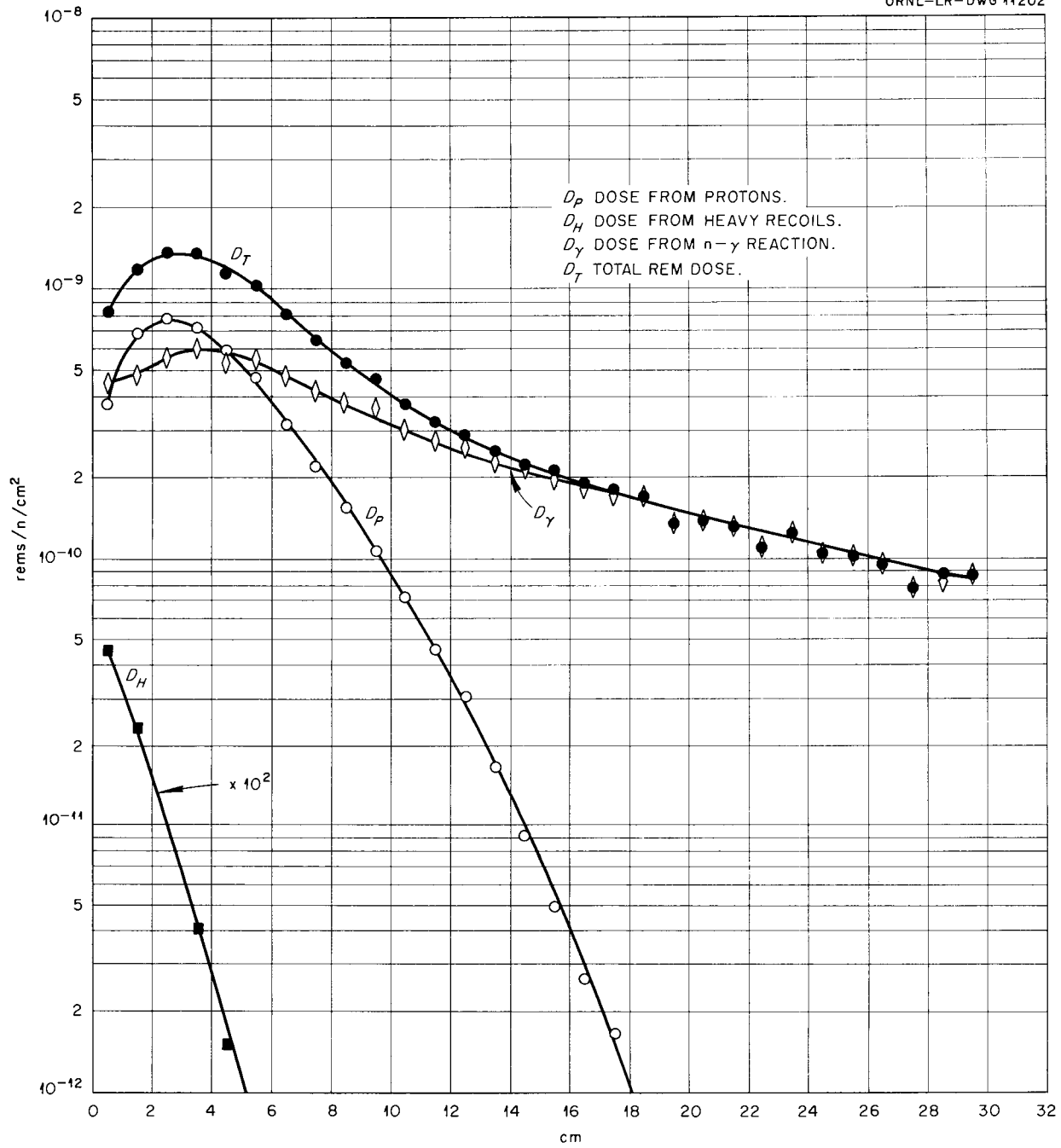


Fig. 79. Biological Dose from 0.0001-Mev Neutron Beam.

UNCLASSIFIED  
ORNL-LR-DWG 11205

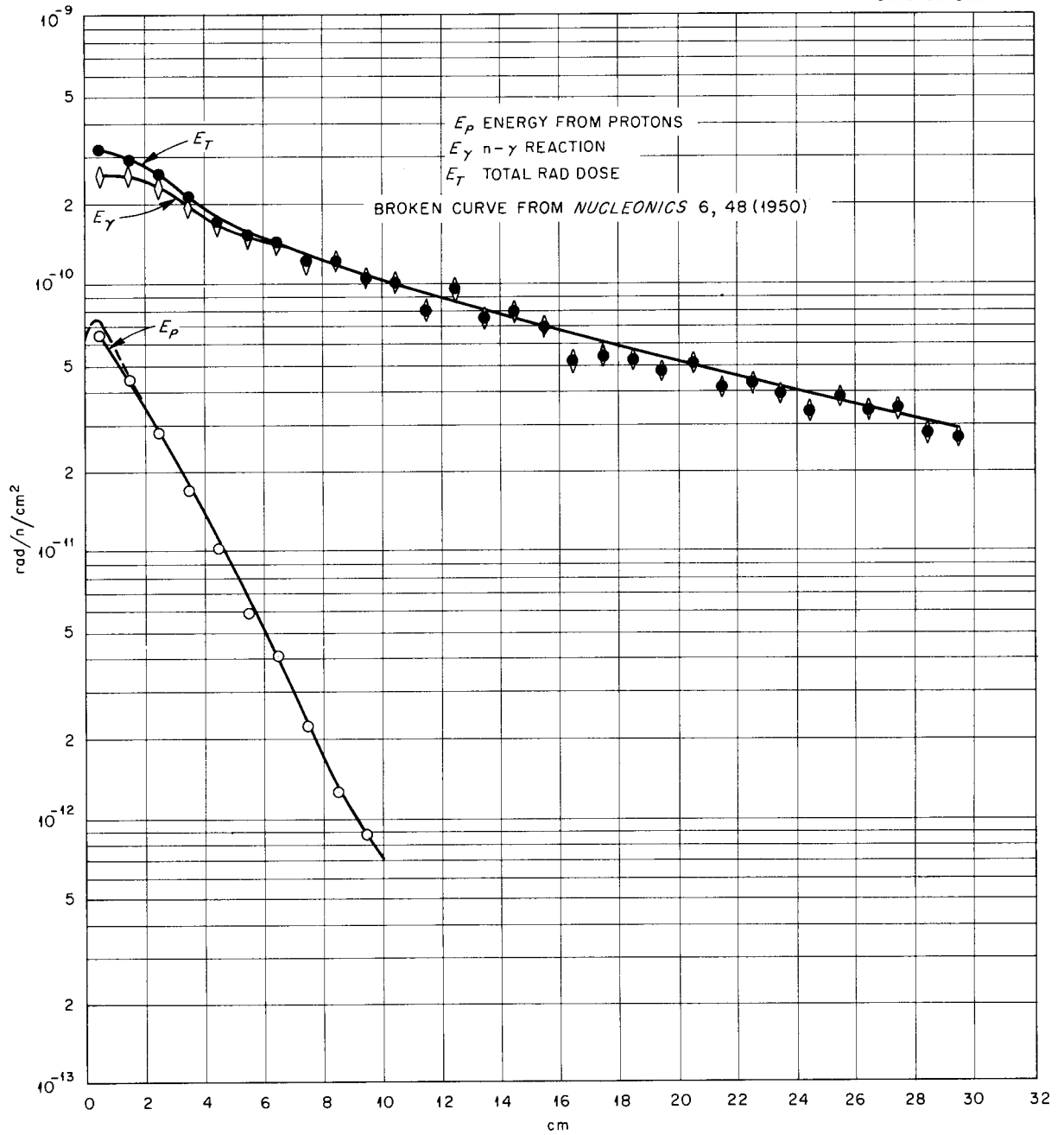


Fig. 80. Absorbed Dose from Thermal Neutron Beam.

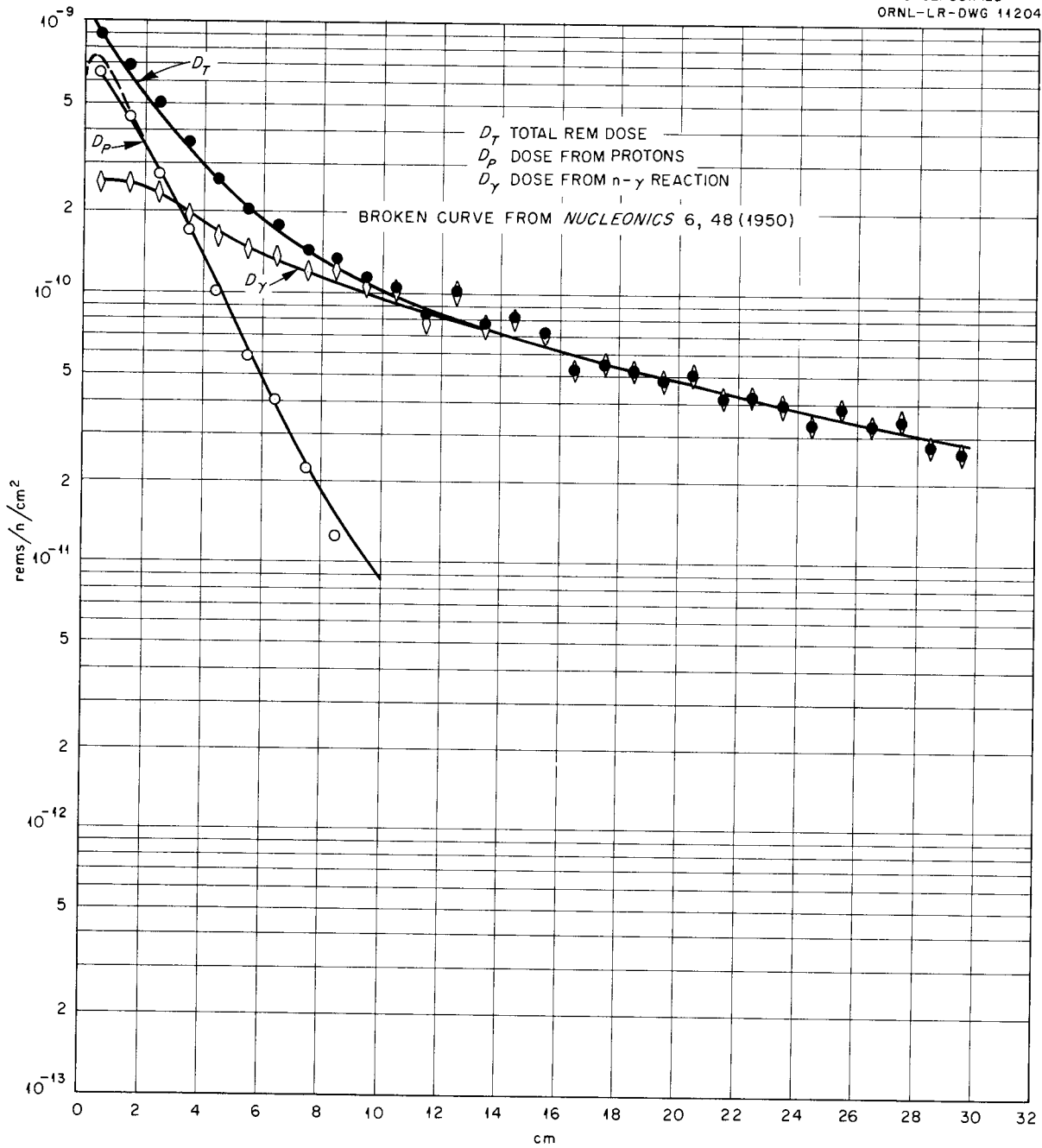


Fig. 81. Biological Dose from Thermal Neutron Beam.

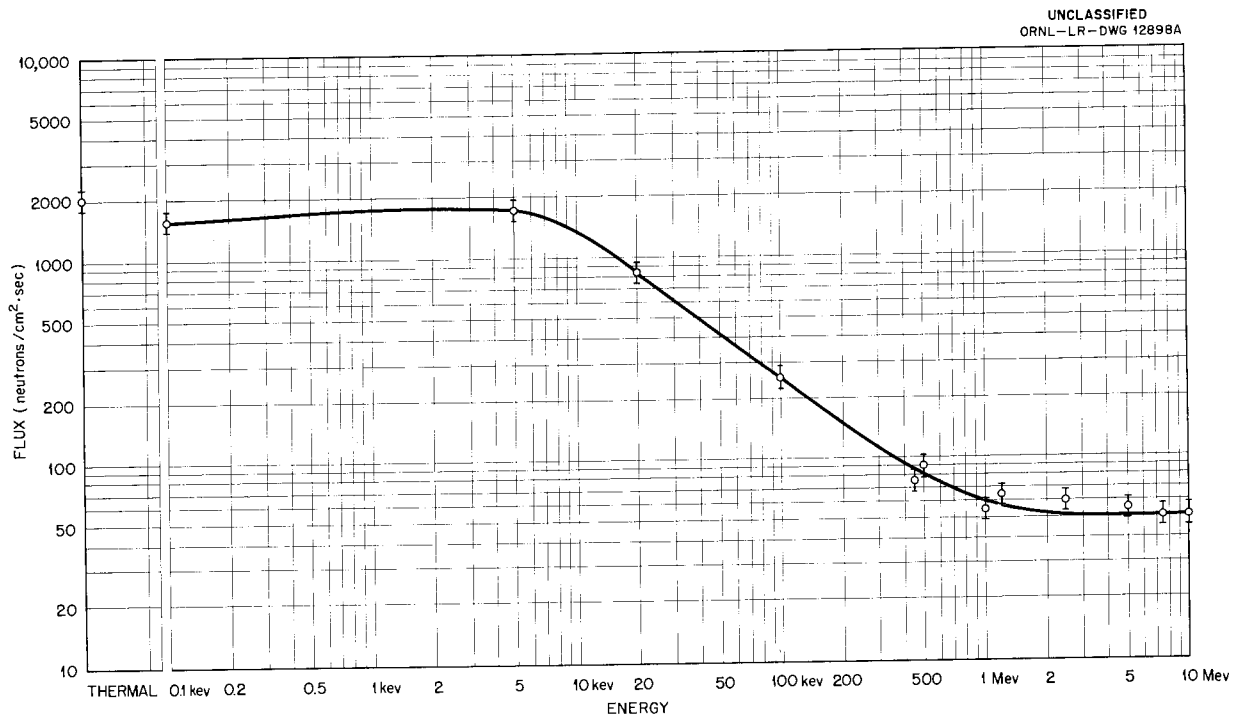


Fig. 82. Maximum Permissible Flux of Neutrons as Function of Neutron Energy (0.3 rem/40 hr).

The absorbed gamma dose rate from polonium-beryllium has been measured as 25% of the absorbed neutron dose rate (both measured in tissue rad units). Generally, the value of the gamma dose rate from such a source is taken as 10% of the neutron dose rate. In a previous report<sup>22</sup> this value of 10% was assumed, which led to the conclusion that the contribution from inelastic scattering and capture of neutrons to the response of the carbon-carbon dioxide ionization chamber was significant. By using the value of 25% as measured with the new dosimeter, essentially all the current in the ionization chamber can be accounted for as gamma radiation and recoil atoms, thus invalidating the earlier conclusion that inelastic scattering and hydrogen capture of neutrons by the gas-and-water-tight cover and the carbon walls of the chamber were significant. The differences noted in the response of the chamber when different materials are used for the gas-and-water-tight cover can be attributed to gamma absorption. Correction for the recoil-atom response has been shown to be neces-

sary in some measurements and the correction is made according to the method outlined previously.<sup>22</sup>

#### Evaluation of Gases for Fast-Neutron Dosimeter

A preliminary study to determine the usefulness of cyclopropane as a counting gas in the fast-neutron dosimeter was reported previously.<sup>23</sup> In addition to ethylene and cyclopropane there are several other commercially available gases such as propene, butene-1, butene-2, and isobutylene, which have the same carbon-to-hydrogen ratio,  $C_N H_{2N}$ , as the polyethylene liner used in the counter. The integral-pulse-height curves for four of these gases, in which were used plutonium alpha particles (the source for calibration of the standard fast-neutron dosimeter), are shown in Figs. 89-92. The per cent resolution was calculated from each of the integral-pulse-height curves and the resolution was plotted as a function of the high voltage (Fig. 93) and as a function of the electronic gain (Fig. 94) for each of the gases. The electronic gain is that amplification necessary to make approximately 50% of the counter pulses equal to or

<sup>22</sup>F. J. Davis *et al.*, *HP Semiann. Prog. Rep.* Jan. 31, 1956, ORNL-2049, p 54, esp. 58.

<sup>23</sup>*Ibid.*, p 56.

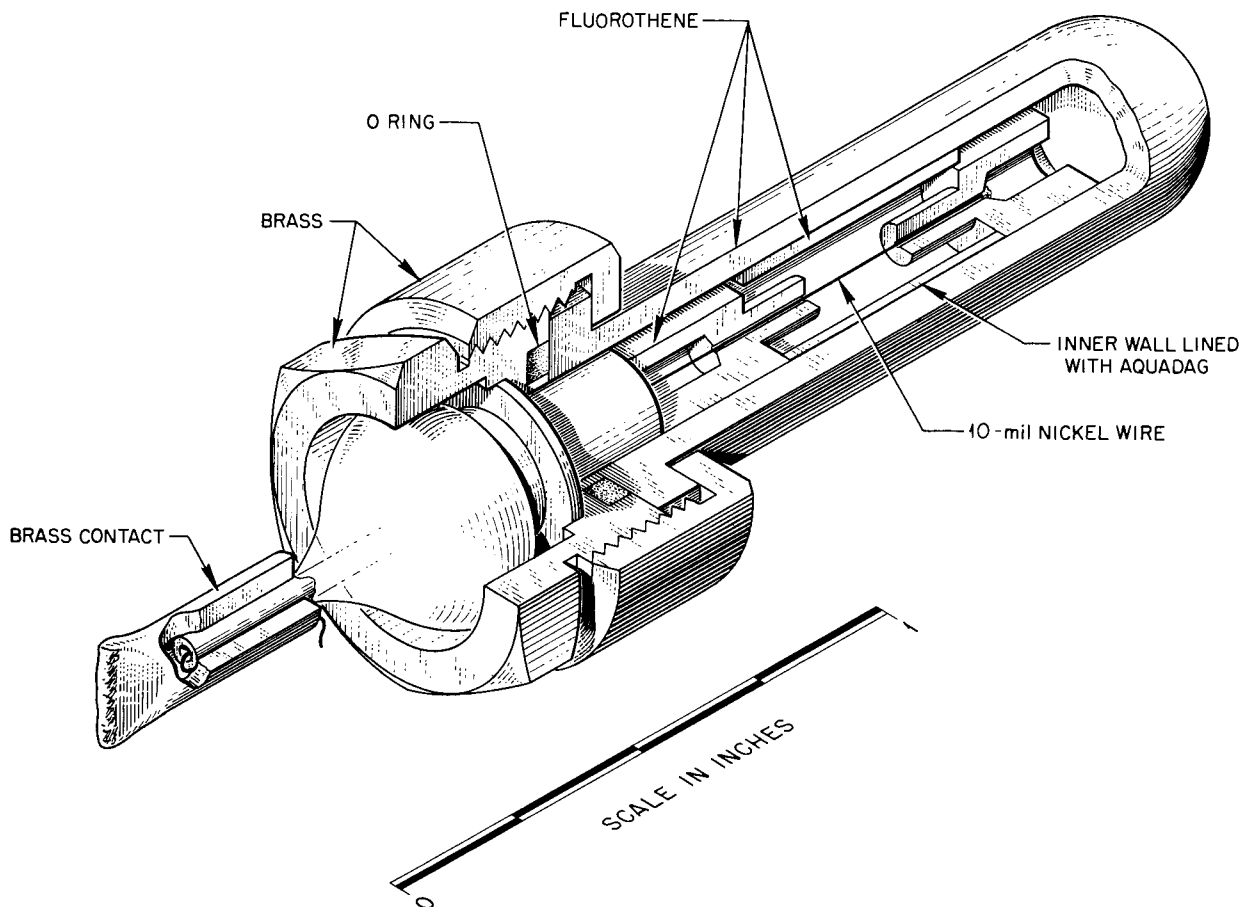


Fig. 83. Gamma Dosimeter.

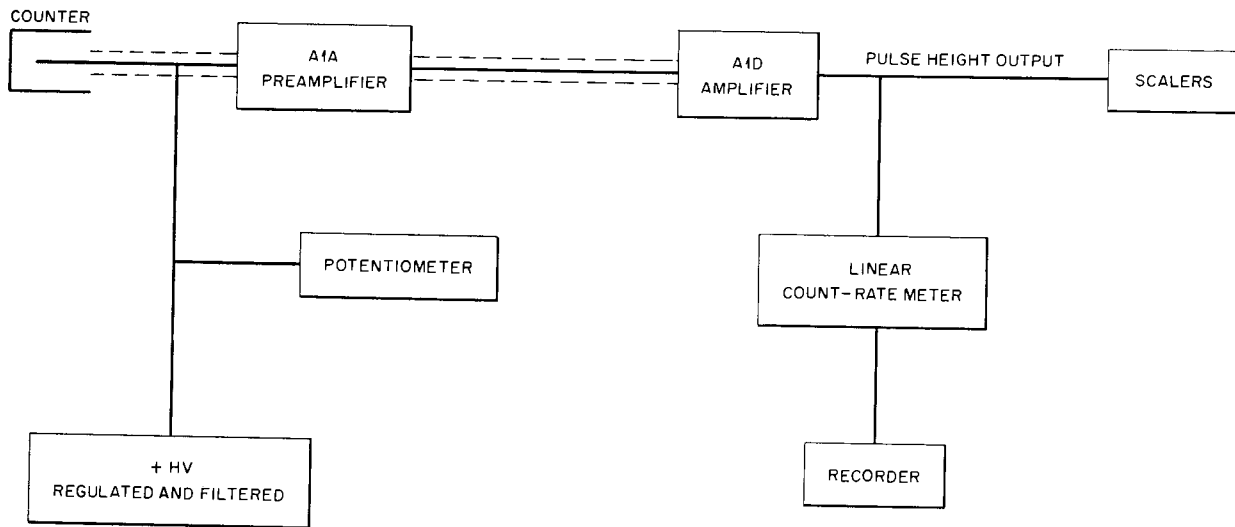


Fig. 84. Dosimeter Apparatus.

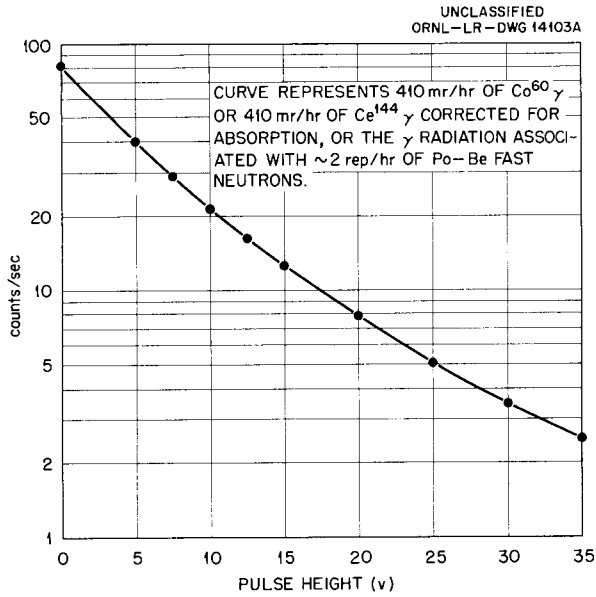


Fig. 85. Typical Pulse Height Distribution.

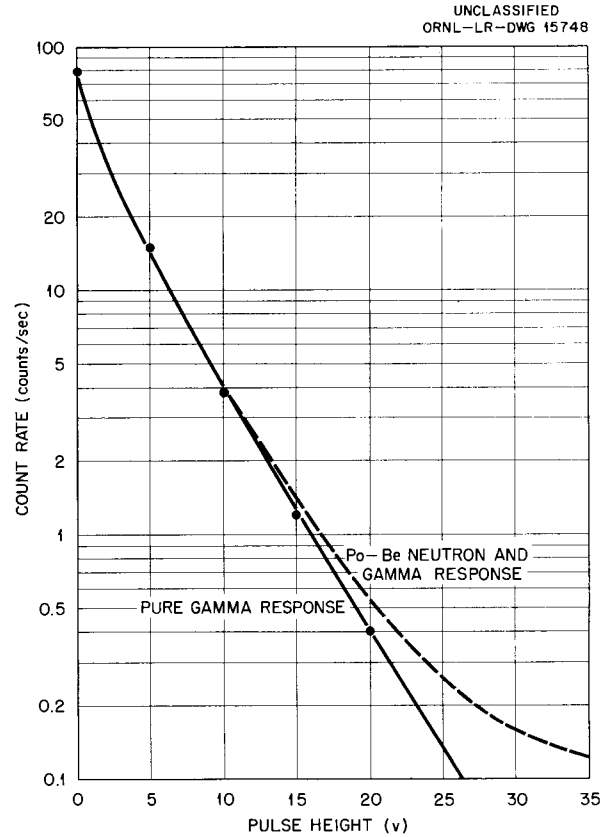


Fig. 87. Pulse Height Distributions for Counter Voltage That Is Too Low.

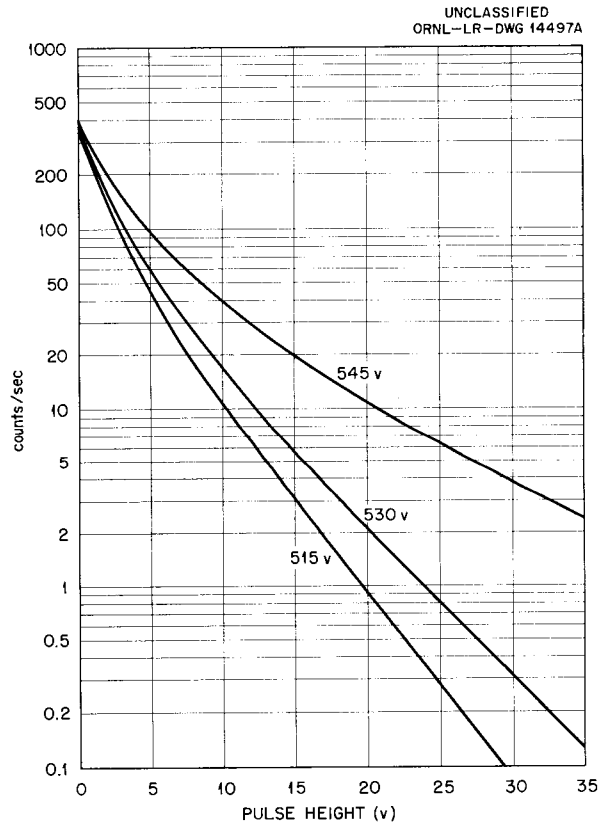


Fig. 86. Pulse Height Distribution as a Function of Voltage on Counter. (For gamma radiation, constant gain,  $\text{CS}_2$ -filled fluoroethene)

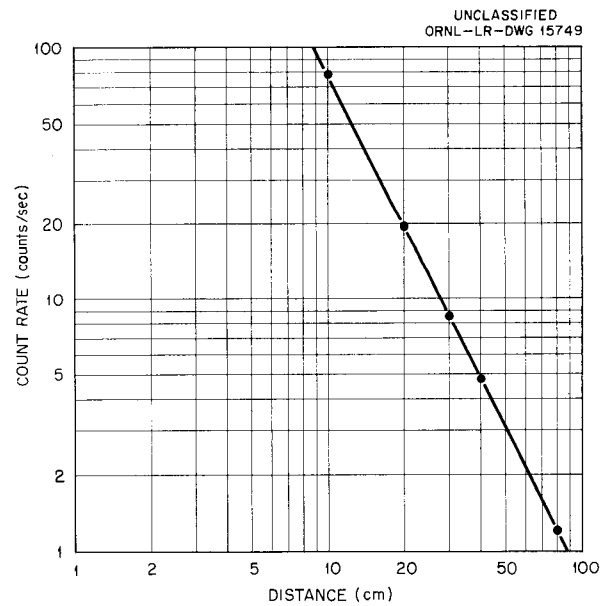


Fig. 88. Integral Count Rate as a Function of Source-Counter Distance. (Pulse height selector at 6 v)

UNCLASSIFIED  
ORNL-LR-DWG 15750

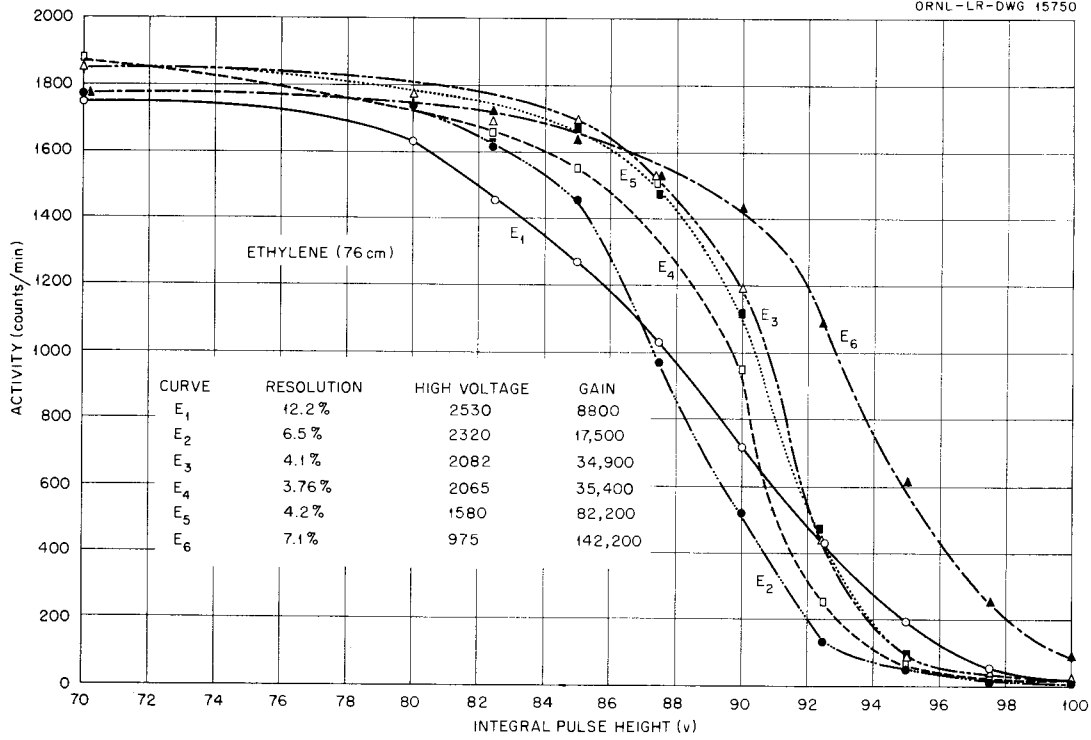


Fig. 89. Integral Pulse Height Curve for Ethylene at 76 cm.

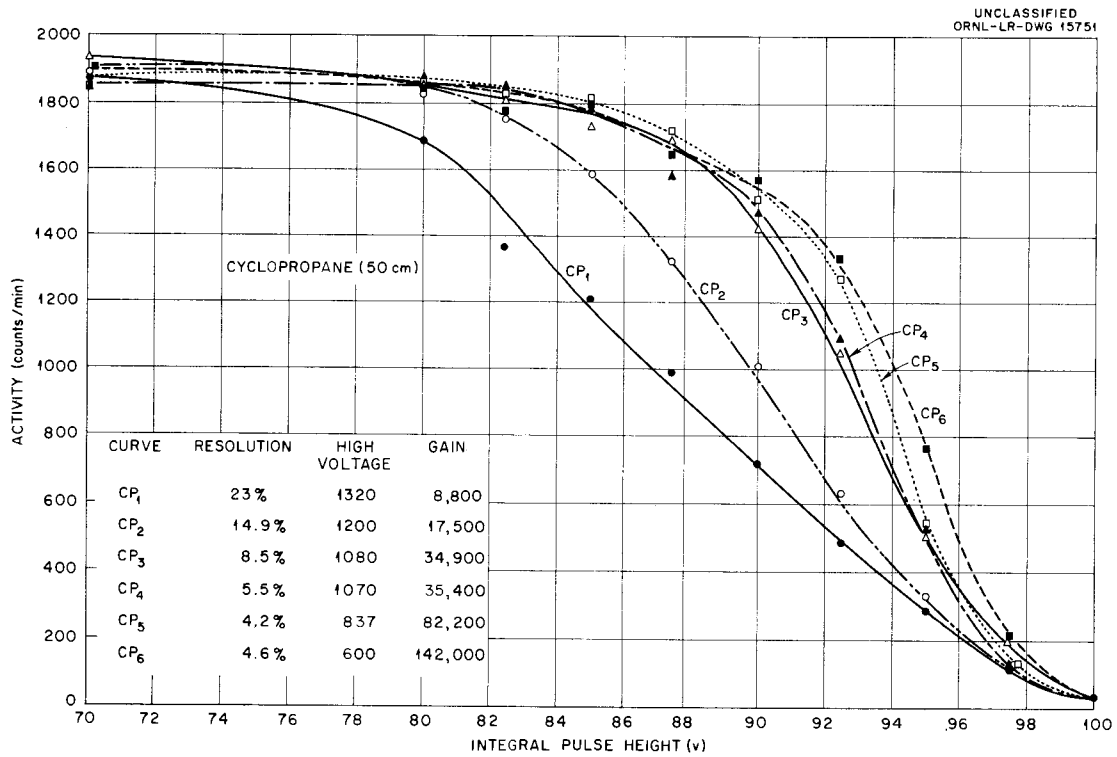


Fig. 90. Integral Pulse Height Curve for Cyclopropane at 50 cm.

UNCLASSIFIED  
ORNL-LR-DWG 15752

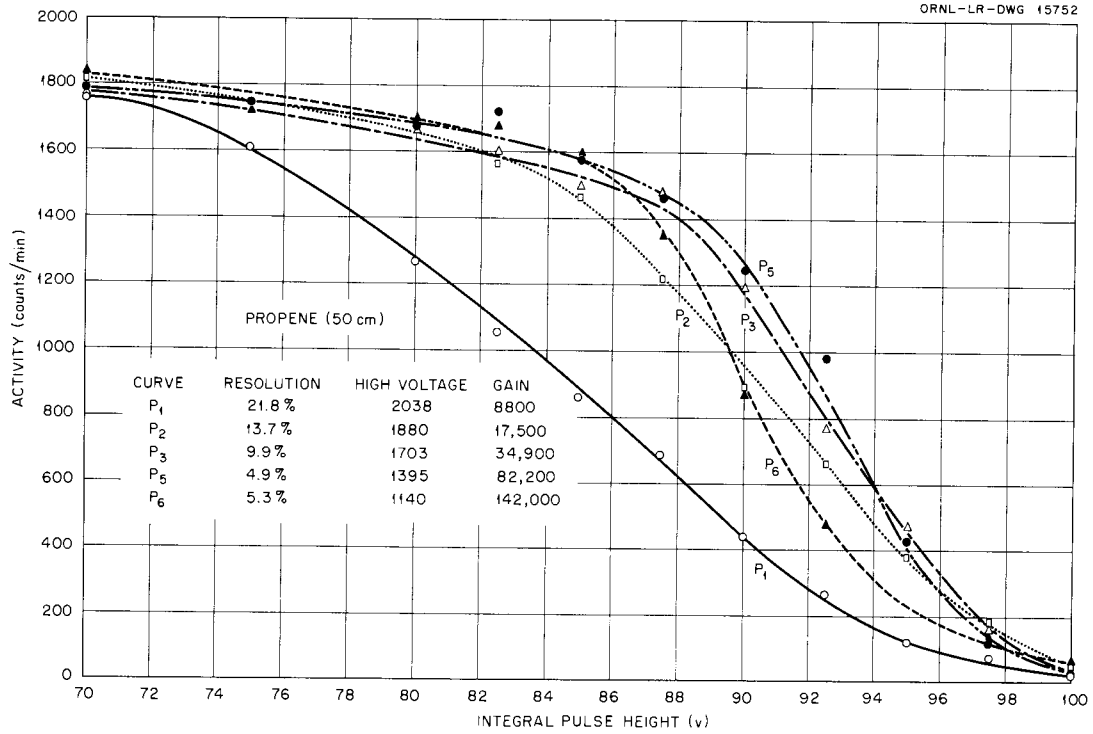


Fig. 91. Integral Pulse Height Curve for Propene.

UNCLASSIFIED  
ORNL-LR-DWG 15753

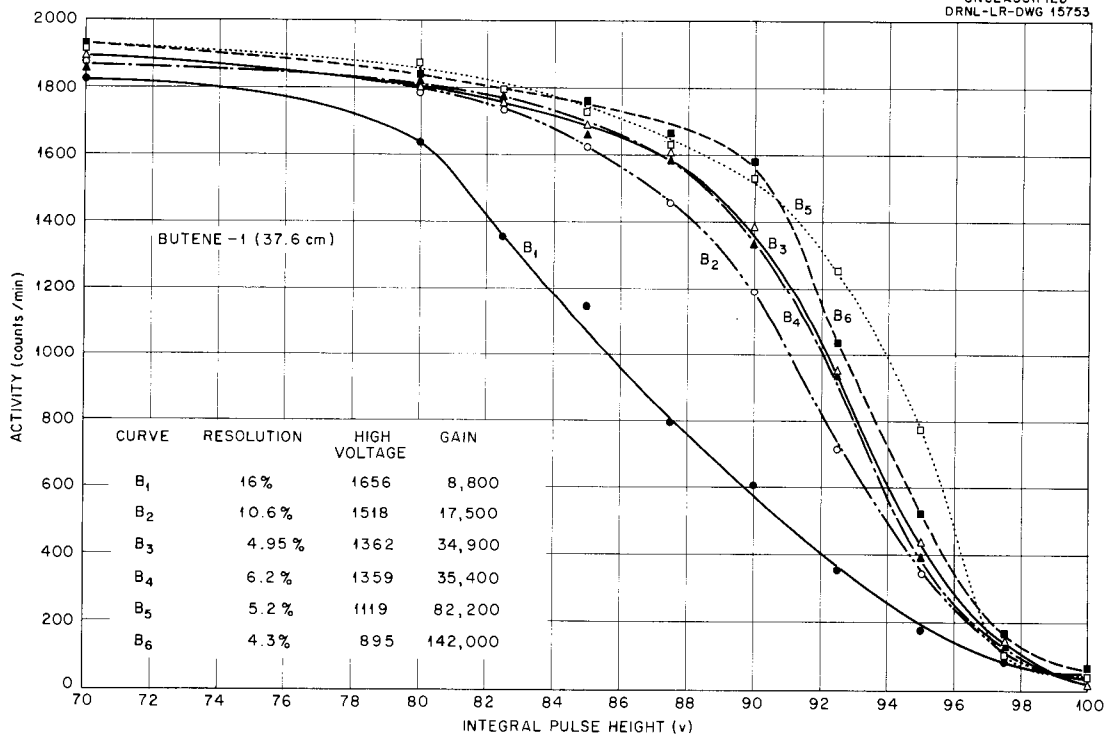


Fig. 92. Integral Pulse Height Curve for Butene-1 at 37.6 cm.

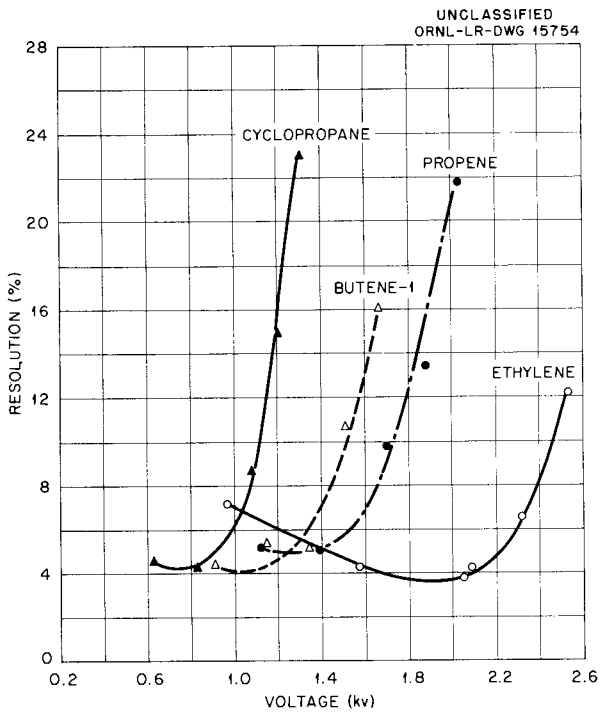


Fig. 93. Resolution vs High Voltage for Ethylene, Cyclopropane, Propene, and Butene-1.

larger than 90 v in amplitude. The high voltage as a function of electronic gain for each of the gases is shown in Fig. 95.

The curves allow the gas, electronic gain, and high voltage to be selected that will give the optimum operating conditions for a given fast-neutron measurement. In addition, the curves indicate the direction of future development in proportional counter dosimetry.

The  $W$  values (electron volts per ion pair) for the above gases and several similar gases have been determined by using the equipment previously described.<sup>24</sup> The  $W$  values for  $Pu^{239}$  alpha particles are as follows:

Gas	$W$ values (ev/ion pair)
Ethylene	27.9
Cyclopropane	25.9
Propene	27.2
Isobutylene	26.6
Butene-1	26.5
Butene-2 ( <i>cis</i> )	26.3
Butene-2 ( <i>cis</i> and <i>trans</i> )	26.3

<sup>24</sup>T. E. Bortner and G. S. Hurst, *Phys. Rev.* **93**, 1236 (1954).

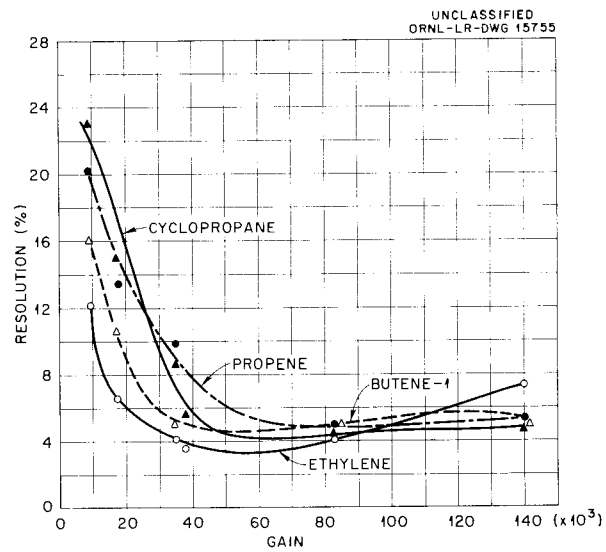


Fig. 94. Resolution vs Electronic Gain for Ethylene, Cyclopropane, Propene, and Butene-1.

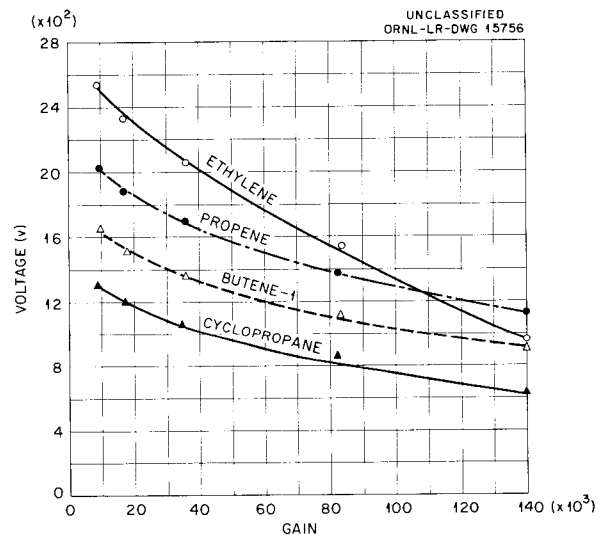


Fig. 95. High Voltage vs Electronic Gain for Ethylene, Cyclopropane, Propene, and Butene-1.

### Neutron-Threshold-Detector Program

A method for measuring the spectrum of neutrons with a series of foil detectors has been described.<sup>25-27</sup> The detectors consist of  $Au^{197}$ ,

<sup>25</sup>G. S. Hurst *et al.*, ORNL-1671. (Secret)

<sup>26</sup>F. J. Davis *et al.*, *HP Semiann. Prog. Rep.* Jan. 31, 1956, ORNL-2049, p 54.

<sup>27</sup>G. S. Hurst *et al.*, *Rev. Sci. Instr.* **27**, 153 (1956).

$\text{Pu}^{239}$ ,  $\text{Np}^{237}$ ,  $\text{U}^{238}$ , and  $\text{S}^{32}$ . The amount of induced activity in the detecting elements is determined with scintillator counters, and the neutron spectrum is constructed.

The scintillation counting efficiency for  $\text{Pu}^{239}$ ,  $\text{Np}^{237}$ , and  $\text{U}^{238}$  has been increased by a factor of approximately 18 by counting all pulses representing an energy of 0.5 Mev or greater instead of 1.1 Mev or greater and by counting the samples between  $2 \times 4$  in. NaI crystals rather than  $1 \times 1\frac{1}{2}$  in. crystals. In the case of  $\text{Np}^{237}$  a correction for neutron activation is made by observing the 1.04-Mev  $\text{Np}^{238}$  peak with a single-channel analyzer approximately 3 days after irradiation.

The  $\text{S}^{32}(n, p)\text{P}^{32}$  reaction is used to determine approximately the number of neutrons having energy greater than 2.5 Mev. The reaction produces  $\text{P}^{32}$ , which is a 1.71-Mev beta emitter with a 14.3-day half life. The  $\text{P}^{32}$  beta is counted with a plastic scintillation counter. The previous method was to use a sulfur disk with a thickness slightly greater than the range of the 1.71 beta. This limited the sensitivity to the area of sulfur that could be counted on a given detector.

A simple, reproducible method for concentrating  $\text{P}^{32}$  into a small area from a large volume of  $\text{S}^{32}$  has been found. A volume of activated sublimed sulfur in a thin aluminum dish is melted on a hot plate, and when the sulfur has melted, it is ignited and allowed to burn out completely, leaving the  $\text{P}^{32}$  attached to the aluminum dish. The yield has been determined (roughly) to be greater than 90%.

To determine the reproducibility of the method, ten consecutive burnings were made in the same aluminum dish and from a single batch of neutron-irradiated sulfur. The count rates as determined after each burning are shown in Fig. 96. The point at 12.9 g is undoubtedly a counter error as the points above this fall on the curve. The method increases the count rate by a factor of approximately 7 for a thickness of sulfur slightly greater than the range of the 1.71-Mev beta.

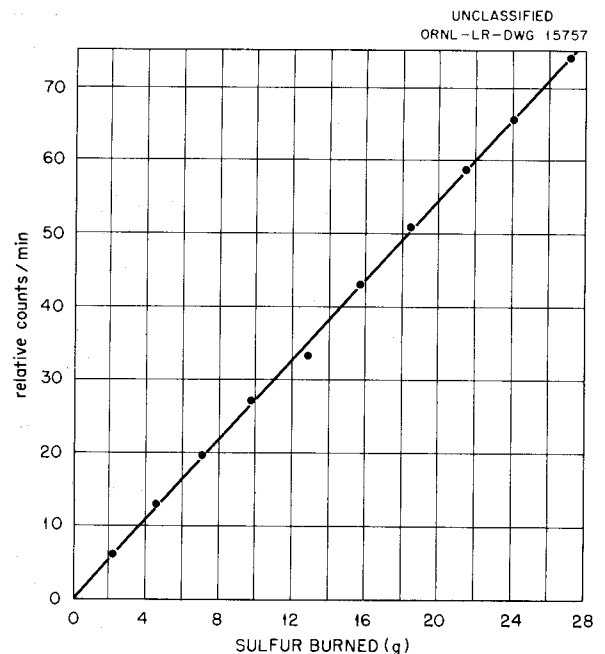


Fig. 96. Count Rate After Various Amounts of Sulfur Were Burned.

A  $1\frac{1}{2}$ -in. sulfur disk, which weighed 18.05 g, was exposed to approximately  $2 \times 10^8$  neutrons/cm<sup>2</sup> from a polonium-beryllium source. The count rate after burning and a short time after the exposure was approximately 170 counts/min or 9.3 counts/min/g of  $\text{S}^{32}$ .

Two pounds of unirradiated sulfur was burned in a 4-in.-dia aluminum dish and counted on a  $4\frac{1}{2}$ -in. plastic scintillator. No detectable count above counter background was noted. Since the amount of sulfur that can be counted on a given sensitive counting area is no longer a limiting factor, the sensitivity of neutron detection by the  $\text{S}^{32}(n, p)\text{P}^{32}$  method can be increased by many orders of magnitude.

## EDUCATION, TRAINING, AND CONSULTATION

E. E. Anderson

### AEC FELLOWSHIP PROGRAM

E. E. Anderson                      M. F. Fair

The present group of 20 AEC Fellows in Radiological Physics completed the year of graduate study at Vanderbilt University in June. The records for the year show that 70% of the group earned an average of B or better. The group is now at ORNL for training in Applied Health Physics and a ten-week course in Reactor Engineering. Four of the group were granted a six-month extension of their Fellowship and will work on research problems either at ORNL or at Vanderbilt University to complete the requirements for a master's degree. The AEC Fellows for the 1955-56 program were selected in March and the group (29 in number) will enroll at Vanderbilt University in September.

### OTHER ACTIVITIES

E. E. Anderson                      M. F. Fair  
   K. Z. Morgan

A six-week advanced course in Health Physics was conducted for ten medical officers from the Advanced Radiobiology Course of the Armed Forces Special Weapons Project and one officer from the Army Chemical Center.

K. Z. Morgan presented a 12-hr course in Health Physics as a part of the July course, "Nuclear Energy Fundamentals for Industry," offered at

North Carolina State College. The 12 hr included a demonstration of Health Physics instruments used to measure dose, and lectures and discussion on "Maximum Permissible Exposure Values," "Control of Radiation by the Health Physicist," and "Shipping of Radioisotopes."

An introductory course in Nuclear Physics, including the fundamentals of radiation protection, was presented for the staff members and summer participants of the Ecology Section.

The Section conducted lectures and discussion periods on particular phases of Health Physics for:

1. the ORNL Orientation Program,
2. MIT Practice School,
3. foreign visitors,
4. a group of Reactor School students,
5. Instrument Division,
6. Electronuclear Division,
7. REED Group,
8. ORINS Radioisotope Techniques Course, and
9. ORINS-UT-AEC Military Veterinary Radiological Health Course.

A course in mathematics was conducted for the Laboratory Apprentice Training Program.

At the request of the Swedish Atomic Energy Company, E. G. Struxness and R. J. Morton spent four weeks in Stockholm discussing and advising on "Waste Disposal Problems in the Nuclear Energy Field." E. G. Struxness made brief visits to Norway, England, Holland, and France for informal discussions on the same subject.

## PUBLICATIONS

E. E. Anderson, F. C. VonderLage, and R. T. Overman, "Education and Training in Nuclear Science and Engineering in the United States," *Proceedings of the International Conference on the Peaceful Uses of Atomic Energy, Geneva, August 8-20, 1955* **1**, 463-470, United Nations, New York, 1956.

T. H. J. Burnett, "Estimating Airborne Radioactive Particulate Hazards - A Review of Sampling Criteria," *Am. Ind. Hyg. Assoc. Quar.* **17**, 80-84 (1956).

M. J. Cook, K. Z. Morgan and A. G. Barkow, "An Experiment Designed to Test the Validity of the Current Practice of Using Single Exposure Data to Calculate Maximum Permissible Concentration in Water for Continuous Exposure to Radioisotopes," *Am. J. Roentgenol. Radium Therapy Nuclear Med.* **75**, 1177-1187 (1956).

E. D. Gupton, "Proposed Dosage Determination in Beta-Gamma-X-Ray Film Dosimetry at ORNL," *Proceedings of the Health Physics Conference, Ohio State University, June 13-15, 1955, Columbus, Ohio* (May 1956).

F. N. Huffman, *Spatial Distribution of Electron Depth Dose in Aluminum*, ORNL-2137 (August 1, 1956).

G. S. Hurst, J. A. Harter, P. N. Hensley, W. A. Mills, M. Slater, and P. W. Reinhardt, "Techniques of Measuring Neutron Spectra with Threshold Detectors - Tissue Dose Determination," *Rev. Sci. Instr.* **27**(3), 153-156 (1956).

B. Kahn, "Leaching of Some Fission Products from Soil," *Anal. Chem.* **28**, 216-218 (1956).

F. Kalil and J. M. Garner, Jr., "System Continuously Records Water Level and Contamination," *Nucleonics* **14**(7), 56-60 (1956).

W. J. Lacy, R. R. Rollins, and L. M. Lawless, "The Removal of Radioactive Material from Water by Serial Coagulation, Ion Exchange, and Charcoal Adsorption," *Salty Dog VII*, ERDL-1451 (June 22, 1956).

H. J. Moe, "Ionization of Acetylene Mixtures and Other Mixtures by  $\text{Pu}^{239}$  Alpha Particles," ORNL-2136 (July 25, 1956).

K. Z. Morgan, "Organization of Professional Health Physicists," *Proceedings of Health Physics Conference, Ohio State University, June 13-15, 1955, Columbus, Ohio* (May 1956).

K. Z. Morgan, W. S. Snyder and M. R. Ford, "Maximum Permissible Concentration of Radioisotopes in Air and Water for Short Period Exposure," *Proceedings of the International Conference on the Peaceful Uses of Atomic Energy, Geneva, August 8-20, 1955* **13**, 139-158, United Nations, New York, 1956.

R. J. Morton and E. G. Struxness, "Ground Disposal of Radioactive Wastes," *Am. J. Public Health* **46**, 156-163 (1956).

R. J. Morton and C. P. Straub, "Removal of Radionuclides from Water by Water Treatment Processes," *J. Am. Water Works Assoc.* **48**, 545 (1956).

R. H. Ritchie, "Shielding Problems," *Proceedings of Health Physics Conference, Ohio State University, June 13-15, 1955, Columbus, Ohio* (May 1956).

B. G. Saunders, "Cloud Chamber for Counting Nuclei in Aerosols," *Rev. Sci. Instr.* **27**(5), 273-277 (1956).

C. P. Straub, W. J. Lacy, and R. J. Morton, "Methods for Decontamination of Low Level Radioactive Liquid Wastes," *Proceedings of the International Conference on the Peaceful Uses of Atomic Energy, Geneva, August 8-20, 1955* **9**, 24-27, United Nations, New York, 1956.

## HEALTH PHYSICS PROGRESS REPORT

C. P. Straub, "Criteria for Waste Disposal," *Proceedings of Health Physics Conference, Ohio State University, June 13-15, 1955, Columbus, Ohio* (May 1956).

C. P. Straub, "Problems of Radioactive Waste Disposal," *Sewage and Ind. Wastes* **28**, 787-794 (1956).

E. G. Struxness, A. J. Luessenhop, S. R. Bernard, and J. C. Gallimore, "Uranium Distribution and Excretion in Man," *Proceedings of the International Conference on the Peaceful Uses of Atomic Energy, Geneva, August 8-20, 1955* **10**, 186-196, United Nations, New York, 1956.

E. G. Struxness, R. J. Morton, and C. P. Straub, "Disposal of High Level Radioactive Liquid Wastes in Terrestrial Pits," *Proceedings of the International Conference on the Peaceful Uses of Atomic Energy, Geneva, August 8-20, 1955* **9**, 684-691, United Nations, New York, 1956.

J. W. Thomas, "Air Sampling for Radioactive Gases," *Proceedings of the Health Physics Conference, Ohio State University, June 13-15, 1955, Columbus, Ohio* (May 1956).

J. W. Thomas and R. E. Yoder, "Aerosol Penetration Through a Lead-Shot Column," *A.M.A. Archives of Industrial Health* **12**, 550-555 (1956).

J. W. Thomas and R. E. Yoder, "Aerosol Size for Maximum Penetration Through Fiberglass and Sand Filters," *A.M.A. Archives of Industrial Health* **13**, 545-549 (1956).

A. C. Upton, F. P. Conte, G. S. Hurst, and W. A. Mills, "The Relative Biological Effectiveness of Fast Neutrons, X-rays, and  $\gamma$ -Rays for Acute Lethality in Mice," *Radiation Res.* **4**, 117-131 (1956).

## PAPERS

J. A. Auxier and G. S. Hurst, *A Fast Neutron Insensitive Gamma Dosimeter*, Health Physics Society, June 25-27, 1956, Ann Arbor, Michigan.

S. R. Bernard and E. G. Struxness, *The Distribution and Excretion of Uranium in Man*, Health Physics Society, June 25-27, 1956, Ann Arbor, Michigan.

R. D. Birkhoff, H. H. Hubbell, Jr., and R. M. Johnson, *Ionization in a Cavity in a Beta-Radioactive Medium*, American Physical Society, March 29-31, 1956, Nashville, Tennessee.

R. D. Birkhoff, J. S. Cheka, H. H. Hubbell, Jr., R. M. Johnson, and R. H. Ritchie, *Measurement of Electron Flux in a Radioactive Medium*, American Physical Society, April 26-28, 1956, Washington, D. C.

T. E. Bortner and G. S. Hurst, *Electron Drift Rate in Pure Gases and Gas Mixtures*, American Physical Society, March 29-31, 1956, Nashville, Tennessee.

T. H. J. Burnett, *Air Pollution Aspects of Power Reactors*, Ninth Municipal and Sanitary Engineering Conference, April 17, 1956, University of Florida, Gainesville.

J. S. Cheka, *A Neutron Film Dosimeter*, Health Physics Society, June 25-27, 1956, Ann Arbor, Michigan.

J. M. Garner and O. W. Kochtitzky, *Radioactive Sediments in the Tennessee River System*, American Society of Civil Engineers, June 7, 1956, Knoxville, Tennessee.

M. I. Goldman and C. P. Straub, *Ground Disposal of Liquid Radioactive Wastes*, Meeting of the American Institute of Mining Engineers, February 22, 1956, New York.

G. S. Hurst, *Ionization by Alpha Particles in Mixtures of Gases*, Gordon Conference of American Association for the Advancement of Science, July 9-13, 1956, New Hampton, New Hampshire.

K. Z. Morgan, *Maximum Permissible Internal Dose of Radionuclides - Recent Changes in These Values*, American Nuclear Society Conference, June 8, 1956, Chicago, Illinois.

R. H. Ritchie, *Boundary Effects in Plasma Losses of Electrons in Thin Films*, American Physical Society, April 26-28, 1956, Washington, D. C. (Presented by R. D. Birkhoff).

C. C. Sartain, *Linearity of a Cloud Chamber*, American Physical Society, March 29-31, 1956, Nashville, Tennessee.

B. G. Saunders, *Cloud Chamber for Counting Nuclei in Aerosols*, American Physical Society, March 29-31, 1956, Nashville, Tennessee.

W. S. Snyder, *The Variation of Neutron Dose with Neutron Energy and Geometry*, Health Physics Society, June 25-27, 1956, Ann Arbor, Michigan.

C. P. Straub, *Fundamentals of Underground Waste Disposal*, National Convention of the American Society of Civil Engineers, February 14, 1956, Dallas, Texas.

E. G. Struxness, *A Survey of Ground Disposal for Liquid Wastes*, Health Physics Society, June 25-27, 1956, Ann Arbor, Michigan.

A. D. Warden, D. M. Davis and J. C. Hart, *Potential Hazards Associated with the Sale and Smelting of Uranium Contaminated Steel and Copper*, American Industrial Hygiene Association Meeting, April 1956, Philadelphia, Pennsylvania.

R. E. Yoder and J. W. Thomas, *The Filtration of Aerosols by Sand*, Health Physics Society, June 25-27, 1956, Ann Arbor, Michigan.

# UNCLASSIFIED

## LECTURES

E. E. Anderson, *Opportunities in the Field of Health Physics*, University of Rochester, May 2, 1956, New York.

E. E. Anderson, Moderator of Panel on *Training of Radiologic Physicists*, Annual Conference of Teachers of Clinical Radiology, February 11, 1956, Chicago, Illinois.

E. E. Anderson, *Radioactive Materials, Safety, and Economy*, Nuclear Engineering Lecture Series, University of Alabama, Birmingham Center, February 29, 1956.

K. E. Cowser, *Studies of Seepage Pits for Disposal of Radioactive Liquid Wastes*, presented to the following groups:

1. Steering Committee on Disposal of Radioactive Waste Products in Geologic Structures, Earth Sciences Division, National Academy of Sciences, National Research Council, February 15, 1956, Oak Ridge, Tennessee.
2. Mineralogy Club, April, 1956, Oak Ridge, Tennessee.
3. Chemical Technology Seminar, June 12, 1956, Oak Ridge, Tennessee.
4. Health Physics Division, Ecology Summer Participants, June 22, 1956, Oak Ridge, Tennessee.

K. E. Cowser, *Field Studies in Waste Disposal Research*, Health Physics Division, AEC Radiological Physics Fellowship Students, June 6, 1956.

F. M. Empson, *Waste Disposal - The Entrainment Well*, Chemical Technology Division, January 10, 1956.

M. I. Goldman, *Power Reactor Waste Disposal*, Seminar on Public Health Aspects of Nuclear Power, University of Minnesota, March 26, 1956, Minneapolis.

M. I. Goldman, *Environmental Radiocontamination and Waste Disposal*, Veterinary Radiological Health Course, March 6, 9, and April 10, 1956, Oak Ridge Institute of Nuclear Studies.

M. I. Goldman, *Chemical Reprocessing of Nuclear Fuels and Fission Product Waste Disposal and Nuclear Reactor Safety*, Training Course at the Sanitary Engineering Center, May 2, 1956, Cincinnati, Ohio.

K. Z. Morgan, *Internal Radiation Hazards*, U. S. Naval Medical School, March 13, 1956, Bethesda, Maryland.

G. G. Robeck, *Environmental Radiocontamination and Waste Disposal*, Veterinary Radiological Health Course, June 11, 1956, Oak Ridge Institute of Nuclear Studies.

F. W. Sanders, *Waste Disposal - Evolution of K-42 from Hot and Boiling Solutions*, Chemical Technology Division, January 10, 1956.

C. P. Straub, *Radioactive Waste Disposal*, a series of lectures to the AEC Fellowship Students in Radiological Physics at Vanderbilt University, May 21-22, 1956, Nashville, Tennessee.

C. P. Straub, *Radiological Health Aspects of Sanitary Engineering*, training course for Reserve Public Health Service and Military Sanitary Engineers at the Robert A. Taft Sanitary Engineering Center, June 11 and 22, 1956, Cincinnati, Ohio.

E. G. Struxness, *Ground Disposal of Radioactive Wastes*, Royal Institute of Technology, sponsored by AB Atomenergei (Atomic Energy Co.) Stockholm, for students of the Swedish Reactor School, May 18, 1956, Stockholm, Sweden.

E. G. Struxness, *Ground Disposal of Radioactive Wastes*, the Norwegian Radium Hospital, sponsored by the Ministry of Health for members of their Advisory Committee on Radiological Protection, May 28, 1956, Oslo, Norway.

R. E. Yoder, *Waste Disposal - The Filtration of Aerosols by Sand*, Chemical Technology Division, January 10, 1956.